

RELATIONSHIP BETWEEN THE GASIFICATION
REACTIVITIES OF COAL CHAR AND THE
PHYSICAL AND CHEMICAL PROPERTIES OF
COAL AND COAL CHAR

James L. Johnson

Institute of Gas Technology
3424 S. State Street
Chicago, Illinois 60616

INTRODUCTION

A variety of experimental investigations have studied, at elevated pressures, the gasification kinetics of coal chars in hydrogen and in gases containing steam and hydrogen. The bulk of these investigations, however, have been primarily concerned with the characterization of gasification rates as a function of environmental conditions such as temperature, pressure, and gas composition, and have provided little systematic information concerning relationships between gasification reactivities and the physical and chemical properties of coal or coal char.

This study was therefore initiated to evaluate possible relationships between gasification reactivities and simple compositional parameters for coal chars derived from a wide variety of coals and coal-maceral concentrates. The internal structural changes that occur during the course of gasification of a few coal chars of varying rank were also explored. The gasification reactivities of individual coal chars were determined in hydrogen or in a 50:50 steam-hydrogen mixture at 35 atmospheres, using a high-pressure thermobalance. Most tests were conducted at 1700°F, although, in a special series of tests designed to investigate the catalytic effects of exchangeable cations on lignite char reactivities, temperatures were varied from 1400° to 1700°F. The following results are discussed in this paper:

- The relationship between the initial carbon content and the gasification reactivities determined in the hydrogen at 1700°F, for coal chars derived from 36 coals and maceral concentrates ranging in rank from anthracite to lignite.
- The effect of exchangeable cation concentrations (sodium and calcium) on gasification reactivities of lignites in hydrogen at 1700°F and in steam-hydrogen mixtures at 1400° to 1700°F.
- The surface area and pore volume variations that occur during gasification in hydrogen and in steam-hydrogen mixtures at 1700°F of coal chars derived from anthracite, metallurgical coking coal, high-volatile A bituminous coal, sub-bituminous A coal, and lignite.

EXPERIMENTAL PROCEDURE

The high-pressure thermobalance used in this work to obtain gasification reactivity factors has been described previously (4). The main feature of this apparatus is that the weight of a small, fixed-bed sample of coal char (1/2 to 1 gram) contained in a wire-mesh basket can be continuously measured as it undergoes gasification in a desired gaseous environment at constant temperature and pressure. In all tests conducted, -20+40 U. S. sieve size particles were used, and gas flow rates in the reactor were maintained at sufficiently high values to result in negligible gas conversion. Under these conditions, coal-char gasification could be considered to occur under constant known environmental conditions. Coal chars were produced by initially exposing the raw coals to nitrogen at 1 atmosphere for

60 minutes, at the same temperature to be used during subsequent gasification in hydrogen or in steam-hydrogen mixtures. The weight loss versus time characteristics obtained during gasification in individual tests were then used as a basis for computing gasification reactivity factors, using a procedure described below.

Certain of the solid feeds and residues were analyzed for internal surface area, pore volume, and true density. Surface areas were computed from adsorption isotherms obtained with a Model 2100 Orr surface area-pore volume analyzer manufactured by the Micromeretics Corp., which was also used to obtain true densities in helium. Adsorption isotherms obtained in nitrogen at 77°K were interpreted with the BET equation to compute surface area, and isotherms obtained in carbon dioxide at 298°K were interpreted with the Dubinin-Polanyi equation as modified by Kaganer (7) to compute surface area. In general, surface areas computed from nitrogen and carbon dioxide adsorption isotherms were not in agreement, and values obtained in carbon dioxide were considered to be most reflective of equivalent internal surface area, which is consistent with the findings of other investigators (2, 3, 6, 7, 12). Apparently, the penetration of nitrogen into the microporous structure of coals or carbonized coal chars is severely limited by slow, activated diffusion processes at 77°K, leading to very low apparent surface areas; on the other hand, for partially gasified coal chars having more open microporous structures, capillary condensation of nitrogen can lead to unreasonably high apparent surface areas (1, 8). Adsorption isotherms obtained with carbon dioxide at the higher temperature of 298°K facilitate activated diffusion into microporous structures, and capillary condensation is inhibited by the lower relative pressures employed (0.003 to 0.02). Although there is some question concerning whether carbon dioxide adsorption isotherms should be interpreted in terms of micropore volume (8, 9, 10, 11) rather than micropore surface area (2, 3, 6, 7, 12), the distinction is not of importance in empirical correlations with gasification kinetic parameters. This is because the calculation methods used to compute numerical values of micropore volume and micropore surface area are virtually identical, differing only in the numerical constants used. Thus, reported values of micropore volumes can be converted to corresponding values of micropore surface area by a fixed constant. In this study we have chosen to compute surface area values, favoring the argument that carbon dioxide adsorption on a carbon surface should be restricted to a monolayer thickness, as a result of the quadruple interaction of the carbon dioxide molecules with the π -bonds of the carbon surface (2, 7).

An Aminco mercury intrusion porosimeter capable of a hydrostatic pressure of 15,000 psi was used to obtain pore volume distributions for pores having diameters greater than about 120 angstroms. Pore volume distributions for pores between about 12 and 300 angstroms were obtained from adsorption isotherms obtained in nitrogen at 77°K at relative pressures up to about 0.93. Good agreement was obtained with these two methods in the overlap region from 180 to 300 angstroms, similar to results reported by Gan *et al.* (3).

DEFINITION OF RELATIVE REACTIVITY FACTOR, f_L

Weight loss versus time characteristics obtained in individual thermobalance tests were interpreted to obtain relative reactivity factors for the coal chars used, based on a quantitative model developed previously at the Institute of Gas Technology to describe the gasification kinetics of bituminous coal chars as a function of temperature, pressure, gas composition, pretreatment temperature, and carbon conversion (4). The essential features of this model are described below.

Coal-char gasification in gases containing steam and hydrogen are assumed to occur via three main reactions:

where —

f_o = reactivity factor dependent only on the inherent nature of the coal char

T_p = pretreatment temperature, °R

T = gasification temperature, °R.

Equation 3 is only applicable for $T_p > T$; for $T_p \leq T$, then $f_L = f_o$.

At constant environmental conditions, Equation 1 can be integrated to yield —

$$M(X) = \int_0^X \frac{\exp(\alpha X^2)}{(1-X)^{2/3}} dX = f_L k_T \theta \quad 4)$$

Based on Equation 4, a plot of $M(X)$ versus θ should yield a straight line having a slope equal to the term $f_L k_T$. Values of $M(X)$ can be computed from experimental thermobalance data, using Equation 2 to obtain values of X and using the defined value of α to evaluate the integral in Equation 4. Note that, for tests conducted in pure hydrogen, the value of α is 0.97; with this value, the term $(1-X)^{2/3} \exp(0.97 X^2)$ is approximately equal to $(1-X)$, over nearly a complete range of X . For this case, $M(X) = -\ln(1-X)$ and values of the specific gasification rate, $(dX/d\theta)/(1-X)$, are constant and equal to $f_L k_T$.

Figure 1 shows two types of behavior noted in this study in experimental plots of $M(X)$ versus θ . Line A is typical of the characteristics obtained with the majority of coal chars tested, with linearity exhibited over the complete range of base carbon conversion. The line shown does not extrapolate to the origin because char samples initially exposed to the gasifying environment in the thermobalance require 1 to 2 minutes to heat up to reactor temperature. A characteristic of the type shown for Case B was obtained with some coal chars, usually low-rank materials, indicating an initial period of transient reactivity, which decreased during the first 5 to 10 minutes and remained constant thereafter. For coal chars exhibiting this type of behavior, only the linear portion of the curve corresponding to constant reactivity was used to evaluate experimental values of $f_L k_T$.

Values of the reactivity factor, f_L , were then obtained by dividing the term $f_L k_T$ by the value of k_T defined in the model (4) for the reaction conditions used.

RESULTS

Correlation of Reactivity Factors With Carbon Content in Raw Coals

The reactivity factors for coal chars derived from 36 coals and coal maceral concentrates were determined in hydrogen at 1700°F and 35 atmospheres. The distribution of coals used with respect to rank and lithotype is described in Table 1. In this study a variety of correlations were evaluated in attempting to quantitatively relate these reactivity factors with simple, compositional parameters included in ultimate, proximate, and petrographic analyses of the raw coals. The best success, however, was achieved with one of the simplest correlations considered — a relationship between reactivity factors and initial carbon contents. This correlation is illustrated in Figure 2, where the line drawn corresponds to the expression:

$$f_L = 6.2Y(1 - Y) \quad 5)$$

where -

f_L = relative reactivity factor of coal char

Y = concentration of carbon in raw coal (dry, ash-free), g/g coal.

Table 1. NUMBERS OF EACH COAL TYPE USED IN CORRELATION

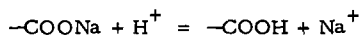
<u>Coal Rank</u>	<u>Whole</u>	<u>Vitrain</u>	<u>Fusian</u>	<u>Total</u>
Lignite	1	1	1	3
Subbituminous C	2	1	--	3
Subbituminous B	1	2	2	5
Subbituminous A	3	2	1	6
High-Volatile C Bituminous	1	2	1	4
High-Volatile B Bituminous	1	1	4	6
High-Volatile A Bituminous	4	2	--	6
Low-Volatile Bituminous	2	--	--	2
Anthracite	<u>1</u>	<u>--</u>	<u>--</u>	<u>1</u>
Total	16	11	9	36

For reasons discussed below, it should be emphasized that, for lignite coal chars, the correlation shown in Figure 2 is applicable only when the raw lignite is initially treated in acid to remove exchangeable cations.

The standard deviation of experimental reactivity factors shown in Figure 2 and of reactivity factors calculated from Equation 5 is about 0.1, which is equivalent to the reproducibility of experimentally determined reactivity factors. Interestingly, the correlation proposed does not uniquely distinguish between maceral types.

Effects of Exchangeable Cation Concentration on Lignite Char Reactivity

If reactivity factors determined for coal chars derived from untreated raw lignites were included in Figure 2, then a considerable amount of scatter would be apparent above the correlation line at low carbon concentrations. One phase of this study, however, showed that the reactivities of lignite chars obtained from lignites initially treated in HCl or HCl-HF acid were generally significantly less than the corresponding reactivities exhibited by lignite chars derived from untreated lignites. This was not observed with several bituminous and subbituminous coal chars. This behavior apparently resulted from a catalytic effect of exchangeable cations inherently present in raw lignites in carboxyl functional groups, which can be removed in acid by the following type of reaction:



With this explanation, one can reasonably expect that this catalytic effect would predominate in lignites and would decrease rapidly with increasing coal rank, corresponding to a rapid decrease in the amount of coal oxygen combined in carboxyl functional groups.

A series of tests were conducted to obtain a quantitative measure of the effects of exchangeable cation concentration (sodium and calcium) on char reactivity factors for gasification in hydrogen and in steam-hydrogen mixtures. These tests were conducted with lignite chars derived from raw lignites, with the lignite chars derived from raw lignites initially demineralized in hydrochloric acid to remove exchangeable cations and with the lignite chars derived from raw lignites initially demineralized in hydrochloric acid to which various amounts of calcium or sodium were then added by cation exchange in sodium acetate or calcium acetate solutions. Results of one

series of tests corresponding to gasification in hydrogen at 1700°F are shown in Figure 3. The results in Figure 3 were correlated with the expression:

$$f_L/f_L^0 = 1 + 54.7 Y_{Na} + 14.0 Y_{Ca} \quad 6)$$

where -

f_L = reactivity factor of lignite to which sodium or calcium was added

f_L^0 = reactivity factor of acid-treated lignite ($Y_{Na}, Y_{Ca} = 0$)

Y_{Na}, Y_{Ca} = concentration of exchangeable sodium or calcium in lignite before devolatilization in nitrogen, g/g fixed carbon.

Although the correlation given in Equation 6 was developed from data obtained with prepared lignites that did not contain both calcium and sodium at the same time, it does apply reasonably well to untreated lignites containing, in some cases, both calcium and sodium. This is demonstrated in Table 2.

Table 2. COMPARISON OF CALCULATED AND EXPERIMENTAL REACTIVITY RATIOS

Lignite	Y_{Ca}	Y_{Na}	f_L/f_L^0	
	g/g fixed carbon		Calculated	Experimental
Savage Mine, Montana (whole)	0.043	0.000	2.1	1.7
Savage Mine, Montana (vitrain)	0.019	0.004	1.5	1.7
Glenharold Mine, N. Dakota (whole)	0.031	0.009	1.9	2.0
Glenharold Mine, N. Dakota (vitrain)	0.019	0.002	1.3	1.2

A test series was also conducted to determine effects of exchangeable calcium and sodium concentrations on the reactivities on a Montana lignite char in steam-hydrogen mixtures at temperatures from 1400°F to 1700°F. Results obtained are illustrated in Figure 4, which plots values of the kinetic term, $f_L k_T$, as a function of temperature and cation concentration. Although these results have not yet been quantitatively correlated, they apparently show that sodium and calcium significantly enhance gasification in steam-hydrogen mixtures, even more so than for gasification in hydrogen alone. Figure 4 shows that the effect of calcium concentration on reactivities is substantially the same as the effect of sodium concentration at corresponding conditions (contrary to the behavior obtained in pure hydrogen), and that relative catalytic effects tend to decrease with increasing gasification temperature.

A significant additional result of the test series conducted with steam-hydrogen mixtures was that the reactivity of acid-treated Montana lignite ($Y_{Ca}, Y_{Na} = 0$) remains constant for gasification in steam-hydrogen mixtures over a temperature range from 1400° to 1700°F. This is shown in Figure 5, which plots experimental values of $f_L k_T$ versus values of k_T calculated from correlations developed to describe bituminous coal char gasification kinetics (4). The line drawn corresponds to a constant value of $f_L = 1.3$, which is about the same value obtained for gasification in pure hydrogen at 1700°F.

Variations in Internal Char Surface Areas During Gasification

The variations in internal surface areas were measured for several chars at different stages of gasification in hydrogen or steam-hydrogen mixtures. The compositions of the coals from which these chars were prepared are given in Table 3. Figure 6 shows the variations in surface area measured in carbon dioxide with different base carbon conversion fractions for a series of tests conducted with Montana lignite chars. Figure 6 shows that the internal surface area of the Montana lignite char tends to remain constant over a major range of base carbon conversion fractions and is essentially independent of char pretreatment or gasification conditions. The apparent surface areas of carbonized chars ($X = 0$) are lower than the nominal value of partially gasified chars. This difference may reflect that, even with carbon dioxide, penetration into the micropore structure is somewhat inhibited before the structure is opened up by partial gasification.

Figure 7 shows variations in apparent surface area measured in nitrogen for Montana lignite chars. The characteristics shown tend to support the suggestion made previously that, at low levels of conversion, nitrogen penetration into the micropore structure is severely inhibited, but that, at higher carbon conversions, unreasonably high apparent surface areas are obtained because of capillary condensation.

In Figure 8, variations in surface area measured in carbon dioxide (S_{CO_2}) obtained with some other coal chars are compared with results obtained with Montana lignite chars. Although surface areas measured for char derived from anthracite, high-volatile bituminous coal, and lignite remained essentially constant during the course of conversion in hydrogen and steam-hydrogen mixtures, surface areas for the subbituminous coal char generally decreased with increasing carbon conversions during gasification in hydrogen. Interestingly, of the four coal chars tested, only the subbituminous coal char exhibited decreasing specific gasification rates during gasification with hydrogen that paralleled the decrease in surface area. This is shown in Figure 9. Although generalizations based on the kinetic behaviors exhibited by only four coal chars are not justified, these results do suggest that a form of kinetic correlation to describe coal-char gasification rates that is more meaningful than that derived from the Equation 1 may be the following:

$$\frac{dX}{d\theta} = \lambda S k_T (1 - X) \quad 7)$$

where —

λ = relative reactivity per unit of internal surface area

S = internal surface area per mass of carbon present.

With this interpretation, the constancy of the values of f_L and S_{CO_2} of anthracite, high-volatile bituminous, and lignite coal char during gasification in hydrogen corresponds to a constant value of λ for each char. For the subbituminous coal char, λ is also constant, although S_{CO_2} decreases with increasing carbon conversion, apparently because of the growth of crystallites. For the gasification temperatures used, this growth is probably unusual and not characteristic of most coal chars. This is particularly true if the first-order kinetics observed in a variety of previous studies of the gasification of a fairly large number of coal chars in hydrogen are assumed to correspond to constant values of λ and S_{CO_2} for the individual coal char tested.

Table 3. COMPOSITIONS OF COALS USED IN PHYSICAL PROPERTY STUDIES

Coal Identification	Pittsburgh No. 8 (Ireland Mine)		Brazilian Carvao Metallurgical		Rosebud, Colstrip Mine		Savage Mine (Montana)	
	Anthracite	Subbituminous A	Subbituminous A	Whole	Subbituminous A	Whole	Subbituminous A	Whole
Rank	Anthracite	Whole	Whole	Whole	Whole	Whole	Whole	Whole
Lithotype	Whole	Whole	Whole	Whole	Whole	Whole	Whole	Whole
Ultimate Analysis, mass %								
Carbon	83.40	69.47	66.70	69.60	66.70	69.60	65.13	65.13
Hydrogen	2.37	3.78	4.57	4.52	4.57	4.52	4.13	4.13
Oxygen	2.62	6.59	4.57	19.31	4.57	19.31	24.20	24.20
Nitrogen	0.84	1.39	1.22	0.99	1.22	0.99	0.89	0.89
Sulfur	1.03	3.75	1.90	0.65	1.90	0.65	0.57	0.57
Ash	9.74	15.02	21.04	4.93	21.04	4.93	5.08	5.08
Total	100.00	100.00	100.00	100.00	100.00	100.00	100.00	100.00
Proximate Analysis, mass % (dry)								
Volatiles	6.77	22.70	31.80	42.10	31.80	42.10	43.62	43.62
Fixed Carbon	83.49	62.28	47.20	53.00	47.20	53.00	51.30	51.30
Ash	9.74	15.02	21.00	4.90	21.00	4.90	5.08	5.08
Total	100.00	100.00	100.00	100.00	100.00	100.00	100.00	100.00

Interestingly, in the kinetic model previously referred to, the value of α in Equation 1 is approximately 1.7 for a variety of gas compositions containing steam and hydrogen at elevated pressures. Empirically, this value corresponds to decreasing values of λ with increasing carbon conversions when interpreted in terms of Equation 7. This occurs even when the total internal surface areas remain constant during conversion in steam-hydrogen mixtures, as was shown in Figure 6 for Montana lignite char.

Some additional evidence was obtained in this study that can be interpreted in terms of the formulation given in Equation 7. Figure 10 shows values of S_{CO_2} obtained during gasification of a coal char derived from Brazilian metallurgical coal, at various temperatures, with hydrogen and steam-hydrogen mixtures. With this material, the char surface area, S_{CO_2} , is not a function of carbon conversion level and is the same in hydrogen and in steam-hydrogen mixtures, but decreases with increasing gasification temperature. The reactivity factor, f_r , which is characteristic of results obtained at a specific temperature, also decreases with increasing temperature and is proportional to internal char surface area, as shown in Figure 11. This particular char then can be considered to have a constant value of λ , independent of temperature, conversion, or gasification medium, but does exhibit a decreasing internal surface area with increasing temperature, a feature that probably reflects its use as a metallurgical coking coal.

Variations in Char Pore Volumes During Gasification

Figure 12 illustrates typical pore-volume distributions of partially gasified coal chars. With the exception of untreated Montana lignite (Curve F), the features exhibited in Figure 12 appear to be generally similar to the distributions obtained by Stacy and Walker (9) with some coal chars resulting from a fluid-bed hydrogasification. Whereas Curves A through E tend to show a plateau at a pore diameter of about 55 angstroms, possibly indicative of the lack of development of significant transitional pores, Curve F shows a significant variation in pore volume through this range of pore diameters. It may be pertinent, therefore, that the gasification rates of untreated Montana lignite char in a steam-hydrogen mixture were about 7 times faster than the largest of the gasification rates obtained with chars corresponding to Curves A through E. It is thus possible that, with sufficiently large gasification rates, dynamic modifications that tend to occur within coal structures as carbon is removed are inhibited.

The plateau in pore-volume variations at a pore diameter of 55 angstroms exhibited by most coals tested has suggested the following simplified representation of pore-volume characteristics: Total pore volume accessible via pores less than 55 angstroms is defined as "micropore" volume, and pore volume accessible via pore openings having diameters between 55 and 20,000 angstroms is defined as "macropore" volume. Micropore and macropore volumes obtained with different coal chars are shown in Figures 13 and 14 as a function of the base carbon conversion fraction. Note that in these figures, volumes are represented per mass of initial base carbon rather than per mass of remaining carbon and, therefore, are proportional to volumes on a per particle basis. Figure 13 shows surprisingly little variation in macropore volume with increasing conversion for Curves A through E. In viewing these results, remember that the true density of base carbon in these coal chars is about 2 grams/cu cm, corresponding to a total volume of 0.5 cu cm/gram of initial base carbon. Thus, if the space initially occupied by gasified base carbon were added to the macropore volume, macropore volumes would increase significantly with increasing carbon conversion. The results shown in Figure 13, however, indicate that this is not generally the case, with the exception of Curve F, which does show a sharp increase in macropore volume up to conversions of about 0.8.

Figure 14 shows that micropore volumes tend to initially increase with increasing carbon conversion, reach a maximum, and then decrease with increasing conversion, approaching zero at complete conversion. Interestingly, the micropore-volume characteristics corresponding to untreated Montana lignite char gasified in a steam-hydrogen mixture are essentially identical to the characteristics for the other Montana lignite chars, as opposed to the behavior noted in Figures 12 and 13. Thus, the rapid gasification rates that evidently affect structural transitions at a "macro" level apparently do not affect structural transitions on a "micro" level. This is consistent with the results discussed previously, which showed an insensitivity in lignite-char-surface areas to initial acid treatment or to gasification conditions.

The variations in total particle volume with base carbon conversion measured with the mercury porosimeter are shown in Figure 15. The volumes represent the sum of solid volume plus pore volumes accessible via pore openings having diameters of less than 120 microns. As indicated in Figure 15, total particle volumes tend to decrease with increasing base carbon conversion fraction, particularly at conversions greater than about 0.5. Because these results were somewhat unexpected when initially observed, some additional tests were conducted to obtain photographic evidence of quantitative changes that occurred in individual external coal-char particle dimensions before and after gasification in hydrogen at 1700°F. In this series of tests, a few particles each of anthracite, high-volatile A bituminous coal, and Montana lignite were initially photographed in several orientations under optically calibrated conditions; were gasified in the thermobalance to relatively high levels of carbon conversion; and were then photographed again. Detailed examination of the photographs obtained did show a significant reduction in particle volumes, consistent with the results shown in Figure 15. The fraction of volume reduction of each type of char was independent of initial particle diameter in the range from about 200 to 800 microns. This fact and the fact that external topological characteristics remained unchanged except for a diminishment in size indicated that the observed shrinkage occurred throughout individual particles and was not the result of a "shrinking core" phenomenon.

SUMMARY AND CONCLUSIONS

The overall evidence obtained in this study suggests the tentative conclusion that gasification of coal chars with hydrogen and steam-hydrogen mixtures occurs primarily at char surfaces located within micropores. This conclusion is supported by the relationships indicated between specific gasification rates and internal char surface areas, particularly for gasification in hydrogen. With the majority of coal chars, internal surface area remains constant during gasification and is independent of gasification conditions, possibly indicating an invariance in average crystallite dimensions during the gasification process. With some coal chars, however, surface areas tend to decrease with increasing conversion or increasing gasification temperature, which would be indicative of a growth in crystallite dimensions.

Particle shrinkage occurs during coal-char gasification, due almost solely to contraction of the microporous phase (solids plus pores accessible via openings with diameters less than 55 angstroms), possibly because of the continuous re-orientation of individual carbon crystallites. Macropore cavities also shrink at higher levels of conversion, but in a manner analogous to cavities in a metallic solid undergoing thermal contraction. Although accessible macropore volumes may increase somewhat during the initial stages of conversion, this increase may correspond to an increasing accessibility of the macropore cavities present initially. Although there are some significant differences in the variations in surface areas and pore volumes for various coal chars during gasification, the different coal chars tested exhibit a surprising similarity in variations in average micropore diameter with increasing base carbon conversion. This is shown in Figure 16, which plots

values of the average micropore diameter, \bar{D} , versus the base carbon conversion fraction, X. The average micropore diameter was computed from the expression -

$$\bar{D} = \frac{4V}{S_{CO_2}}$$

where -

V = micropore volume (accessible pore-opening diameter <55Å).

Although the relative gasification reactivity factor, f_r , can be considered to be the product of two terms - "char surface area" and "reactivity per unit of char surface area" - this study has not produced enough data to evaluate correlations between these separate parameters and other coal properties.

The study has shown, however, that f_r itself correlates well with the initial carbon content of raw coals for most of the coal chars tested. Lignites represent a special case, because of the catalytic effects of exchangeable cations, particularly sodium and calcium, which predominate in lignites because carboxyl functional groups are present. This catalytic effect is greater for gasification in steam-hydrogen mixtures than in hydrogen alone and tends to decrease with increasing gasification temperature.

ACKNOWLEDGMENT

This work was conducted at the Institute of Gas Technology with primary support from the American Gas Association.

REFERENCES

1. Dubinin, M. M., "Chemistry and Physics of Carbon," Vol. II. (Ed. P. L. Walker, Jr.). Marcel Dekker, Inc., New York, 1966, p. 51.
2. Everett, D. H., Proc. Chem. Soc. **38**, (1957).
3. Gan, H., Nandi, S. P. and Walker, P. L., "Porosity in American Coals," Stock No. 2414-00059, U.S. Government Printing Office, Washington, D.C. 1972.
4. Johnson, J. L., in Advances in Chemistry Series No. 131, "Coal Gasification," 1974.
5. Kaganer, M. E., Zh. Fiz. Khim. **33**, 2202 (1959).
6. Marsh, H. and Siemieniewska, Fuel (London) **44**, 355 (1965).
7. Marsh, H. and Wynne-Jones, W.F.K., Carbon **1**, 281 (1964).
8. Spencer, D.H.T. and Bond, R. L., in Advances in Chemistry Series No. 55, "Coal Science," 724, 1966.
9. Stacy, W. O. and Walker, P. L., "Structure and Properties of Various Coal Chars," Stock No. 2414-00058, U.S. Government Printing Office, Washington, D.C., 1972.

10. Toda, Y., "Study on Pore Structure of Coals and Fluid Carbonized Products," Report No. 5 of the National Institute for Pollution and Resources. Japan, 1973.
11. Toda, Y., Hatauci, M., Toyoda, S., Yoshida, Y. and Honda, H., Fuel 50 (2), 187 (1971).
12. Walker, P. L. and Patel, R. L., Fuel 49 (1), 91 (1970).

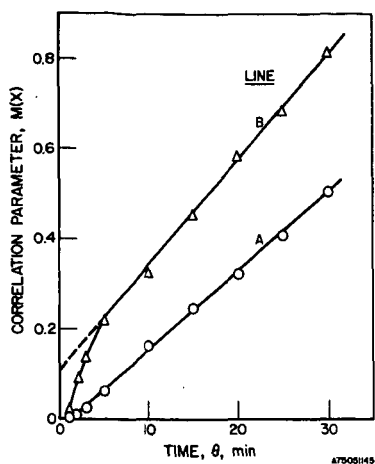


Figure 1. TYPES OF CORRELATION CHARACTERISTICS

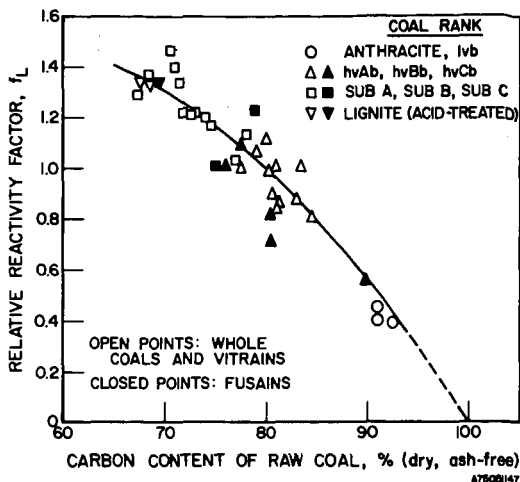


Figure 2. CORRELATION OF REACTIVITY FACTORS

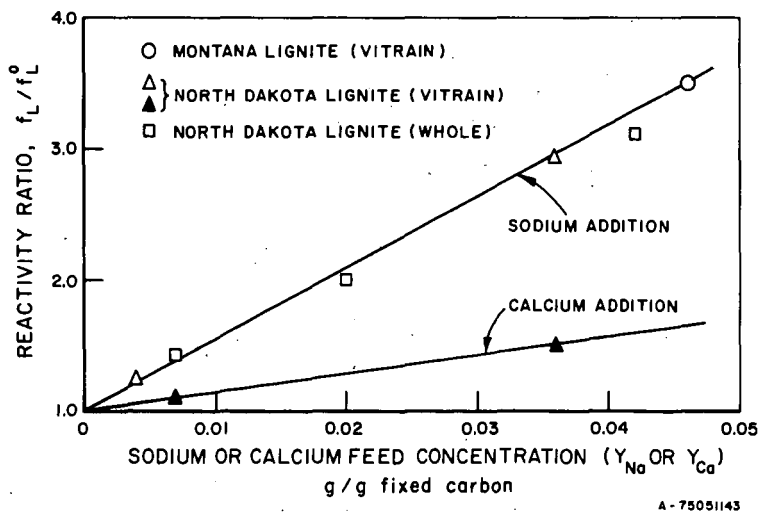


Figure 3. EFFECT OF CATION CONCENTRATION ON REACTIVITY OF LIGNITE CHAR IN HYDROGEN AT 1700°F AND 35 ATMOSPHERES

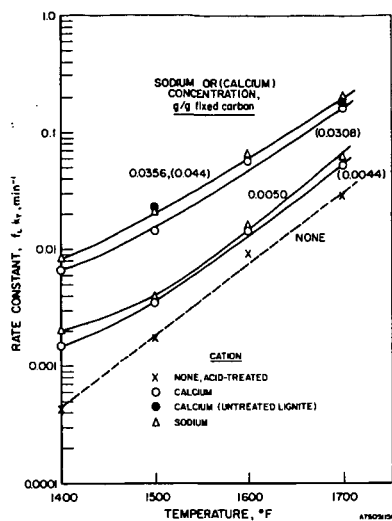


Figure 4. EFFECT OF CATION CONCENTRATION ON REACTIVITY OF MONTANA LIGNITE CHAR IN STEAM-HYDROGEN MIXTURES AT 1400° TO 1700°F AND 35 ATMOSPHERES

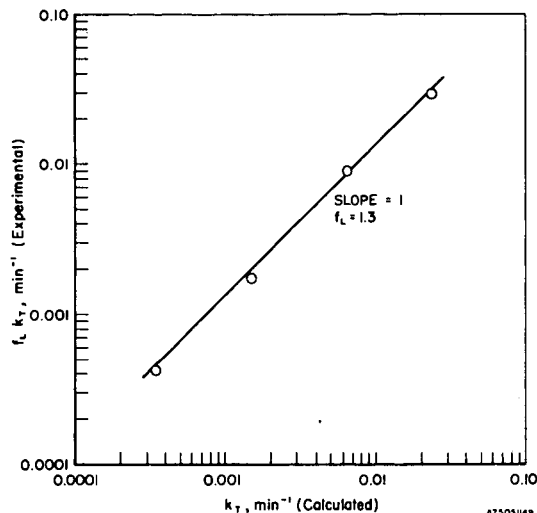


Figure 5. REACTIVITY OF ACID-TREATED MONTANA LIGNITE CHAR IN STEAM-HYDROGEN MIXTURES AT 1400° TO 1700°F AND 35 ATMOSPHERES

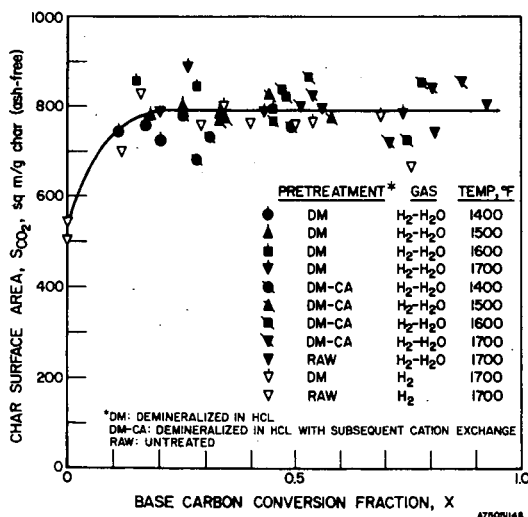


Figure 6. VARIATIONS IN SURFACE AREA MEASURED IN CARBON DIOXIDE (S_{CO_2}) WITH BASE CARBON CONVERSION FRACTION FOR MONTANA LIGNITE CHARS GASIFIED AT VARIOUS CONDITIONS

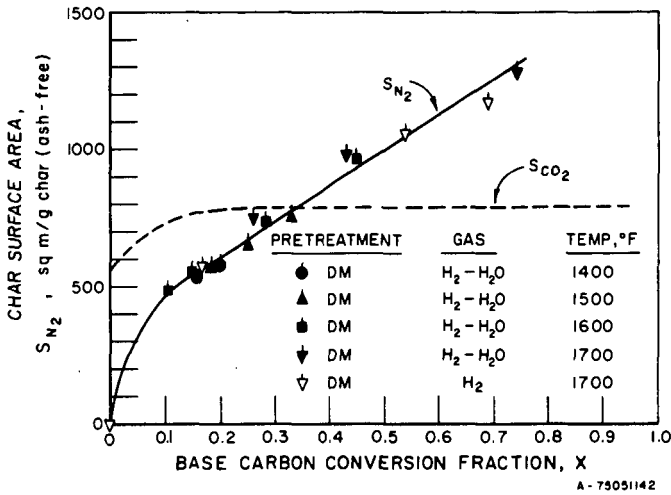


Figure 7. VARIATIONS IN APPARENT SURFACE AREA MEASURED IN NITROGEN WITH BASE CARBON CONVERSION FRACTION FOR MONTANA LIGNITE CHARS GASIFIED AT VARIOUS CONDITIONS

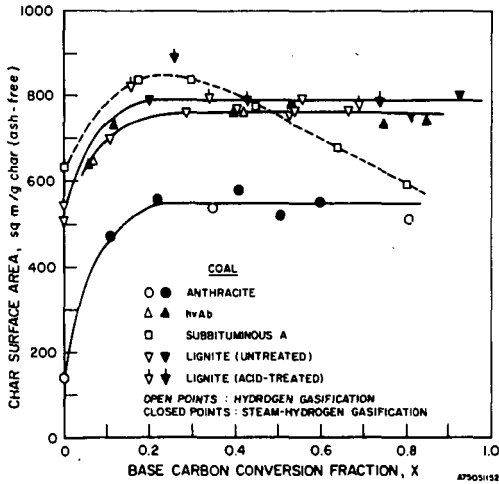


Figure 8. VARIATIONS IN S_{CO_2} WITH BASE CARBON CONVERSION FRACTION FOR DIFFERENT COAL CHARS GASIFIED IN HYDROGEN AND STEAM-HYDROGEN MIXTURES AT 1700°F AND 35 ATMOSPHERES

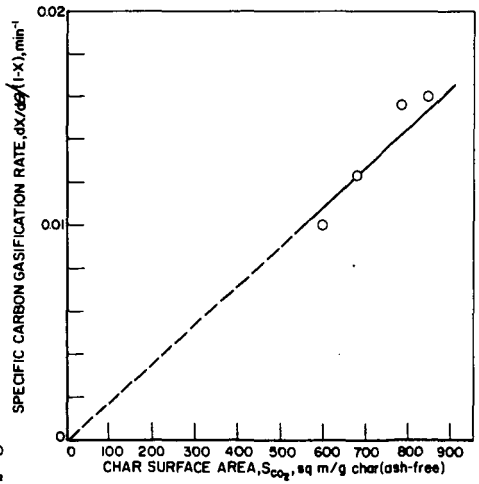


Figure 9. RELATIONSHIP BETWEEN SPECIFIC CARBON GASIFICATION RATE AND S_{CO_2} FOR GASIFICATION OF ROSEBUD SUBBITUMINOUS A COAL CHAR IN HYDROGEN AT 1700°F AND 35 ATMOSPHERES

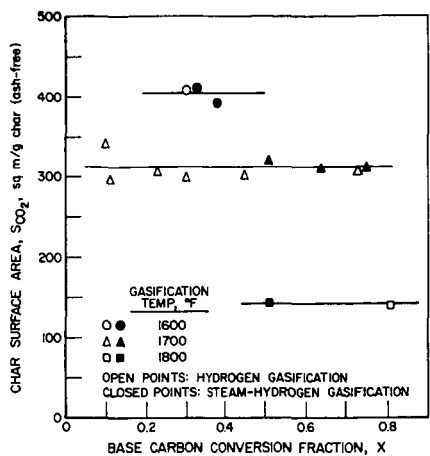


Figure 10. EFFECT OF GASIFICATION TEMPERATURE ON INTERNAL SURFACE AREA OF CARVAO METALLURGICAL COAL CHAR

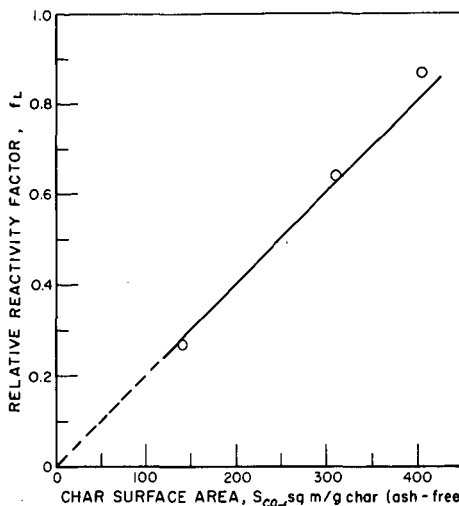


Figure 11. RELATIONSHIP BETWEEN REACTIVITY FACTOR, f_L , and S_{CO_2} FOR CARVAO METALLURGICAL COAL CHAR

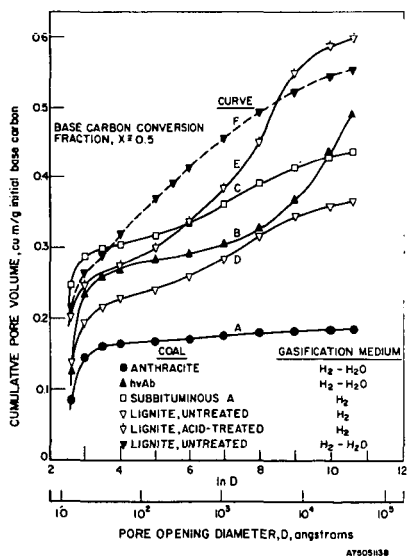


Figure 12. TYPICAL PORE VOLUME DISTRIBUTIONS FOR DIFFERENT COAL CHARS GASIFIED IN HYDROGEN AND STEAM-HYDROGEN MIXTURES AT 1700°F and 35 ATMOSPHERES

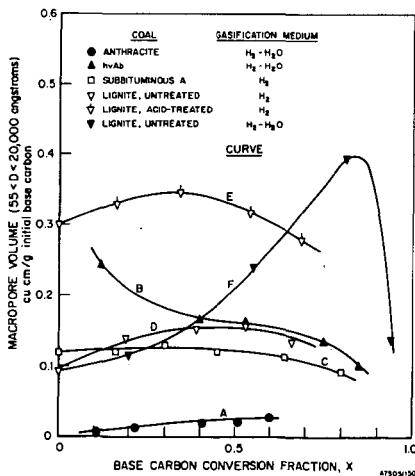


Figure 13. RELATIONSHIP BETWEEN MACROPORE VOLUME AND BASE CARBON CONVERSION FRACTION FOR DIFFERENT COAL CHARS

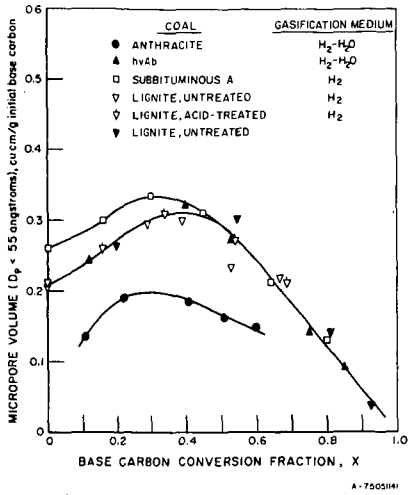


Figure 14. RELATIONSHIP BETWEEN MICROPORE VOLUME AND BASE CARBON CONVERSION FRACTION FOR DIFFERENT COAL CHARS

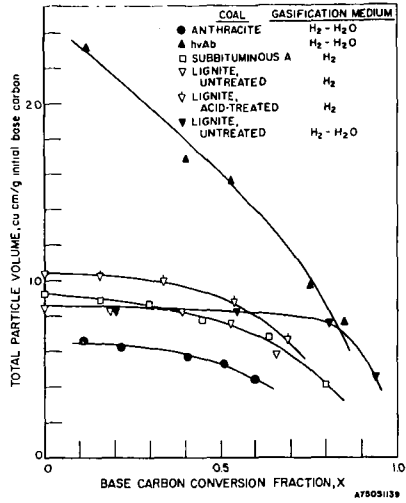


Figure 15. RELATIONSHIP BETWEEN TOTAL PARTICLE VOLUME AND BASE CARBON CONVERSION FRACTION FOR DIFFERENT COAL CHARS

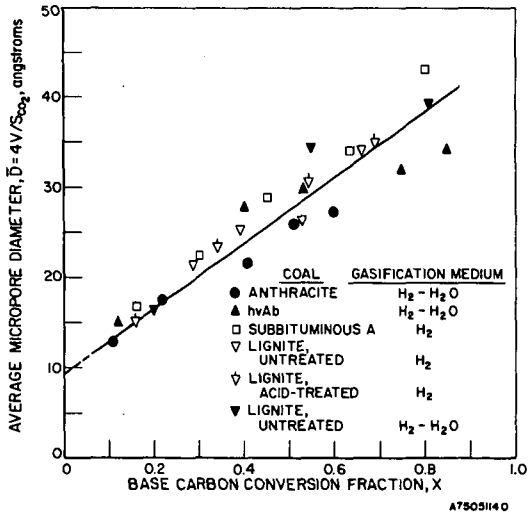


Figure 16. RELATIONSHIP BETWEEN AVERAGE MICROPORE DIAMETER AND BASE CARBON CONVERSION FRACTION FOR DIFFERENT COAL CHARS

RAPID DEVOLATILIZATION AND HYDROGASIFICATION OF BITUMINOUS COAL.

D.B. Anthony, H.C. Hottel, J.B. Howard, and H.P. Meissner, Department of Chemical Engineering, Massachusetts Institute of Technology, Cambridge, Massachusetts 02139

Rapid devolatilization and hydrogasification of a Pittsburgh Seam bituminous coal were studied and an approximate coal conversion (weight loss) model was developed that accounts for secondary char-forming reactions among volatiles. Approximately monolayer samples of small coal particles supported on wire mesh heating elements were electrically heated in hydrogen and hydrogen/helium mixtures. Coal weight loss was measured as a function of residence time (0.05-20 sec.), temperature (400-1100°C), heating rate ($10^2 - 10^4$ °C/sec.), total pressure (0.001 - 100 atm), hydrogen partial pressure (0 - 100 atm), and particle size 50 - 1000 μ m). Rate of weight loss under these conditions appears to be controlled by thermal decomposition reactions that form volatiles and initiate a sequence of secondary reactions leading to char. Thermal decomposition is modelled as a large number of parallel first-order reactions having a statistical distribution of activation energies (20-89 kcal/mole). The contribution of secondary reactions to weight loss is described by a selectivity expression derived from the assumption that char formation by these reactions competes with hydrogenation reactions and diffusional escape of volatiles from the particle.

J. A. Gray, P. J. Donatelli, P. M. Yavorsky

U.S. Energy Research and Development Administration
Pittsburgh Energy Research Center
4800 Forbes Avenue
Pittsburgh, Pennsylvania 15213

INTRODUCTION

Of the many processes currently under development which will convert coal to environmentally acceptable solid, liquid, and gaseous fuels utilizing pyrolysis, synthesis gas, solvent extraction, or hydrogenation techniques, the direct hydrogenation of coal to a raw gas that is easily upgraded to pipeline quality is a promising approach. Such a process is under development by the E.R.D.A., Pittsburgh Energy Research Center and is known as HYDRANE (1, 2).

Briefly, the HYDRANE flow sheet is as follows. Pulverized raw coal is fed to the top zone of the hydrogasifier, operated at 70 atm and 750°-900° C, where it falls freely as a dilute cloud of particles through a hydrogen-rich gas containing some methane from the lower zone. About 20 pct of the carbon in the raw coal is converted to methane, causing the coal particles to lose their volatile matter and agglomerating characteristics and to form very porous, reactive char particles. This char falls into the lower zone, operated at 70 atm and 900°-980° C, where hydrogen feed gas maintains the particles in a fluidized state and reacts with an additional 25 pct of the carbon to make methane. The product gas exists from the bottom of the dilute-phase zone and is cleaned of entrained solids, tars and oils, and some unwanted gases. After cleanup, catalytic methanation of the small amount of residual carbon monoxide gives a pipeline quality, high-Btu, substitute natural gas. Char from the lower zone of the hydrogasifier is reacted with steam and oxygen to make the needed hydrogen.

This process has the following advantages:

1. External hydrogen consumption per unit of methane produced is low because the hydrogen already in the coal is efficiently utilized,
2. Process costs associated with coal pretreatment, inherent in other coal conversion processes based on caking bituminous coal feedstocks, are eliminated,
3. 95 percent of the product methane is produced directly in the hydrogasifier thus requiring very little catalytic methanation,
4. Simple reactor design,
5. Produces low-sulfur char byproduct for hydrogen generation and low-sulfur tars, and
6. Utilizes sensible heat of the residual char from the hydrogasifier in the hydrogen generation plant.

Because of these advantages, coal and oxygen (the costliest items in gasification) requirements are minimized for the process, and thermal efficiency and carbon utilization are high at 78 pct and 44 pct, respectively (3, 4).

Much of the hydrogasification kinetic data on the laboratory scale, free-fall, dilute-phase reactor has already been published (5, 6) as well as data from a semiflow bench-scale reactor (7). In this paper we review previous and some recent kinetic data with regard to the type of reactor used to obtain the data, and the effect of the type of reactor on the conversion data. The conversion of the non-mineral elements in the coal during hydrogasification and the char yield are shown to be related to the carbon conversion regardless of the reactor geometry used, so that the constituent conversions can be calculated once the carbon conversion is known. This simplifies the reactor design in that only the carbon conversion need be kinetically defined for a particular reactor geometry.

EXPERIMENTAL REACTORS

"Hot-Rod" Reactors (HR)

In 1955 El Paso Natural Gas Company entered into a cooperative agreement with the then U.S. Bureau of Mines Synthetic Fuels Research Branch to investigate the hydrogenation of a subbituminous New Mexico coal to produce high-Btu gas and low-boiling aromatics. Part of the agreement called for tests in a reactor in which dry coal could be rapidly brought to the desired operating temperature and pressure. A normal autoclave required over an hour to reach temperature. Consequently, the effect of the heating and cooling cycles on the reaction could not be discerned. In late 1955, Hiteshue conceived the apparatus known as the "hot-rod" reactor and completed the El Paso project using it. The apparatus along with conversion data were first reported by Hiteshue, Anderson, and Schlesinger in 1957 (8) and again during 1960-1964 (9, 13).

The "hot-rod" reactor, shown in Figure 1, was a 70-inch long stainless steel tube (type 304) having a 5/16-inch inside diameter and a 5/8-inch outside diameter. A coal or char sample weighing 8 grams and screened to 30 x 60 U.S. sieve size was inserted into the tube between two porous stainless steel disks such that a 32-inch length was available to fluidize the sample. The tube was heated with electrical current by connecting it to a transformer that was capable of supplying 700 amperes at 9 volts. With this method of heating, the reactor, sample, and feed gas were heated from room temperature to 800° C in about 2 minutes and to 1200° C in about 4 minutes. At the end of the experiments, the reactor and sample were cooled to room temperature in about 10 seconds by spraying with cold water. The flowsheet of the entire apparatus is shown in Figure 2 and has been discussed in detail in the previously cited references.

Free-Fall Dilute Phase Reactor (FDP)

The agglomeration of bituminous coals in hydrogen is a major problem in designing a reactor for their continuous hydrogenation to produce a high-Btu gas. It has been shown that bituminous coals, both caking and noncaking, will agglomerate when rapidly heated in hydrogen at 500 psig and 500° C or at 6,000 psig and 500° to 800° C (10, 13, 14). Texas lignite agglomerated at 6,000 psig and 800° C but did not agglomerate at 500 psig and 500° C. Chars produced from carbonizing bituminous coals, cokes, graphite and anthracite, and a highly oxidized hvAb coal did not agglomerate. Feldmann (6) observed that at least 10 pct of the volatile matter in Pittsburgh seam hvAb coal, originally containing 36 pct volatile matter, had to be removed to obtain a char that would not agglomerate at 1,000 psig and 800° C in hydrogen in subsequent "hot-rod" reactor tests.

Lewis and Hiteshue (15) designed an entrained flow reactor for continuously hydrogenating both caking (hvAb) and noncaking (hvCb) coals. They believed that if the suspension of coal in the feed gas was dilute enough (dilute phase), particle-

particle collision and subsequent agglomeration could be avoided. The reactor was a 1/8-inch inside diameter, 60-foot long helical tube, and was operated at 600 psig and 800° C. The coal was entrained at a rate of 60 gms/hr in hydrogen where the hydrogen velocity was 2 fps. Experiments with the helical reactor were unsuccessful because of solids plugging at about the 500 to 550° C zone in the helical tube. Changing to a straight, horizontal tube reactor having an internal diameter of 5/16 inches and a length of 20 feet did not alleviate the plugging problem.

A 4-inch diameter vertical reactor where the coal particles would not contact the reactor wall during devolatilization was found to operate very successfully. It was further shown that reducing the diameter to less than 3 inches caused plugging, again due to coal particles contacting the reactor wall. Figure 3 shows the laboratory dilute-phase reactor that evolved from these studies.

A large amount of kinetic data has been reported for this reactor using Pittsburgh seam hvAb and Illinois #6 hvCb coals (5, 6, 16, 17). Details of the laboratory reactor and method of operation are discussed in the previous references.

The present FDP reactor is a 3.26-inch inside diameter pipe that is heated through the wall and contained in a 10-inch diameter pressure shell. Coal is injected into the top of the reactor through a 5/16-inch inside diameter, water-cooled nozzle using a rotary feeder and part of the feed gas. The coal free-falls through a 5-foot long reactor concurrently with the feed gas at a particle residence time of less than a second. Agglomeration is avoided because the rapid heating devolatilizes the particles before many particle collisions with the wall or other particles can occur. The char product is recovered from a cooled hopper after each experiment and is analyzed. Gas flows and compositions are measured over steady state periods of the experiment so that mass balances can be calculated.

Two-Stage Integrated Reactor

In order to react fresh dilute phase char with hydrogen as in the integrated reactor system described previously, and to measure reactivity and methane yield at carbon conversion levels expected in a commercial reactor, a two-stage laboratory hydrogasifier was built consisting of a dilute-phase reactor integrated with a second stage reactor that could be operated as either a moving-bed or fluid-bed reactor. Figure 4 illustrates the version using a fluid-bed second stage. Because the diameter of the coal particles increased substantially due to swelling and some agglomeration during devolatilization, a char crusher was used to reduce the particle size to a level acceptable for fluidization. In the moving-bed version, no crusher was used as shown in Figure 5.

The true composition of product gas from the individual stages could not be determined directly because a large amount of mixing occurred between gas near the bottom of the dilute phase reactor and gas near the top of the second stage reactor. The overall methane yield for the two-stage unit was determined in some cases, and these yields were compared to yields from previous dilute phase reactor experiments. The mixing problem was not unexpected since there was no gas seal leg used between the two reactors because of the small scale of the equipment. The mixing was caused from convection currents created from the falling char particles and the hot reactor walls. The operation of the two-stage hydrogasifier is described in much greater detail elsewhere (18).

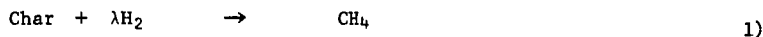
KINETIC MODEL

Within about the first few inches of free-fall in the FDP reactor, the coal particles are rapidly heated and devolatilized yielding a "popcorn" char (19). It is generally accepted that during the period of devolatilization, chemical bonds

such as methylene bridges, oxygen bonds, and side chains are easily broken resulting in evolution of hydrogen rich volatile matter and a large number of free radical structures (5, 20, 21, 22). These free radicals can react with hydrogen forming hydrocarbon gases and solid species that are active for further hydrogenation to volatile material or combine by polymerization to form a highly aromatic, unreactive char structure. During free-fall, but after rapid devolatilization has occurred (after about 6 inches), the solid carbon is very reactive in behavior as though not enough time has elapsed for significant polymerization to proceed (5). However, when the char is further reacted with hydrogen in a second-stage reactor such as a fluidized-bed or moving-bed, the hydrogasification rate is about two orders of magnitude slower (1, 18). Thus, the coal structure and reactivity change constantly during reaction.

Feldmann (5) has proposed that for kinetic modeling purposes the carbon in the raw coal can be divided into three types during hydrogasification. Type 1 carbon is the highly reactive species which is flashed off almost instantaneously during rapid heat-up and devolatilization, Type 2 is the solid carbon which readily hydrogasifies during most of the particle free-fall, and Type 3 is the low-reactivity carbon contained in the remaining, polymerized char structure. Johnson (23) has proposed a very similar model.

In developing a reaction rate expression for the hydrogasification of coal in the FDP reactor (5), the Type 1 carbon is assumed to devolatilize instantaneously and the remainder of hydrogasification occurs with Type 2 carbon. The reaction can be written as



for the data at high hydrogen partial pressures (P_{H_2} 50-60 atm) (5), and as,



for data at lower hydrogen partial pressures (6). An empirical correlation of λ , the stoichiometric coefficient, has been developed from the high pressure data and is

$$\lambda = \begin{cases} 1.0 & \text{for } x < 0.45 \\ 8x - 2.6 & \text{for } 0.45 \leq x \leq 0.55 \\ 1.8 & \text{for } x > 0.55 \end{cases} \quad 3)$$

where x is the total fractional carbon conversion.

The oil yield has been as high as 5% for Pittsburgh seam hvAb coal and 6% for Illinois #6 hvCb coal. A small amount of carbon oxides are produced (usually less than 4% of the product gas) and are in equilibrium according to the water-gas shift reaction as shown in Figure 6.

The hydrogasification of Type 2 carbon follows the rate equation

$$\frac{dx}{dt} = k P_{\text{H}_2} (\alpha - x) \quad 4)$$

where x is the fractional carbon conversion, P_{H_2} the hydrogen partial pressure, α the

fraction of the carbon which is available for reaction in the regime being considered and k the reaction rate constant. Another way of writing Equation 4 where the devolatilized carbon is not included in the fractional carbon conversion is

$$\frac{dZ}{dt} = k P_{H_2} (\beta - Z) \quad 5)$$

where $Z = (x-E)/(1-E)$ and $\beta = (\alpha-E)/(1-E)$. E corresponds to the fraction of carbon that was devolatilized. Assuming the coal particles being fed to the dilute phase reactor attain terminal velocity and the same temperature as the reactor wall almost immediately, Equation 4 may be applied to the FDP reactor as

$$U_T \frac{dx}{dL} = k P_{H_2} (\alpha - x) \quad 6)$$

where U_T is the particle terminal velocity. Equation 6 is integrated over the reactor length yielding

$$\int_E^x \frac{dx}{\alpha - x} = k P_{H_2} \frac{L}{U_T} \quad 7)$$

In the integration, P_{H_2} is assumed constant and equal to the hydrogen partial pressure in the product gas because extensive backmixing occurs due to the hot reactor walls and the downward flow of char. The fraction of Type 1 carbon is accounted for as E in the integration. Within the constraint that $0 < \alpha \leq 1$, the best fit of carbon conversion data from the FDP reactor is obtained when $\alpha = 1$ (2). This means that essentially all of the carbon is available for hydrogasification.

The hydrogasification of char in a "hot-rod", moving-bed, or fluid-bed reactor follows the same rate expression given by Equation 4, however, the reaction is much slower because most of the carbon that is reacting is of the Type 3 variety. Application of Equation 4 to fluid-bed and moving-bed reactors has been discussed elsewhere (18).

The rate expression does not take into account transitions between the various reactive types of carbon in the coal nor mass transfer resistance. In fact the hydrogasification of char is so complex because of the change in carbon structure during reaction, that the above simple classification of carbon may not apply in all cases. Johnson's model (23) takes into account the continuous deactivation of the char but also adds another constant into the model which must be evaluated using experimental data. Generally the more constants there are in a model, the better the model will fit regardless of the accuracy of the proposed reaction mechanism, and the more experimental data is needed to evaluate the constants. For this reason, Equation 4 was kept simple so that data from various reactors could be easily compared. With this perspective, the data from each of the reactor systems will now be discussed.

EXPERIMENTAL RESULTS

FDP Reactor

Using Equation 7 and a terminal velocity of 9 fps, Feldmann (5) determined E and k values for carbon conversion data at 900° C and 725° C. These values are listed in Table 1. In a later publication, Feldmann (2) reanalyzed the 725° C data as a function of hydrogen partial pressure and presented recent 850°-900° C (total

TABLE 1.- FDP Reactor kinetic data (5)

Reactor Wall Temp., °C	Total Reactor Press., atm	E, %	k $\text{atm}^{-1}\text{hr}^{-1}$
725	103,205	22	6
900	205	14	21

TABLE 2.- Ultimate and proximate analyses of feeds

Run Series	Coals				Chars	
	HR-1	HR-2	FDP	HR-1C	HR-2C	
Wt. %	Pgh hvAb	Pgh hvAb	Pgh hvAb	Ill. #6 hvCb	Pgh hvAb	Ill. #6 hvCb
C	74.2	74.1	78.1	74.4	78.8	83.9
H	5.1	5.1	5.3	5.2	1.9	2.8
N	1.5	1.5	1.6	1.7	1.6	---
S	1.9	1.5	1.1	1.3	1.1	---
O	8.8	7.6	8.2	11.5	1.9	---
Ash	8.5	10.2	5.7	5.9	14.7	10.2
	100	100	100	100	100	---
Moisture	1.9	1.4	1.2	1.4	0	0.9
VM	33.9	35.3	36.4	36.8	---	26.0
FC	56.5	53.1	56.7	55.9	---	---

TABLE 3.- FDP Reactor kinetic data

Reactor Wall, Temp., °C	Total Reactor Press., atm	E, %	k $\text{atm}^{-1}\text{hr}^{-1}$
725	103,205	23.1	5.3*
725	103,205	9.4	14.7
850-900	69-108	21.5	24.7*
850-900	69-108	12.2	33.0

*Total carbon conversion.

pressure 69-108 atm) data (6). The ultimate and proximate analyses of the feed coals are shown in Table 2 for the FDP and "hot-rod" reactors. Figures 7 and 8 show the carbon conversion data as total carbon conversion and as carbon conversion to equivalent methane (carbon in methane and ethane).

The difference between total carbon conversion and carbon conversion to methane is due mainly to the production of carbon oxides and oil. Some experimental error is also introduced in measuring the flowrate and composition of the feed and product gases, and in recovery and analysis of the solid and liquid products. Often the run times were not long enough to collect enough oil so the yield could be accurately measured (2). These errors become obvious when the carbon and ash recoveries are much lower than 100 pct. Figure 9 indicates that the hydrogen partial pressure as well as reactor temperature greatly influences the amount of oil produced, especially below a partial pressure of 30 atm. The increase in oil yield with decreasing hydrogen partial pressure agrees with the divergence of the two carbon conversion curves in Figures 7 and 8. Apparently the higher hydrogen partial pressures enhance the hydrocracking of the oil products. Residence time of the hydrocarbon vapors in the reactor also affects the oil yield causing lower amounts of oil at increasing residence time as shown in Figure 10. As indicated in Figure 5, the oil yield was determined by recovery from the gas sample and main tail gas streams. However, some of the oil was lost by condensation on the char receiver wall and to some extent on the char in the receiver. Therefore the oil yield data are now being reexamined where the yield in the gas sample stream is multiplied by the ratio of the total product gas flowrate to the sample gas flowrate in order to estimate total oil yield. These values will probably be higher than the reported values.

The values of the kinetic parameters in Equation 7 for the data in Figures 7 and 8 are listed in Table 3. These parameters were evaluated both for total conversion and for carbon conversion to equivalent methane. The value of $\alpha = 1$ gave the best fit of the total carbon conversion data and was subsequently used to fit the carbon conversion to methane data. The terminal velocity of a single char particle was calculated using the equation

$$U_T = \left[\frac{3.1g(\rho_s - \rho_g)\bar{d}_p}{\rho_g} \right]^{1/2} \quad 8)$$

for $500 < Re_p = \frac{\bar{d}_p U_T}{\nu_g} < 200,000$ (24), and correcting this value for the effect of the cloud of particles (25). Table 4 lists the parameters used for calculating the terminal velocities. A terminal velocity of 16.5 fps was used for the 850°-900° C data and 10.7 fps (average of 9.9 and 11.5) for the 725° C data.

The total reactor pressure has a large influence on the terminal particle velocity because the pressure determines for the most part the size of the char particles produced and hence the bulk and particle densities. This is illustrated in Figure 11 where the char bulk density is plotted versus total reactor pressure. As the pressure increases, the bulk density increases. The bulk density is higher when the feed gas contains about 50 pct methane instead of pure hydrogen. Apparently, increasing the reactor pressure dampens the explosive emission of gases during the rapid devolatilization reaction. A high concentration of hydrogen in the reactor causes more of the carbon to be reacted out of the particle structure resulting in a lower bulk density char (and lower particle density) than is obtained when the reactor feed gas contains about 50 pct methane. Some char particle size data is listed in Table 5 showing how increases in reactor temperature and pressure cause decreases in the mean char particle diameter.

TABLE 4.- Parameters used to calculate terminal velocity

Temperature, ° C	725	725	900	900
Pressure, atm	205	103	205	69
W, lb/hr ft ²	165	128	145	207
d _p , in.	0.0521	0.0667	0.0345	0.0660
ρ _b , lb/ft ³	13.33	8.0	12.29	5.8
ρ _s [*] , lb/ft ³	36.8	22.1	33.9	16.0
ρ _g , lb/ft ³	1.408	0.7074	1.199	0.4035
μ _g , lb/ft hr	0.05745	0.05745	0.06409	0.06409
U _{TS} , fps	3.3	4.1	2.8	4.6
Re _p	1264	1010	542	573
U _T /U _{TS} ^{**}	3.0	2.8	3.0	3.6
U _T , fps	9.9	11.5	8.4	16.5

* Estimated by the ratio of bulk densities and particle density of 16.0 lb/ft³ (26) for char produced at 850°-900° C and 69 atm, e.g., $\frac{13.33}{5.8} \times 16 = 36.8$.

**Ratio of terminal velocity to single particle terminal velocity at a specific mass feed rate per unit area (25).

TABLE 5.- Effect of reactor temperature and pressure on average char particle size

Press., atm/Temp., ° C	Average Char Particle Diameter*, in.			
	750	800	850	900
69	---	0.0735	0.0628	0.0537
83	---	---	0.0566	0.0501
103	0.0667	---	---	0.0485
205	0.0521	0.0492	0.0529	0.0345

$$\bar{d}_p = \left[\sum_i \frac{x_i}{d_{p_i}} \right]^{-1}, \text{ Pittsburgh seam hvAb coal, 50 x 100 mesh feed.}$$

The effect of feed rate per unit reactor cross section on the average char particle diameter is shown in Figure 12. As the feed rate is increased for a fixed reactor diameter, the number of particle collisions increase and hence the mean char particle size increases due to agglomeration. At a mass feed rate of 221 lb/hr ft², Pittsburgh seam coal yielded an average char particle diameter of 1.70 mm (0.0669 inches) compared to 0.487 mm (0.0192 inches) for char produced from Illinois #6 hvCb coal under identical reactor conditions. The maximum capacity in the dilute-phase section of the two-stage integrated reactor is limited by the size of the char produced in the dilute phase section that may be fluidized adequately in the second-stage fluid-bed section. Therefore, the dilute-phase reactor capacity will be much higher for Illinois coal than for Pittsburgh coal because of the smaller size char particles produced.

The feed rates per unit area in Figure 12 are probably low because the coal is not completely distributed across the dilute-phase reactor cross section before rapid heat-up and devolatilization, when the coal is susceptible to caking. As mentioned earlier, the coal is fed by a 5/16 inch diameter tube into a 3.26 inch diameter reactor. The particles hit the wall of the reactor about 12 inches down from the end of the feed nozzle. If devolatilization is completed within 6 inches from the end of the nozzle, a feed rate calculated to be 300 lbs/hr ft² of reactor cross section actually corresponds to a rate of 1000 lbs/hr ft² of cross-sectional area occupied by the particles. Data from a free-fall carbonizer (27), 12 inches in diameter, at the Morgantown Energy Research Center, show that Pittsburgh coal was processed at 1000 lbs/hr ft² and yielded char with a mean diameter of about 0.508 mm (0.02 inches). The feed coal was 70 pct through 200 mesh.

The reaction rate constants for the FDP reactor are shown on an Arrhenius plot in Figure 13. The relatively low activation energy of 15.1 kcal/mole of carbon reacted appears to indicate that the reaction may be controlled by mass transfer of hydrogen to the reaction sites and not by the rate of hydrogasification. Feldmann (2) has suggested that in the higher temperature range the rate may be better described as proportional to $k_g P_{H_2}$, where k_g is a mass transfer coefficient for hydrogen through the gas film surrounding the particle. This seems reasonable since a straight line could have just as easily fit the total carbon conversion data in Figures 7 and 8. The activation energy for carbon hydrogasification in an entrained flow reactor was determined by Zahradnik and Glenn (21) to be 15 kcal/mole, in agreement with the value obtained in this work. They suggest that this activation energy represents the difference in activation energy between the hydrogasification and polymerization reactions. An Arrhenius plot of Feldmann's (1) in which he calculates k by integrating Equation 7 from zero to x instead of from E to x , shows some low temperature FDP data. The activation energy is 29.8 kcal/mole for temperatures below 580° C, and decreases to 6.4 kcal/mole for temperatures above 580° C. The k values were calculated this way because E could not be determined from the available data and because P_{H_2} was approximately constant. This change in activation energy supports Feldmann's suggestion that the reaction is mass transfer controlled. More comments will be made on these results after reviewing some low-temperature "hot-rod" reactor data.

The data presented for the FDP reactor are based mainly on Pittsburgh seam hvAb coal. This coal was studied extensively because of its extreme swelling and agglomerating properties. If the reactor could process badly caking coal than surely it could easily handle mildly caking coals. Illinois #6 hvCb coal is mildly caking and FDP results on this coal are shown in Figure 14. The conversion of Illinois coal has not been studied over a wide range of hydrogen partial pressure as has the Pittsburgh coal, but does appear to be more reactive based on comparison of the two coals in Figure 14 at the same reactor conditions.

"Hot-Rod" Reactors

The results from the "hot-rod" reactor tests of Hiteshue, Friedman, and Madden (7) will be referred to as HR-1 series when coal is used as the starting reactant and HR-1C when char is used. Unpublished data of Feldmann and Williams will be referred to as HR-2 and HR-2C series. The weight loss and carbon conversion data are shown in Figures 15 and 16, respectively, for the HR-2 series experiments. In most of the HR-2 tests the reactor temperature was maintained low enough that Type 2 carbon conversion appeared to occur over a period of about 6 minutes. Once the temperature exceeded about 600° C, Type 3 carbon was rapidly formed. The conversions at which the curves in Figure 15 or 16 appear to level off correspond to the transition points at which the hydrogasification occurs predominately with Type 3 carbon. For the tests at 800° C, the devolatilization and Type 2 carbon conversion both occur in less than a minute. This is more clearly visible when the rate constants are plotted on the same Arrhenius graph with the FDP data in Figure 13. For the data up to 600° C, Equation 4 was integrated starting from zero carbon conversion, and the values of k and α were determined from a least-squares fit of the data (E was found to be very close to zero in the regression analysis for temperatures below 520° C). For the 800° C data, the integration was started from E with $\alpha = 1$, and again k and E were determined from a least-squares analysis of the data. The values of these parameters are listed in Table 6. The model was also fit to the total weight loss data in Figure 15. As is obvious in Figure 16, the carbon conversions calculated from the carbon analyses were not consistent at 425° C and 69 atm with either the total conversion data in Figure 15 or data at 35 atm. Therefore, the carbon gasification rate constant at 425° C was calculated by extrapolating the line obtained when k is plotted versus k_T (rate constant for total conversion). The k value at 425° C can also be estimated by assuming the curve must pass through 0.0588 (average of two data points) at 6 minutes. This method gives a k value of $0.255 \text{ atm}^{-1} \text{ hr}^{-1}$ compared to $0.383 \text{ atm}^{-1} \text{ hr}^{-1}$ by extrapolation.

In the Arrhenius plot of Figure 13, the low temperature "hot-rod" reactor data appears to be consistent with the dilute-phase reactor data. Unfortunately, low temperature FDP data is very difficult to obtain in order to verify the low temperature "hot-rod" reactor data because of agglomeration and plugging. The high temperature "hot-rod" reactor data cannot verify the FDP data because the heat-up rate and residence times are such that they operate in different carbon conversion regimes. The key difference between the FDP reactor and the "hot-rod" reactor is the coal heat-up rate. In the FDP reactor this rate is on the order of 1000° C/sec whereas in the "hot-rod" reactor the rate is about 7° C/sec. By achieving reaction temperature quickly enough, the kinetics of Type 2 carbon hydrogasification can be observed.

The carbon conversion data for the HR-1 series experiments are shown in Figure 17. In these tests the devolatilization and Type 2 carbon conversion occurred in less than a minute because of the high temperatures. Therefore the curves for the most part represent Type 3 carbon conversion. Johnson (23) has observed in thermobalance experiments that devolatilization and Type 2 carbon conversion are essentially complete within 2 minutes at temperatures above about 800° C. The heat-up rate in the thermobalance tests was about the same as in the "hot-rod" reactor tests. The HR-1 series data were fit using Equation 4 with $\alpha = 1$ and integration starting from E . The kinetic parameters are listed in Table 7. Choosing $\alpha = 1$ simply means that essentially all the carbon beyond the fraction E is Type 3. Here E represents the sum of Types 1 and 2 carbon.

Figure 18 illustrates the effect of the reactor temperature on the amount of carbon that can be hydrogasified as Types 1 and 2. High temperatures and hydrogen

TABLE 6.- Kinetic parameters for HR-2 series data

Temp., ° C	P _{H₂} , atm	α	E	k atm ⁻¹ hr ⁻¹	α_T^{**}	k _T ^{**} atm ⁻¹ hr ⁻¹
425	69	.071*	0	0.383*	.099	0.510
470	69	.189	0	0.447	.261	0.594
490	69	.199	0	0.625	.278	0.838
520	69	.179	0	1.47	.264	2.07
600	69	.232	0	0.976	.272	1.08
600	69	1.0	.175	0.00751	---	---
800	69	.315	0	1.22	.344	1.66
800	69	1.0	.243	0.0123	---	---

* Extrapolated using total conversion k_T values. By another method, the k value is 0.255 atm⁻¹hr⁻¹.

** Subscript T indicates total conversion parameters (total weight loss).

TABLE 7.- Kinetic parameters for HR-1 series data

Temp., ° C	P _{H₂} , atm	α	E	k atm ⁻¹ hr ⁻¹
800	18.0	1.0	.252	0.0282
800	35.0	1.0	.355	0.0154
800	69.0	1.0	.450	0.0169
1200	4.4	1.0	.298	0.363
1200	18.0	1.0	.377	0.137
1200	35.0	1.0	.514	0.350

TABLE 8.- Effect of hydrogen partial pressure on carbon conversion in the hot rod reactor

Test	Temp., ° C	P _{H₂} , atm	Carbon Conversion, pct		
			1 min.	2 min.	5-6 min.
HR-1	800	18	---	---	30.7, 25.7
HR-1	800	35	---	---	39.4, 40.4
HR-1	800	69	---	---	52.0, 55.5, 52.6, 54.6
HR-2	500	35	9.10	12.1	---
HR-2	490	69	10.4	14.5	---
HR-2	600	35	17.6	18.4	---
HR-2	600	69	17.5	17.9	---
HR-2	700	35	---	21.0	---
HR-2	800	35	23.7	24.3	31.2
HR-2	800	69	25.6	25.8	33.9

partial pressures result in a large amount of carbon being hydrogasified in the Types 1 and 2 regime. In fact Moseley and Paterson (22) have shown that at a hydrogen partial pressure of 500 atm and 900° C, the carbon is rapidly gasified to completion.

There is a large difference in the level of Types 1 and 2 carbon conversion between the HR-1 data at 800° C and the corresponding HR-2 tests. This discrepancy is shown in Table 8 and is especially noticeable at 800° C and 69 atm. Under these conditions the conversions from the HR-1 tests range from 52 to 54.6 pct at a residence time of 5 minutes whereas the corresponding conversions for the HR-2 tests ranged from 31.2 to 33.9 pct at a residence time of 6 minutes. The lack of response of conversion to changes in hydrogen partial pressure in the HR-2 tests suggests that the reaction rate was strongly mass transfer controlled. This can be verified by comparing the gas velocities in the HR-1 and HR-2 experiments in Table 9. In the HR-1 tests the superficial hydrogen feed gas velocity was 36 cm/sec compared to a velocity of 1 to 2 cm/sec in the HR-2 tests. Apparently the gas velocity was low enough in the HR-2 tests that at the higher temperatures the mass transfer resistance through the particle gas film was significant. In addition, the slower particle heat-up rate may have contributed to the difference in conversions. Anthony (28) has demonstrated, however, that varying the heating rate from 180 to 10,000° C/sec has no effect on the coal conversion. He found smaller particle sizes and more highly dispersed samples to be extremely important because the flux of volatiles emerging from the coal particle may limit the counter diffusion of hydrogen into the particle. This restriction makes it difficult for the hydrogasification reaction to compete with polymerization reactions that produce a relatively inactive char.

In Table 10 the Types 1 and 2 carbon conversion for FDP and "hot-rod" reactor tests are compared. The HR-2 tests were definitely mass transfer controlled whereas it is difficult to conclude this in the FDP tests compared to the HR-1 tests because of the large difference in residence time. In the FDP reactor the residence time was less than 1 second and in the "hot-rod" reactor it was two orders of magnitude greater. Anthony (28) has shown that Types 1 and 2 carbon conversions are complete after about 3 seconds at 69 atm, 900° C, and a heating rate of 750° C/sec. His starting coal particle size was 70 microns compared to about 220 microns in the FDP experiments. Therefore Types 1 and 2 carbon conversion in the FDP tests probably did not reach completion.

Photographs of some of the chars under a scanning electron microscope reveal the porous structure produced in the FDP and "hot-rod" reactors under various conditions. Figure 19 compares chars produced in the FDP reactor at 725° C, 205 atm (top-left), and at 850° C, 69 atm (bottom-left). The char produced at 69 atm appears to be much more porous and less dense than the char made at 205 atm. As discussed previously, this effect shows up as a large difference in bulk density.

Figure 20 compares chars produced in the "hot-rod" reactor at 600° C, 69 atm (bottom) and at 800° C, 69 atm (top) at different residence times. The low temperature char has much larger pores while the high temperature char has a larger number of very small pores. This difference in the pore size is probably related to the higher emission rate of volatile matter from the particles reacted at 800° C. In addition, the superficial hydrogen velocity in the 600° C test was 0.9 cm/sec versus 1.1 cm/sec in the 800° C test. Both these conditions (high volatiles emission, low gas velocity) limit counterdiffusion of hydrogen into the char structure resulting in less competition for the polymerization reaction. Comparison of the FDP and "hot-rod" char samples indicates that the pore structure of the FDP char is more highly developed with pores having thin walls. The samples in Figure 20 were crushed to 100 pct thru 60 mesh so that the gross pore structure is not as clear as possible.

TABLE 9.- Effect of hydrogen velocity on carbon conversion
in the hot rod reactor at 800° C

<u>Series</u>	<u>Sample</u>	<u>P_{H₂}, atm</u>	<u>H₂ velocity cm/sec</u>	<u>Average Carbon Conv., %</u>	<u>Residence Time, min.</u>
HR-1	Pgh. hvAb Coal	35	36.6	39.9	5
HR-2	Pgh. hvAb Coal	35	2.19	31.2	6
HR-1	Pgh. hvAb Coal	69	36.6	53.7	5
HR-2	Pgh. hvAb Coal	69	1.11	33.9	6
HR-1C	Pgh. hvAb Char	69	36.6	31.4	15
HR-2C	Ill. #6 hvCb Char	69	1.11	31.2	15

TABLE 10.- Comparison of types 1 and 2 carbon conversion
in the FDP and "Hot-Rod" Reactors

<u>Tests</u>	<u>P_{H₂}, atm</u>	<u>Carbon Conv., %</u>
FDP*	35.0	27.2
FDP*	69.0	32.2
HR-1**	35.0	33.2, 32.8
HR-1**	69.0	38.5, 40.3
HR-2**	35.0	23.7
HR-2**	69.0	25.6

*From Figure 8, 850°-900° C.

**800° C.

TABLE 11.- Kinetic parameters for HR-1C series data

<u>Temp., ° C</u>	<u>P_{H₂}, atm</u>	<u>α</u>	<u>E</u>	<u>k atm⁻¹hr⁻¹</u>
800	18.0	1.0	.009	.0234
800	35.0	1.0	.027	.0178
800	69.0	1.0	.144	.0110
800	69.0	1.0	.136	.0137*

*HR-2C data.

Figure 21 shows the char samples from FDP tests at 850° C and 69 atm using a lignite coal feed. The pore structure appears very undeveloped compared to the structure obtained with bituminous coal. Because of the lack of particle swelling with lignite (coal particle also in Figure 21), the penetration of hydrogen into the particle is poorer compared to bituminous coal. Consequently, particle size should have an even stronger influence on the hydrogasification of lignite than with bituminous coals.

The char data in Table 9 are very interesting because the superficial hydrogen velocity had no effect on the carbon conversion. The mass transfer rate into the char particles must be large compared to the char-hydrogen reaction rate. This is not surprising since the reaction rate of Type 3 carbon is very slow, probably much slower than the diffusion rates of hydrogen and gaseous reaction products.

The results of HR-1C series experiments with char produced from Pittsburgh seam hvAb coal are shown in Figure 22. The carbon conversion is of the Type 3 species except for a small amount of rapid initial conversion. The kinetic parameters for these data are listed in Table 11. The results of the HR-2C series experiments are also shown in Table 11 and Figure 22, and agree well with the HR-1C data. The two chars are different in that the HR-2C char was produced from Illinois #6 hvCb coal in the dilute phase reactor at 585° C whereas the HR-1C char was produced from Pittsburgh seam hvAb coal by batch carbonization for 2 hours in helium at 600° C. The HR-2C char contained about 26 pct volatile matter compared to the original 36.5 pct volatile matter in the starting coal. Despite these differences, except for the nearly equal devolatilization temperatures, the reactivities of the two chars are essentially the same. A significant difference in the devolatilization temperatures could have resulted in the chars having differing reactivities (23, 29).

The Arrhenius graph in Figure 13 summarizes the results for all the coals and chars tested and includes some of Johnson's data (23) which was adjusted to calculate k values according to Equation 4. Assuming that it is valid to represent the low temperature "hot-rod" reactor data by the same Arrhenius line as the FDP data, the activation energy for hydrogasification of Type 2 carbon is 15.1 kcal/mole of carbon gasified. The hydrogasification rate of Type 3 carbon is about three orders of magnitude lower than the rate of hydrogasification of Type 2 carbon. The activation energy for the HR-1, HR-1C, and HR-2C data is 24.7 kcal/mole of carbon gasified (Type 3 carbon) compared to a value of 47.1 kcal/mole obtained by Johnson (23) using a thermo-balance. At 600° and 800° C, the HR-2 data was complicated by the transition to Type 3 carbon conversion and a significant amount of mass transfer resistance. At these higher temperatures the apparent activation energy falls off considerably as shown in Figure 13.

Two-Stage Integrated Reactor

The results of the two-stage tests where the first-stage was a FDP reactor and the second-stage either a moving-bed or fluid-bed reactor have been presented elsewhere (18). The kinetic results are summarized in Tables 12, 13, and 14 and are also plotted in Figure 13. Because heat transfer limitations within the char particles caused the true particle temperature to be higher than the measured temperature, the activation energy of the moving bed data is low, and the rate constant values are relatively high at the lower reactor temperatures.

Correlation of Char Yield and Coal H, N, S, and O Conversion Data

In order to predict the conversion of other constituents in the coal during hydrogasification besides carbon conversion, results from ninety-five experiments

TABLE 12.- Kinetic results from two-stage integrated reactor
experiments (18) at 69 atm

<u>Run</u>	<u>Total C</u> <u>Conv., X</u>	<u>Moving</u> <u>Bed C</u> <u>Conv., Z*</u>	<u>Fluid</u> <u>Bed C</u> <u>Conv., Z*</u>	<u>Bed</u> <u>Temp., °K</u>	<u>k</u> <u>atm⁻¹hr⁻¹</u>
2	0.552	---	0.378	1158	0.0145
3	0.536	---	0.356	1158	0.0284
5	0.558	---	0.345	1158	0.0316
11	0.608	---	0.419	1073	0.0450
12	0.551	---	0.335	1118	0.0202
13	0.556	---	0.383	1113	0.0218
14	0.537	---	0.357	1183	0.0139
33	0.620	0.457	---	1178	0.0573
37	0.392	0.131	---	1173	0.0360
38	0.485	0.264	---	1148	0.0396
39	0.417	0.167	---	918	0.0449
43b	0.430	0.186	---	1038	0.0395
44b	0.391	0.130	---	923	0.0260
45b	0.406	0.151	---	933	0.0307
46a	0.399	0.151	---	957	0.0305
48	0.511	0.301	---	1073	0.0299
49	0.536	0.337	---	988	0.0358

TABLE 13.- Hydrogasification of Illinois #6 hvCb coal in a two-stage reactor at 1000 psig - run conditions

Test	46		48		49	
Reactor Zone	FDP*	MB*	FDP	MB	FDP	MB
Temp., ° C	850	684	850	800	850	715
Coal or Char Rate, lb(dry)/hr	10.51	6.68	10.26	5.08	10.32	5.01
Bed Height, in.	---	0	---	36	---	36
Residence Time, min.	---	0	---	10.4	---	10.4
Feed Gas, SCFH	164.4	141.4	181.7	152.0	166.2	150.7
Vol. Pct. H ₂	56.2	99.4	52.0	99.0	50.9	98.6
CH ₄	37.2	---	42.1	---	42.8	---
N ₂	1.05	0.50	1.10	1.00	1.50	1.30
He	5.45	---	4.70	---	4.70	---
Product Gas, SCFH**	168.6	141.4	179.0	124.6	169.8	130.3
Vol. Pct. H ₂	34.8	99.4	32.4	54.2	30.1	58.0
CH ₄	55.1	---	57.2	43.5	58.0	39.0
Run Time, min.	187		193		187	

* FDP: free-fall dilute phase reactor (3 foot heated length); MB: moving-bed reactor.

**For runs 48 and 49, the individual product gas flowrates and the composition of the MB product gas prior to mixing were estimated using the helium tracer data.

TABLE 14.- Hydrogasification of Illinois #6 hvCb coal in a two-stage reactor at 1000 psig - results

Test HY	46	48	49
Conversion, wt. pct.			
MAF Coal	43.1	60.2	60.4
C	33.0	50.7	53.6
H	75.4	96.4	93.4
S	66.7	74.8	76.3
N	59.4	89.7	86.4
O	91.0	99.6	90.0
Gas Yields, SCF/lb dry coal			
CH ₄	3.01	7.80	7.58
C ₂ H ₆	0.11	0.17	0.13
CO	0.43	0.69	0.80
CO ₂	0.10	0.09	0.11
H ₂	-3.21	-11.63	-10.31
H ₂ S*	0.04	0.03	0.07
Oil Yield, lb/lb dry coal	0.048	0.041	0.026
Carbon to Gas and Oils, wt. pct.	24.3	47.7	44.2
Mean Char Particle Diameter, mm	0.433	---	0.397

* About 50% of the converted sulfur appears in the gas product after water scrubbing.

in the FDP reactor and FDP-Fluid Bed integrated reactors were correlated with carbon conversion to yield Figures 23-26. The correlations in Figures 23-25 show that char yield and removal of coal hydrogen and nitrogen can be accurately calculated from carbon conversion, independent of reactor conditions and possibly geometry. For carbon conversions above 20 pct (essentially devolatilization) the oxygen removal usually exceeds 90 pct and can be considered to be complete. The data for sulfur removal are very scattered, possibly because of the error in determining changes in small amounts of sulfur in the coal and char samples. In addition, the hydrogen sulfide that is formed may be in equilibrium with sulfur in the char such that a simple correlation with carbon conversion is not possible.

In Figure 27, the char yields have been recomputed in terms of MAF conversion so that the relationship between carbon conversion and MAF conversion can be shown. A curve is drawn through the data such that it bows away from the unit slope line and passes through (0,0) and (100,100). The data in Figures 23-25 only covered the carbon conversion range 22-55 pct so that for simplicity a straight line was used to fit the data. As the range is widened, however, it becomes obvious that a curve gives a better correlation of the data.

The carbon conversion range covered by the HR-1 and HR-2 series experiments is complete, ranging from 0 to 95 pct. In Figure 28, the MAF conversion is plotted versus carbon conversion and essentially the same curve as used in Figure 27 fits these results. Based on these curves it appears that the correlations of coal constituent conversions with carbon conversion are not only independent of reactor conditions, but also reactor geometry. Figure 29 shows a similar MAF-carbon conversion plot for the HR-1C and HR-2C series char tests. The carbon conversion in Figure 29 does not include the carbon that was lost during devolatilization of the coal to prepare the char.

The conversion of coal H, N, and S in the HR-1 and HR-2 series experiments are shown in Figures 30-32. In Figures 30 and 31, the straight line fits of the H and N data determined previously are shown to be inadequate over a very wide range of carbon conversion. These sets of data are both fit best with curves that are concave downward, similar to the MAF curves. Despite the scatter in the data, the correlation with carbon conversion still appears to be valid. Unlike in the FDP and Two-Stage reactor experiments, ultimate analyses were not run on the coal feed for each test, but only on the entire batch of coal. Consequently, some segregation in the feeds could have occurred causing scatter in the calculation of the H, N, and sulfur conversions. These constituents are present in relatively small amounts and thus their calculated conversions are very sensitive to fluctuations in the feed composition. The sulfur data in Figure 32 shows a more definite trend with carbon conversion than was evident in Figure 26 and shows the latter correlation to be conservative. Work is planned to extend the linear correlations in Figures 23-26 to a regression curve that will fit all of the data, i.e., FDP, HR-1, HR-2, and the Two-Stage reactors. These relationships are very valuable in scale-up design calculations because the displacement of the volatile elements in the coal and the char yield can be accurately predicted for the plant flowsheet.

NOMENCLATURE

- α fraction of the carbon that is available for reaction in the regime being considered.
- α_T fractional weight loss that can be achieved in the reaction regime being considered.
- β same as α except the Type 1 carbon is excluded.
- λ stoichiometric coefficient for the char-hydrogen reaction.
- μ_g gas viscosity, lb/ft hr.
- ρ_b char bulk density, lb/ft³.
- ρ_g gas density, lb/ft³.
- ρ_s char particle density, lb/ft³.
- \bar{d}_p mean char particle diameter, in.
- E fraction of carbon instantaneously devolatilized.
- g gravitational acceleration, ft/sec².
- k char-hydrogen reaction rate constant, atm⁻¹ hr⁻¹.
- k_T weight loss reaction rate constant, atm⁻¹ hr⁻¹.
- L reactor length, ft.
- P_{H_2} partial pressure of hydrogen, atm.
- Re_p char particle Reynolds number.
- t time, sec.
- U_T free-fall velocity of char particles, fps.
- U_{TS} single char particle terminal velocity, fps.
- W coal mass feed rate, lb/hr ft².
- x fractional carbon conversion based on total coal carbon.
- z fractional carbon conversion based on starting char carbon.

References

1. Feldmann, H. F., C. Y. Wen, W. H. Simons, and P. M. Yavorsky. Supplemental Pipeline Gas From Coal by the HYDRANE Process. Presented at the 71st National AIChE Meeting, Dallas, Texas, Feb. 20-23, 1972.
2. Feldmann, H. F. and P. M. Yavorsky. The HYDRANE Process. Presented at the 5th AGA/OCR Synthetic Pipeline Gas Symposium, Chicago, Illinois, Oct. 29-31, 1973.
3. Wen, C. Y., C. T. Li, S. H. Tscheng, and W. S. O'Brien. Comparison of Alternate Coal Gasification Processes for Pipeline Gas Production. Presented at the 65th Annual AIChE Meeting, New York, New York, Nov. 26-30, 1972.
4. Wen, C. Y., coworkers. Optimization of Coal Gasification Processes, Research and Development Rept. No. 66, Interim Rept. Nos. 1 and 2, O.C.R., U.S. Dept. of the Interior, Wash., D. C.
5. Feldmann, H. F., W. H. Simons, J. A. Mima, and R. W. Hiteshue. Reaction Model for Bituminous Coal Hydrogasification in a Dilute Phase. Preprints of Fuel Division, ACS, v. 14, No. 4, Part II, Sept. 1970, pp. 1-13.
6. Feldmann, H. F., J. A. Mima, and P. M. Yavorsky. Pressurized Hydrogasification of Raw Coal in a Dilute-Phase Reactor. Fuel Gasification, Advances in Chem. Series 131, ACS, Washington, D. C., 1974, pp. 108-125.
7. Hiteshue, R. W., S. Friedman, and R. Madden. Hydrogasification of High-Volatile A Bituminous Coal. U.S. Bureau of Mines Report of Investigation 6376, 1964.
8. Hiteshue, R. W., R. B. Anderson, and M. D. Schlesinger. Hydrogenating Coal at 800° C. Ind. & Eng. Chem., 49 (Dec., 1957), pp. 2008-10.
9. Hiteshue, R. W., P. S. Lewis, and S. Friedman. Gaseous Hydrocarbons from Coal. Paper presented at the A.G.A. Operating Section Conference, 1960 (CEP-60-9).
10. Hiteshue, R. W., S. Friedman, and R. Madden. Hydrogenation of Coal to Gaseous Hydrocarbons. U.S. Bureau of Mines Report of Investigation 6027, 1962.
11. Friedman, S., R. W. Hiteshue, and M. D. Schlesinger. Hydrogenation of New Mexico Coal at Short Residence Time and High Temperature. U.S. Bureau of Mines Report of Investigation 6470, 1964.
12. Hiteshue, R. W., R. B. Anderson, and S. Friedman. Gaseous Hydrocarbons by Hydrogenation of Coals and Chars. Ind. & Eng. Chem., 52 (July, 1960), pp. 577-9.
13. Hiteshue, R. W., S. Friedman, and R. Madden. Hydrogasification of Bituminous Coals, Anthracite, and Char. U.S. Bureau of Mines Report of Investigation 6125, 1962.
14. Kawa, W., R. W. Hiteshue, W. A. Budd, S. Friedman, and R. B. Anderson. Agglomeration Studies in the Low-Pressure Hydrogenation of Coal in a Fluidized Bed. U.S. Bureau of Mines Bulletin 579, 1959.
15. Lewis, P. S. and R. W. Hiteshue. Hydrogenating Coal in the Entrained State. Ind. & Eng. Chem., 52 (Nov., 1960), pp. 919-20.
16. Lewis, P. S., S. Friedman, R. W. Hiteshue. High Btu Gas by the Direct Conversion of Coal. Fuel Gasification Advances in Chem. Series 69, ACS, Washington, D. C., 1967, pp. 50-63.

17. Hiteshue, R. W. The Hydrogasification of Raw Coal. Paper presented at the Amer. Gas Assoc. Symposium on Synthetic Pipeline Gas, Pittsburgh, Pa., Nov. 15, 1966.
18. Wen, C. Y., S. Mori, J. A. Gray, and P. M. Yavorsky. Application of the Bubble-Assemblage Model to the HYDRANE Process Fluid-Bed Hydrogasifier. Paper presented at the 67th Annual AIChE Meeting, Wash., D. C., Dec. 1-5, 1974.
19. Feldmann, H. F., W. H. Simons, C. Y. Wen, and P. M. Yavorsky. Simulation of a Reactor System for the Conversion of Coal to Methane by the HYDRANE Process. Paper presented at the 4th International Congress of Chem. Eng., Marianske Lazne, Czechoslovakia, Sept. 11-15, 1972.
20. Given, P. H. The Distribution of Hydrogen in Coals and Its Relation to Coal Structure. *Fuel*, 39 (1960), pp. 147-153.
21. Zahradnik, R. L. and R. A. Glenn. The Direct Methanation of Coal. *Fuel* 50, No. 1, (1971), pp. 77-90.
22. Moseley, F. and D. Paterson. The Rapid High-Temperature Hydrogenation of Coal-Chars Part 2: Hydrogen Pressures up to 1,000 Atmospheres. *J. Inst. of Fuel*, 38 (Sept., 1965), pp. 378-391.
23. Johnson, J. L. Kinetics of Bituminous Coal Char Gasification with Gases Containing Steam and Hydrogen. *Fuel Gasification, Advances in Chem. Series 131*, ACS, Wash., D. C., 1974, pp. 145-178.
24. Kunii, D. and O. Levenspiel. *Fluidization Engineering*. John Wiley & Sons, Inc., New York, 1969, p. 76.
25. Wen, C. Y. and J. Huebler. Kinetic Study of Coal Char Hydrogasification, Rapid Initial Reaction. *Ind. & Eng. Chem. Design & Develop.*, 4 (April, 1965), pp. 142-147.
26. Feldmann, H. F., K. D. Kiang, and P. M. Yavorsky. Fluidization Properties of Coal Char. *Preprints of Fuel Division, ACS*, v. 15, No. 3, Sept. 1971, pp. 62-76.
27. Quarterly Technical Progress Report, Morgantown Energy Research Center, Morgantown, West Virginia, September-December, 1969, p. 2.
28. Anthony, D. B. Rapid Devolatilization and Hydrogasification of Pulverized Coal. Sc.D. Thesis, Dept. of Chem. Eng., M.I.T., Cambridge, Mass., Jan., 1974.
29. Blackwood, J. D., B. D. Cullis, and D. J. McCarthy. Reactivity in the System Carbon-Hydrogen-Methane. *Aust. J. Chem.* 20 (1967), pp. 1561-70.

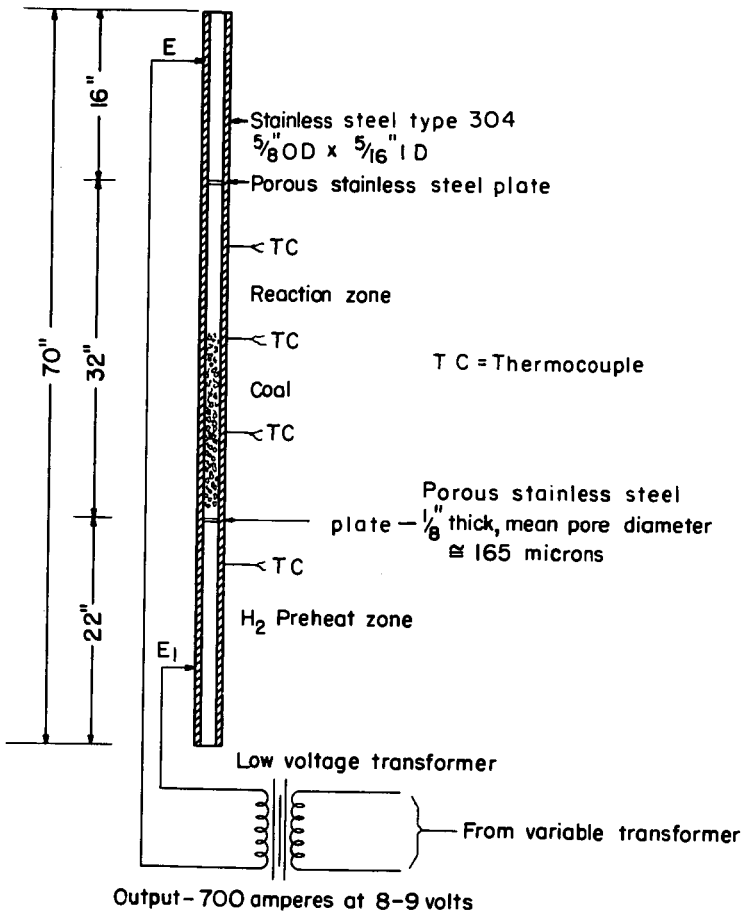


Figure 1 - "Hot-rod" reactor.

L-4753
12-12-56

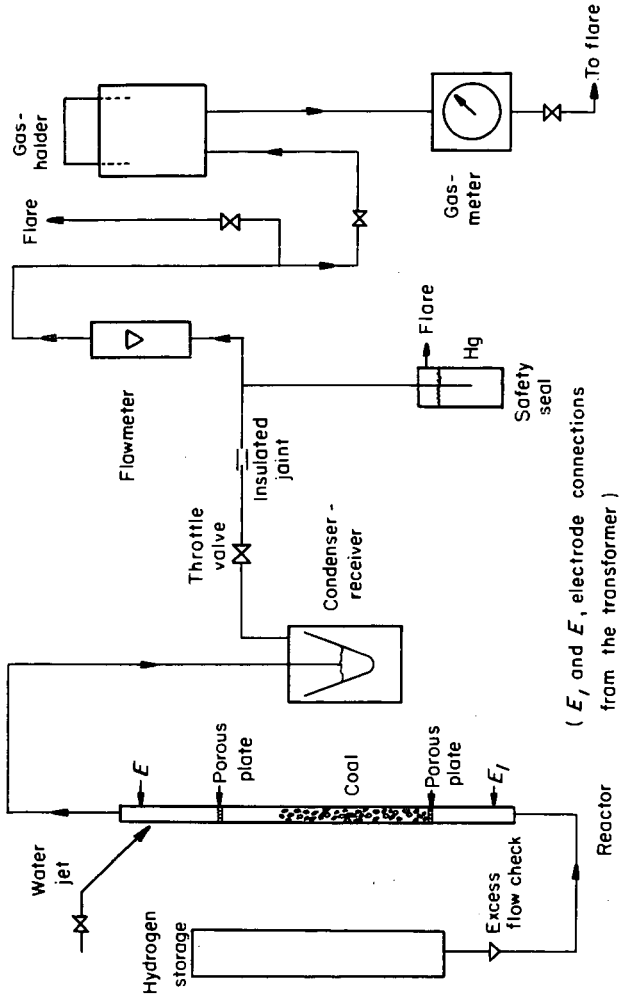


Figure 2 - Flow sheet of "hot rod" apparatus .

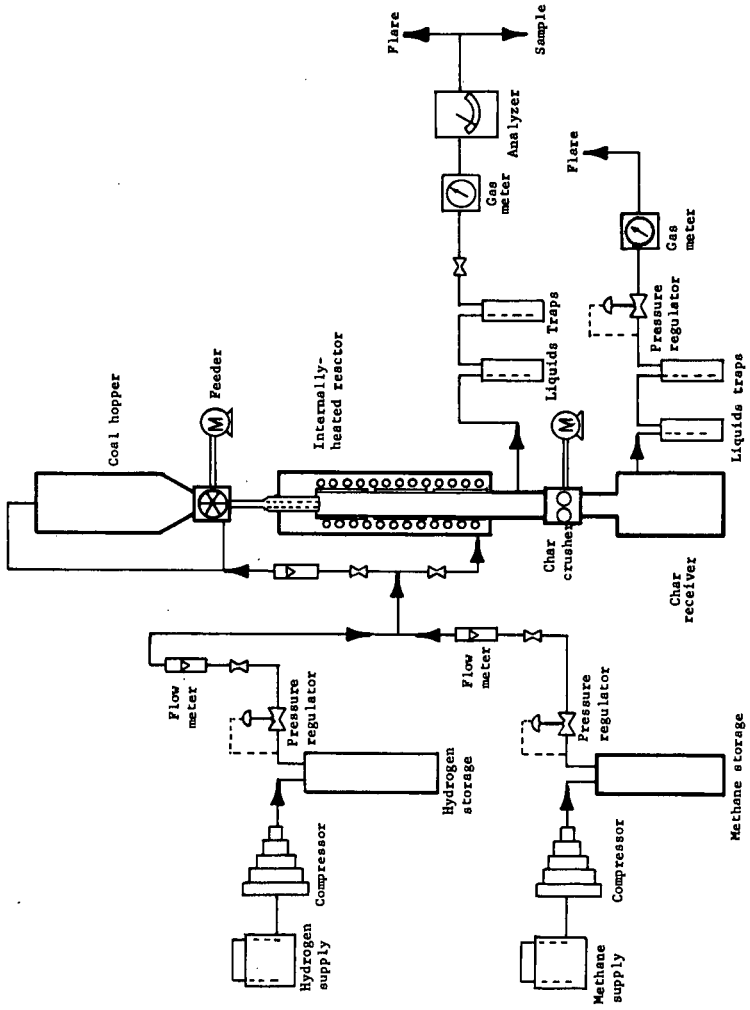


FIGURE 3.- Simplified Flowsheet: Hydrogasification of Coal in Dilute Phase. L-12449

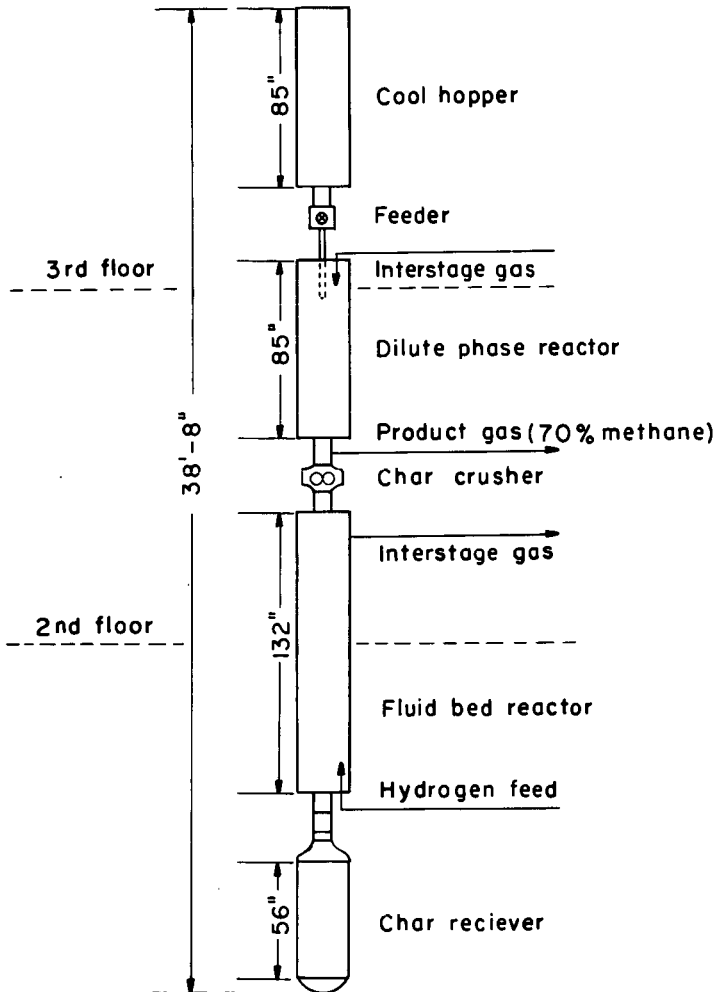


Figure 4 - Integrated hydrogasification unit.

L- 12914

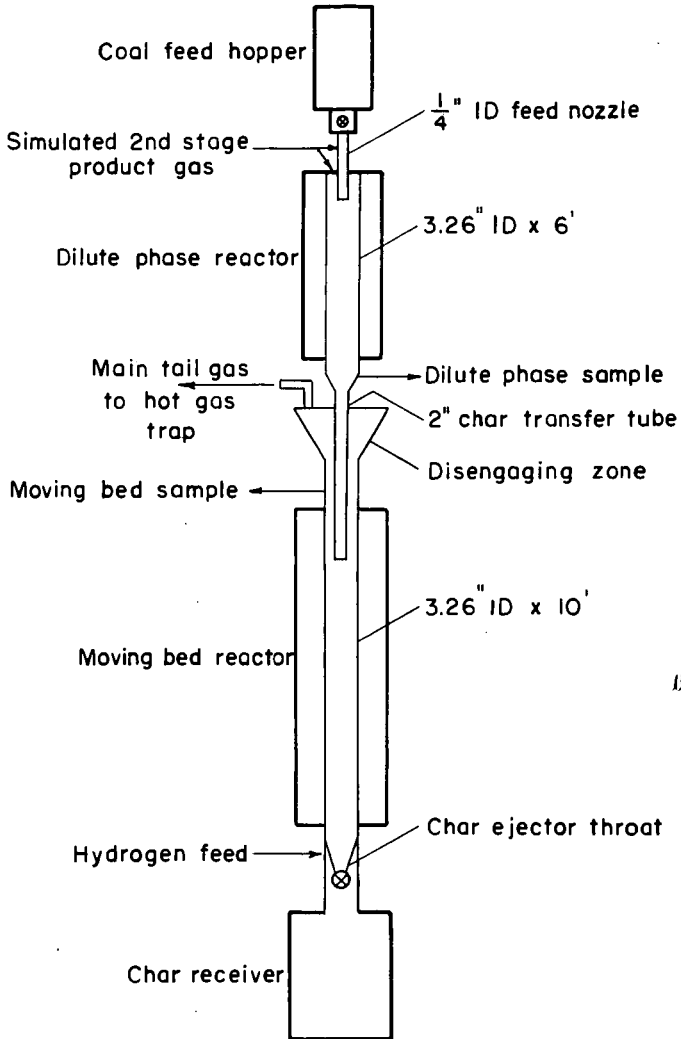


Figure 5 — Integrated two-stage hydrogasifier

L-13753

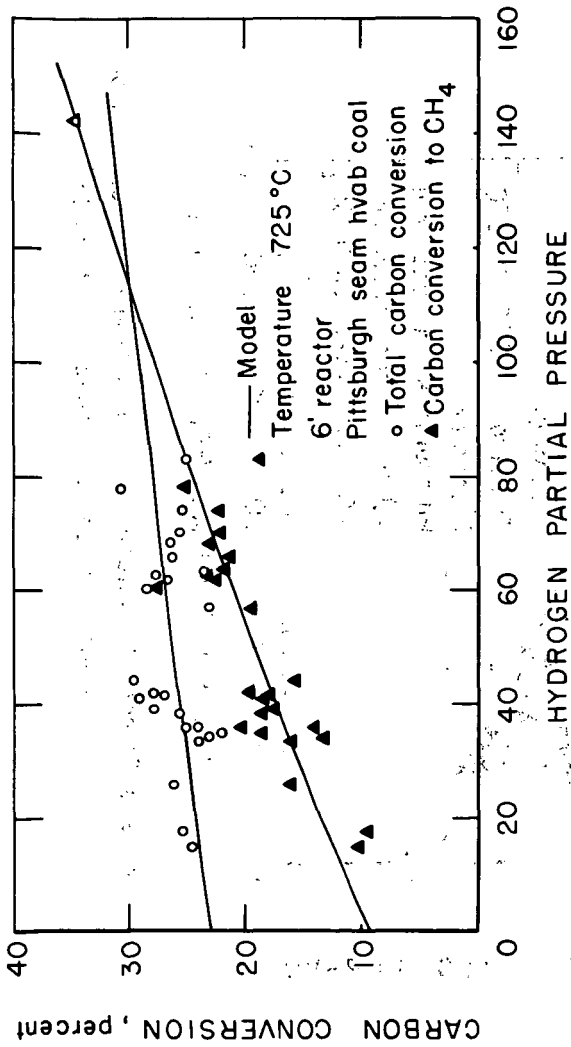


Figure 7 - Effect of hydrogen partial pressure on total carbon conversion and carbon conversion to methane.

5-15-75 L-14296

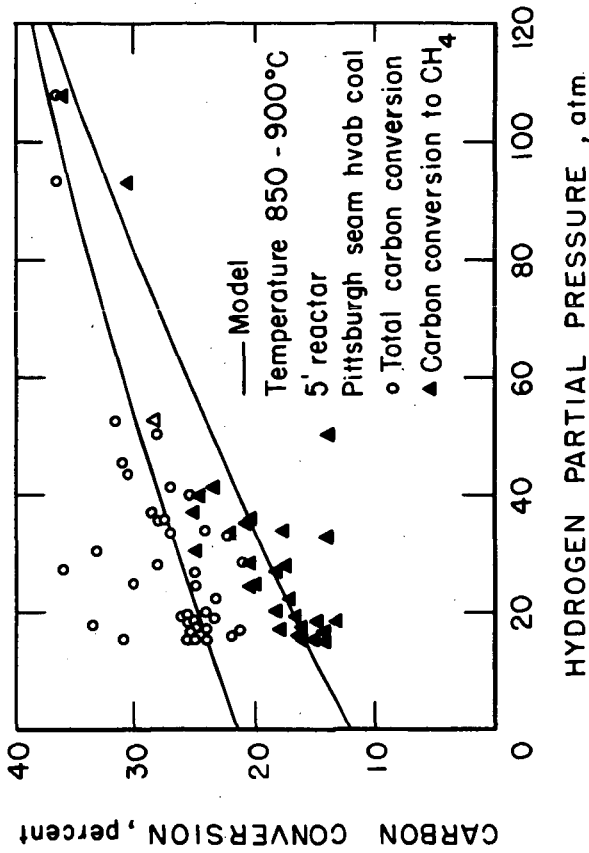


Figure 8-Effect of hydrogen partial pressure on total carbon conversion and carbon conversion to methane.

5-16-75

L-14295

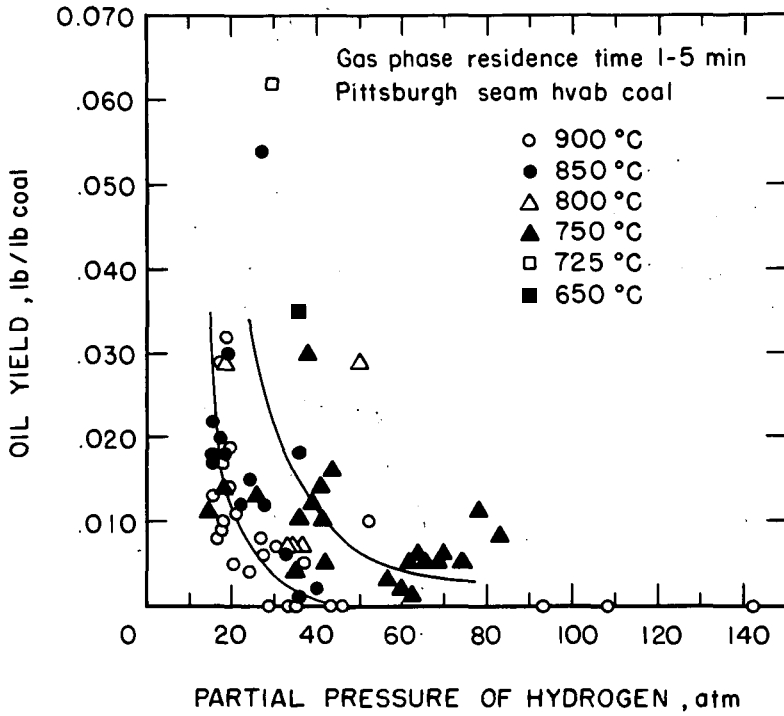


Figure 9 - Effect of hydrogen partial pressure on oil yield.

5-20-75

L-14294

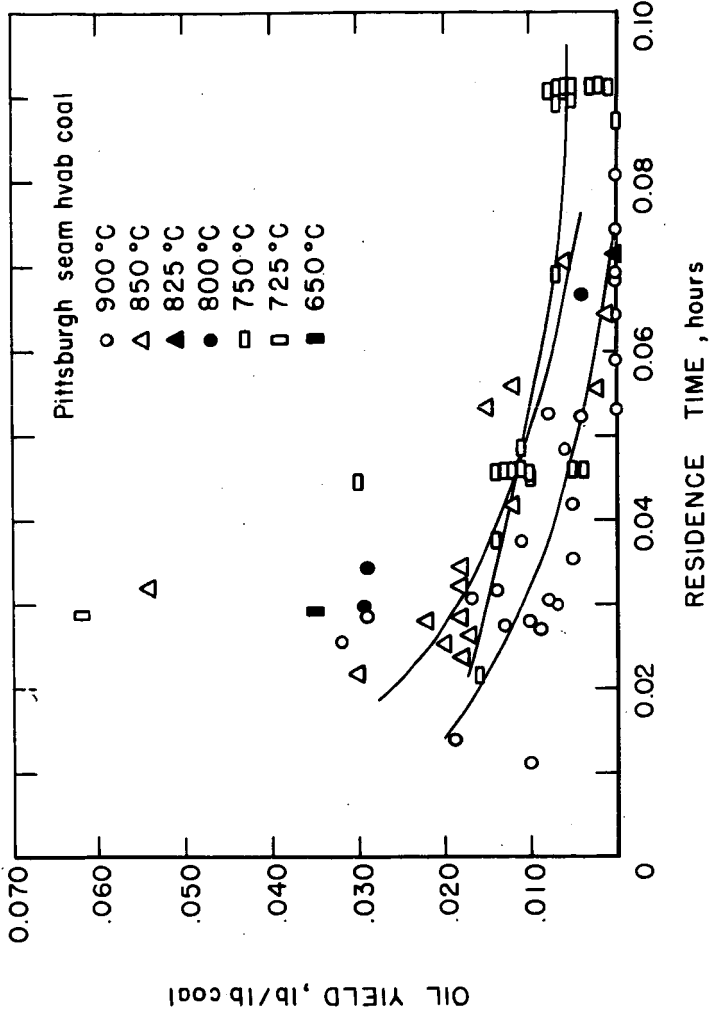


Figure 10-Effect of gas phase residence time on oil yield.

5-21-75

L-14297

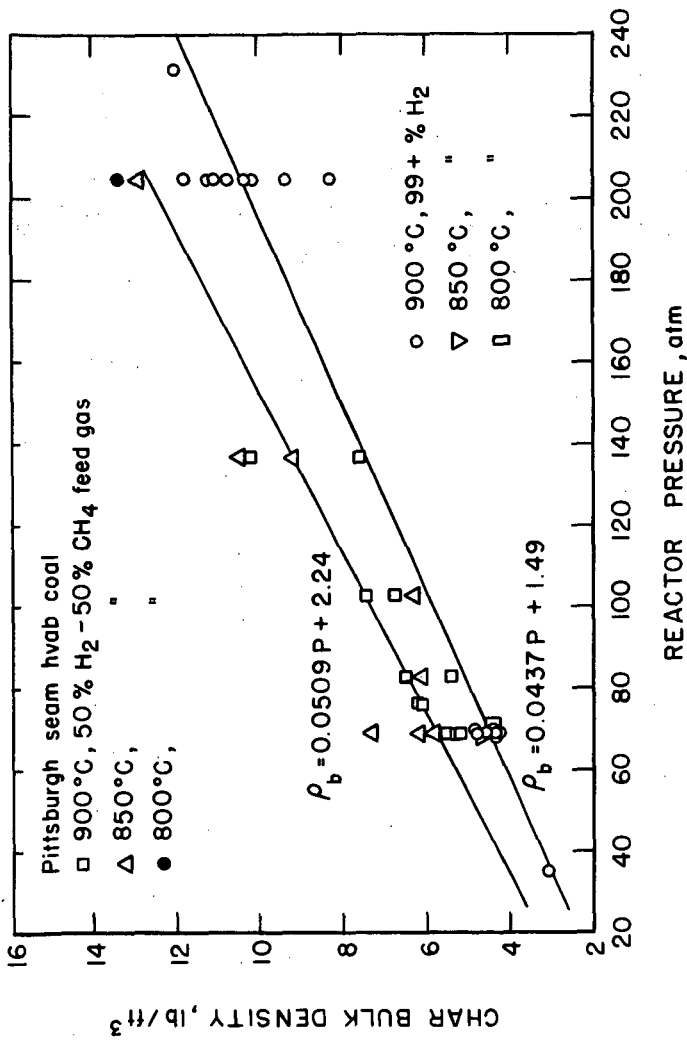


Figure 11 - Effect of total reactor pressure on char bulk density.

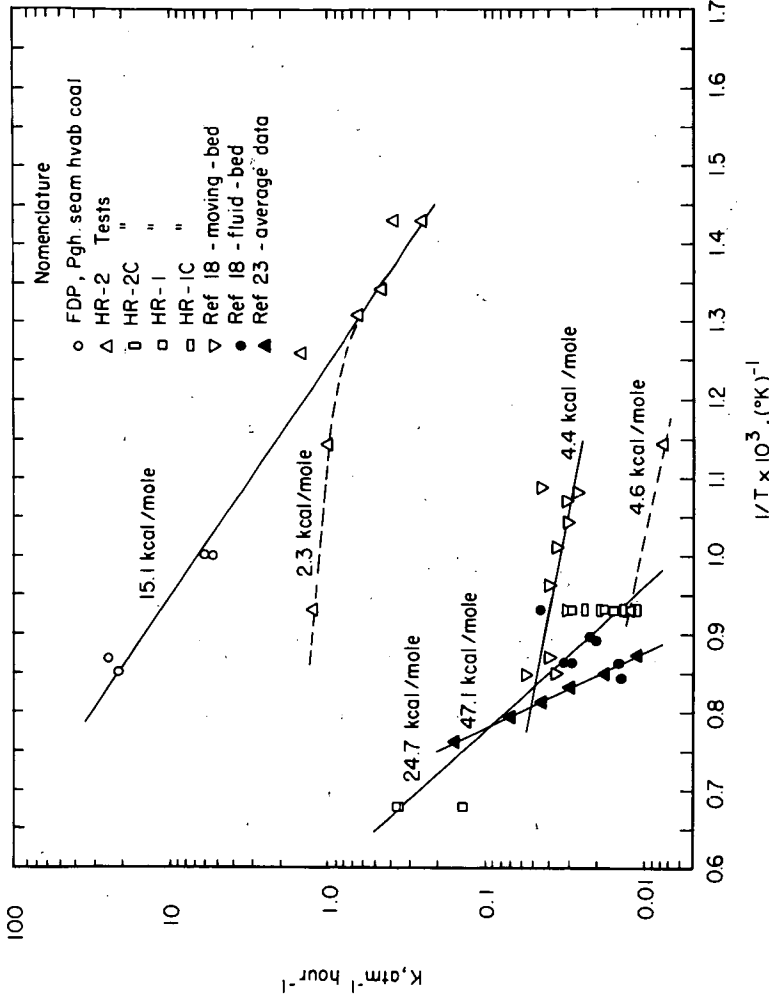


Figure 13 - Temperature dependence of the hydrogasification reactor rate constants for coal and char.

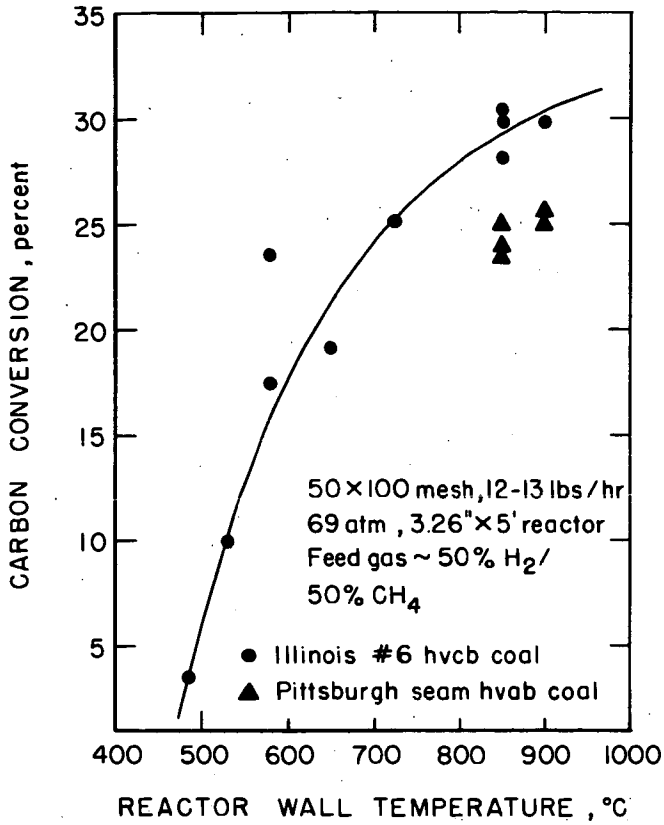


Figure 14 - Carbon conversion in the FDP reactor for Illinois #6 hvcb coal.

5-16-75

L-14292

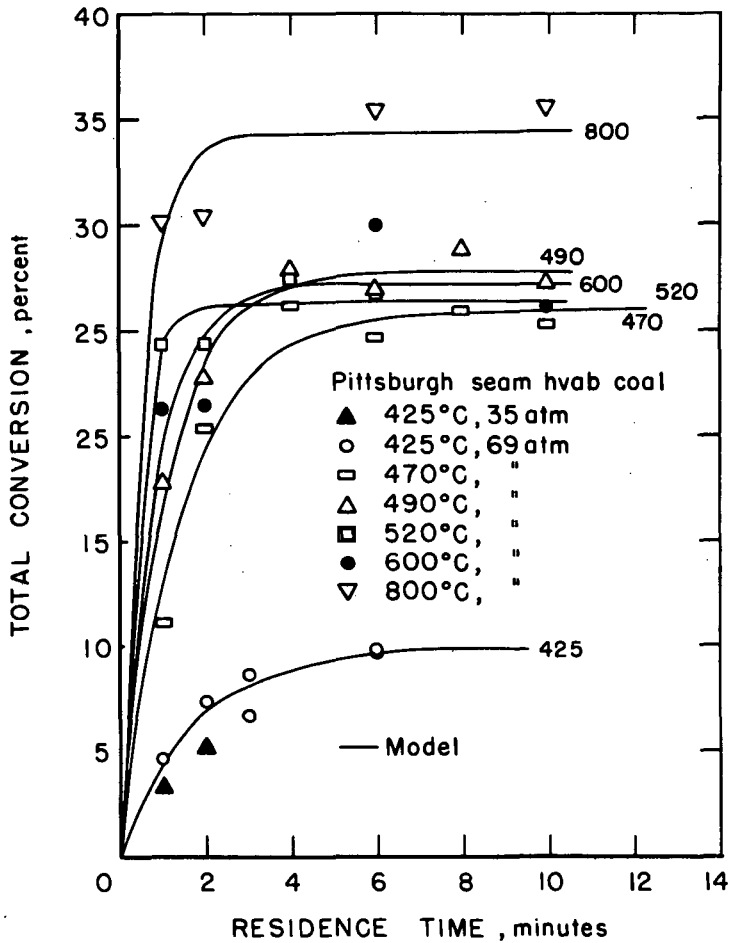


Figure 15 - Effect of temperature and time on total conversion in "hot rod" reactor, HR-2 tests.

5-22-75 L-14300

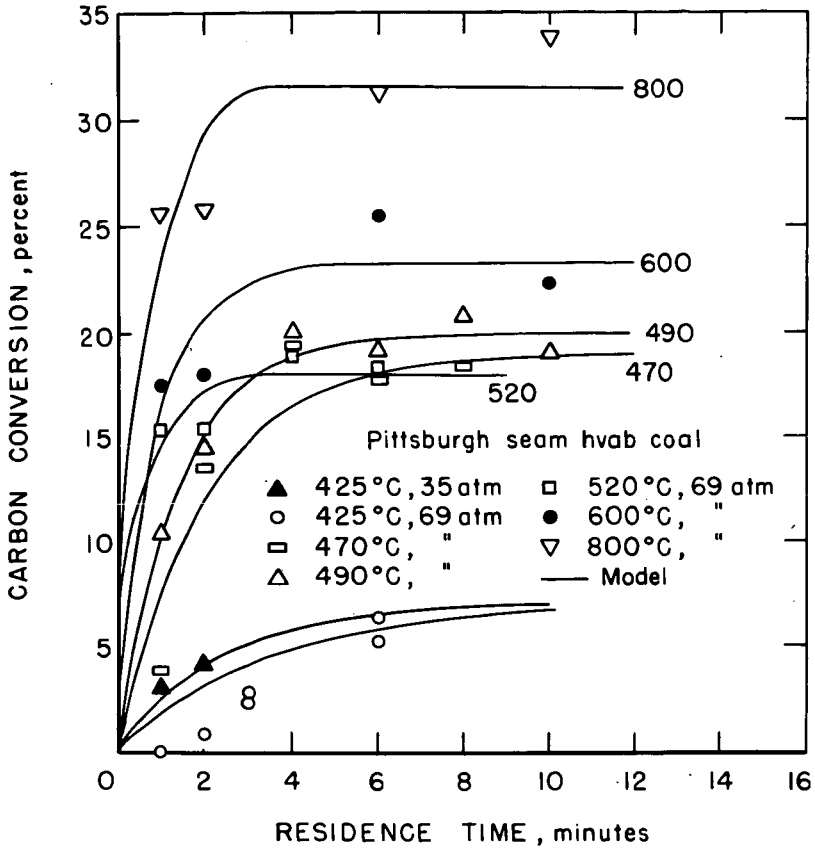


Figure 16- Effect of temperature and time on carbon conversion in "hot rod" reactor, HR-2 tests.

5-27-75 L-14301

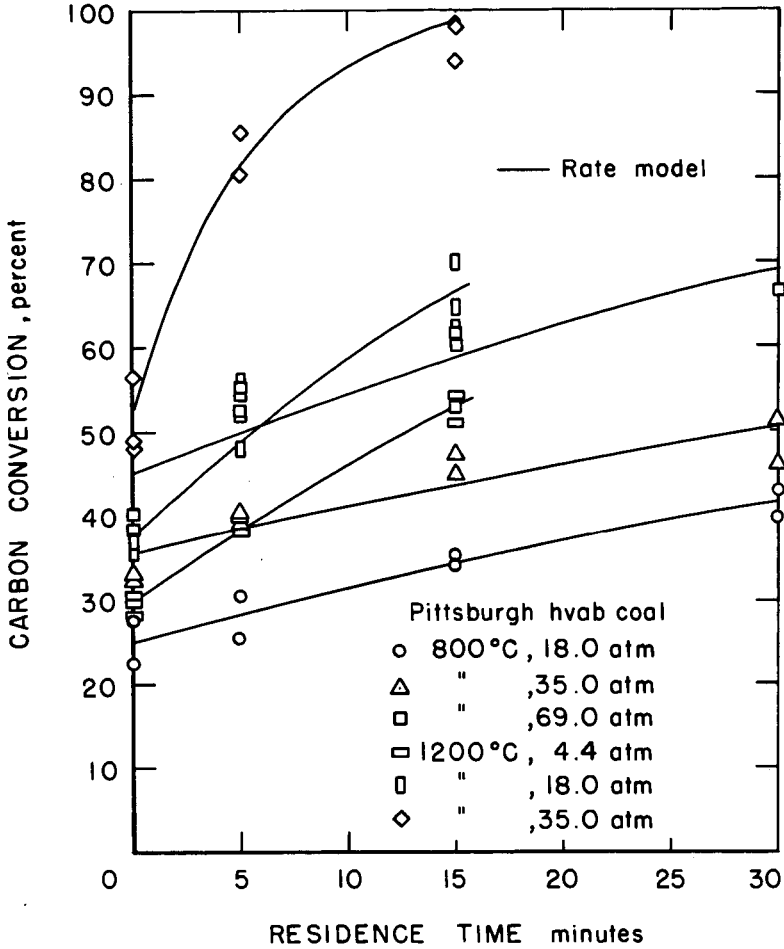


Figure 17- Carbon conversion data for the HR-1 series experiment .

5-21-75 L-14299

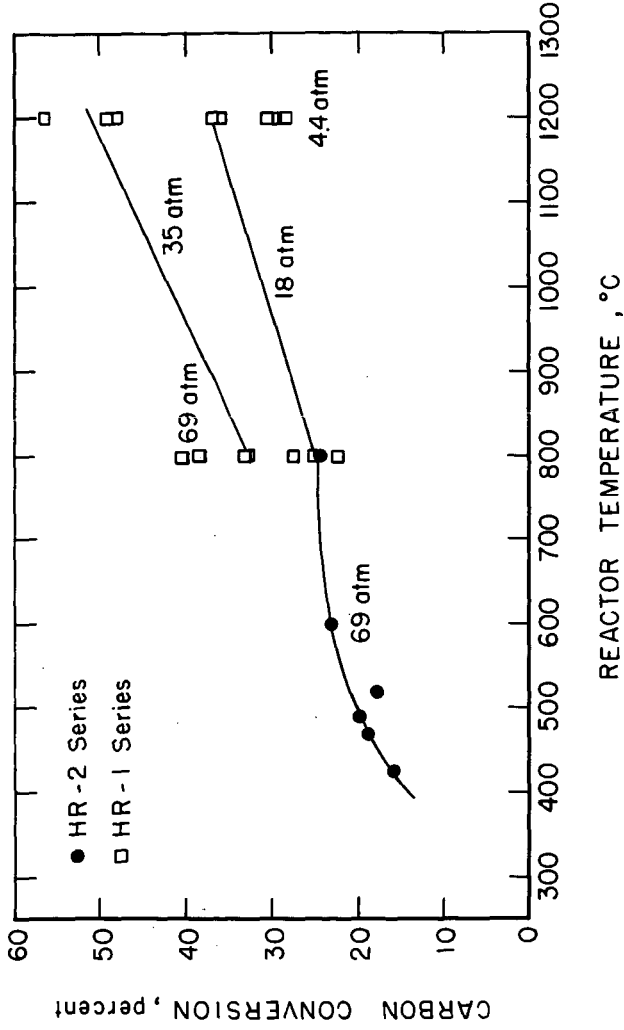


Figure 18-Effect of reactor temperature on types 1 & 2 carbon conversion.

5-15-75 L-14289

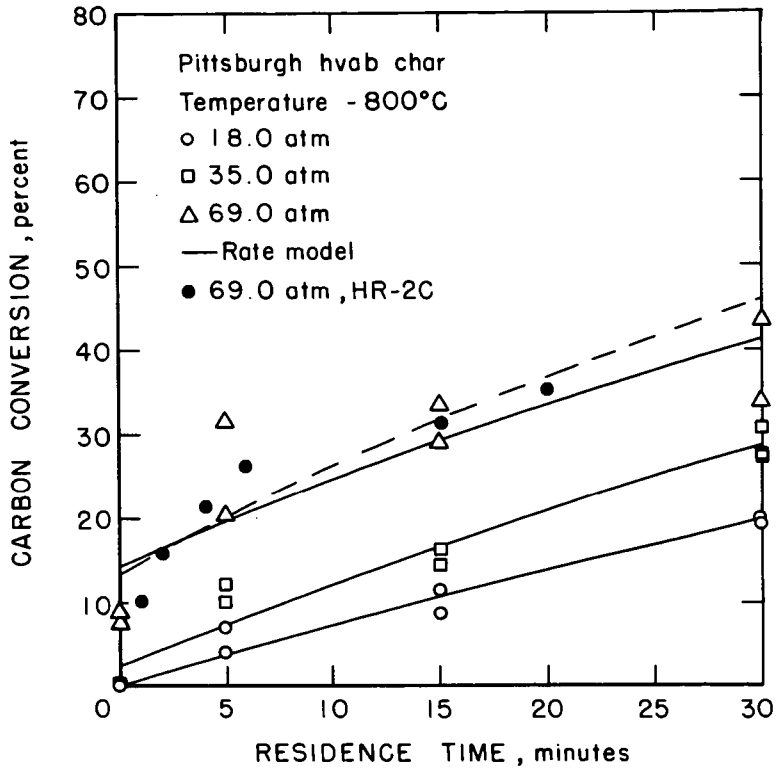


Figure 22- Carbon conversion data for the HR-1C series experiments.

5-15-75

L-14290

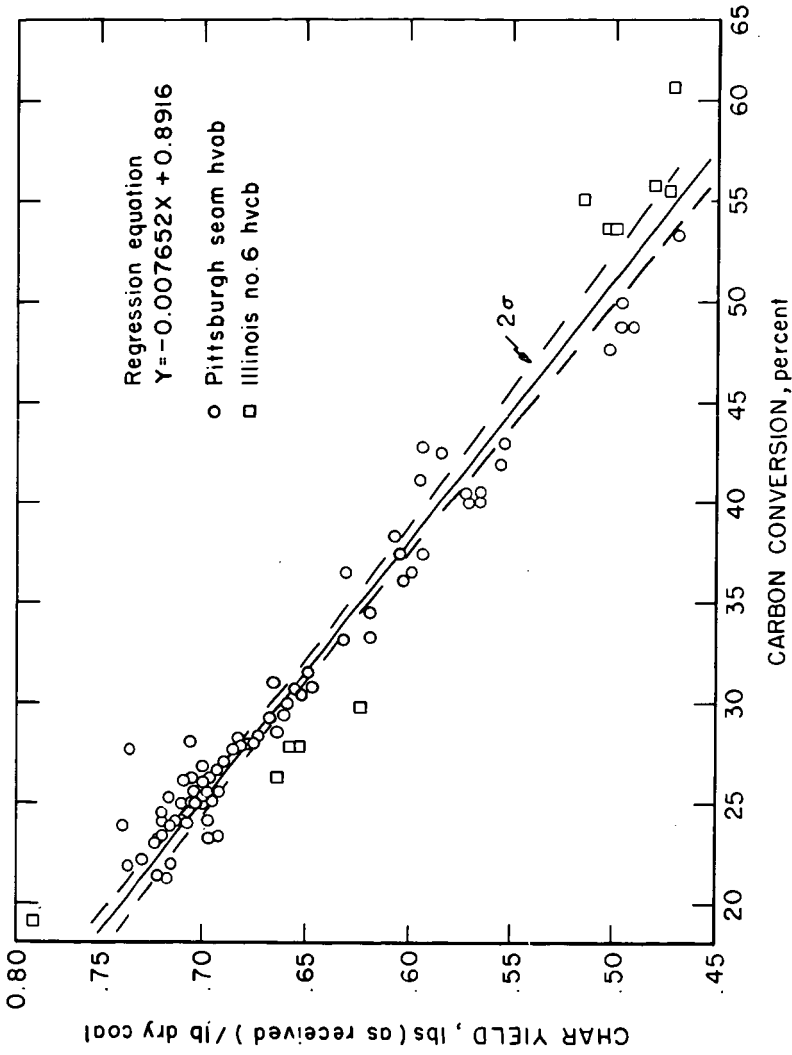


FIGURE 23 - Char yield as a function of carbon conversion during hydrogossification.

L-13708

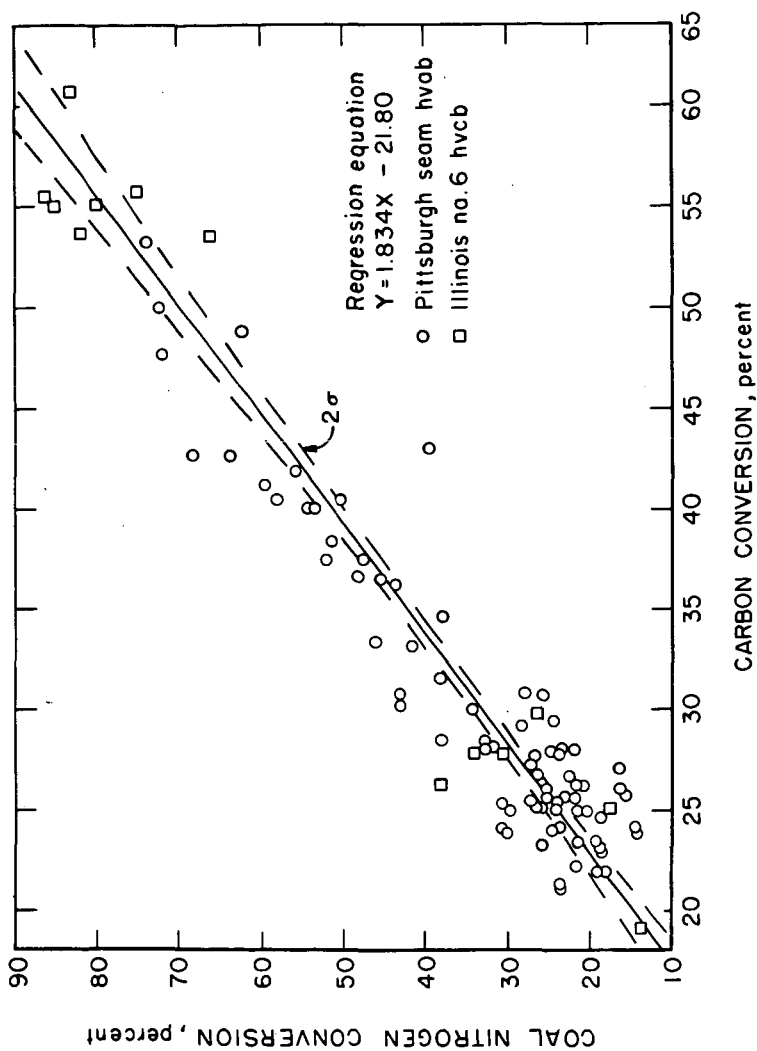


FIGURE 25-Cool nitrogen conversion as a function of carbon conversion during hydrogasification.

L-13712

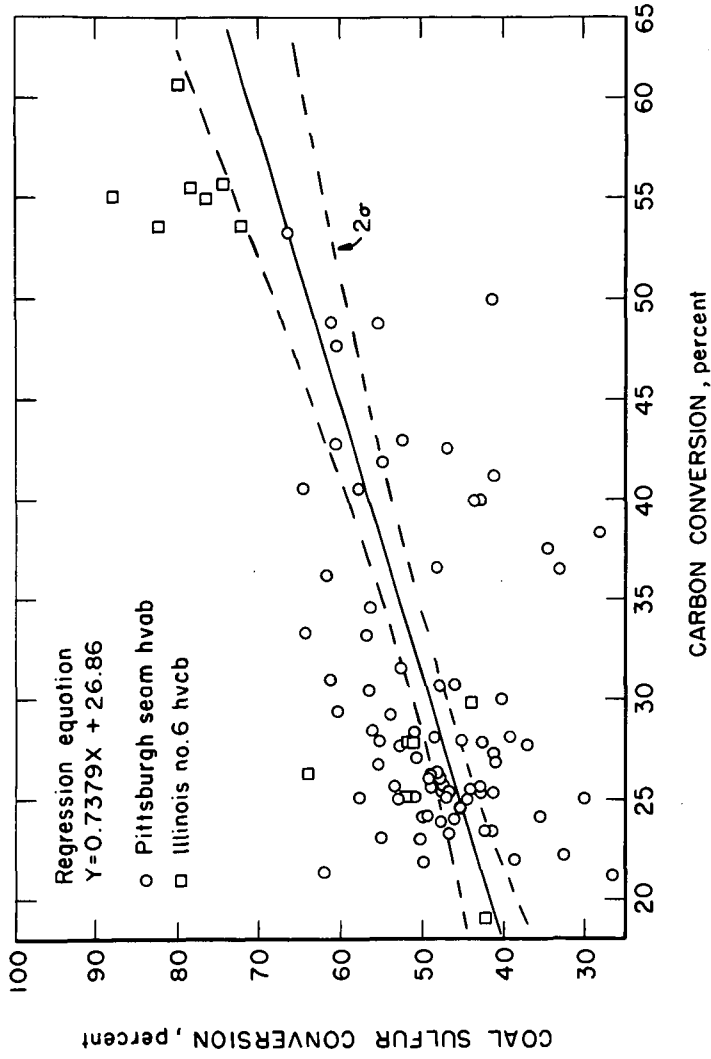


FIGURE 26-Sulfur conversion as a function of carbon conversion during hydrogossification.

L-13710

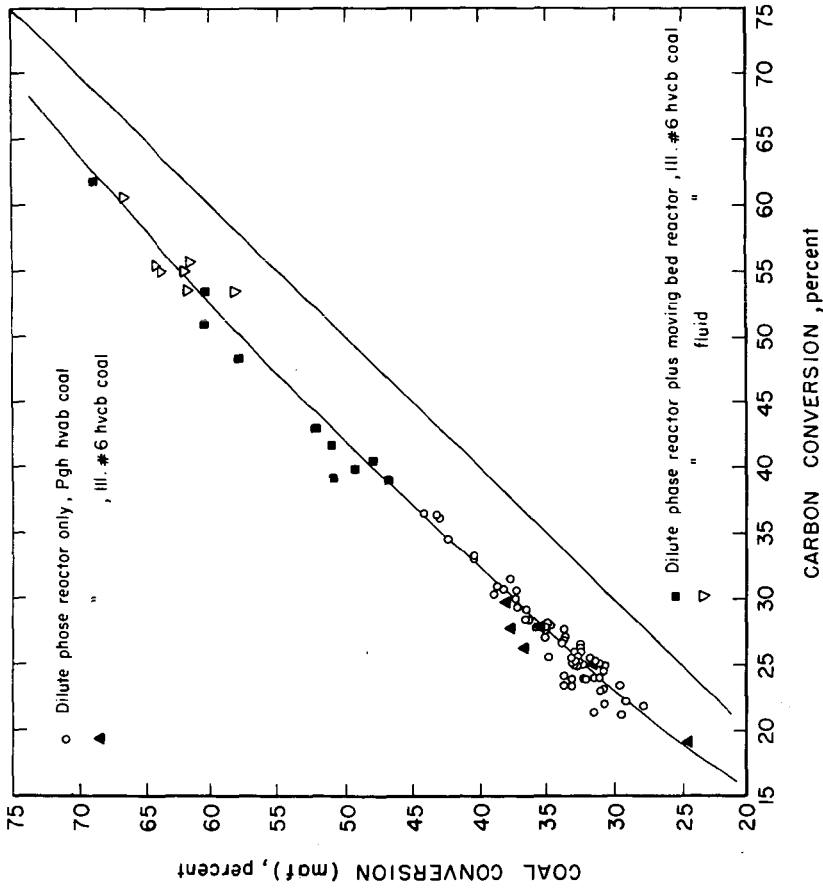


Figure 27-Coal conversion (maf) as a function of carbon conversion during hydrogasification.

5-23-75 L-14305

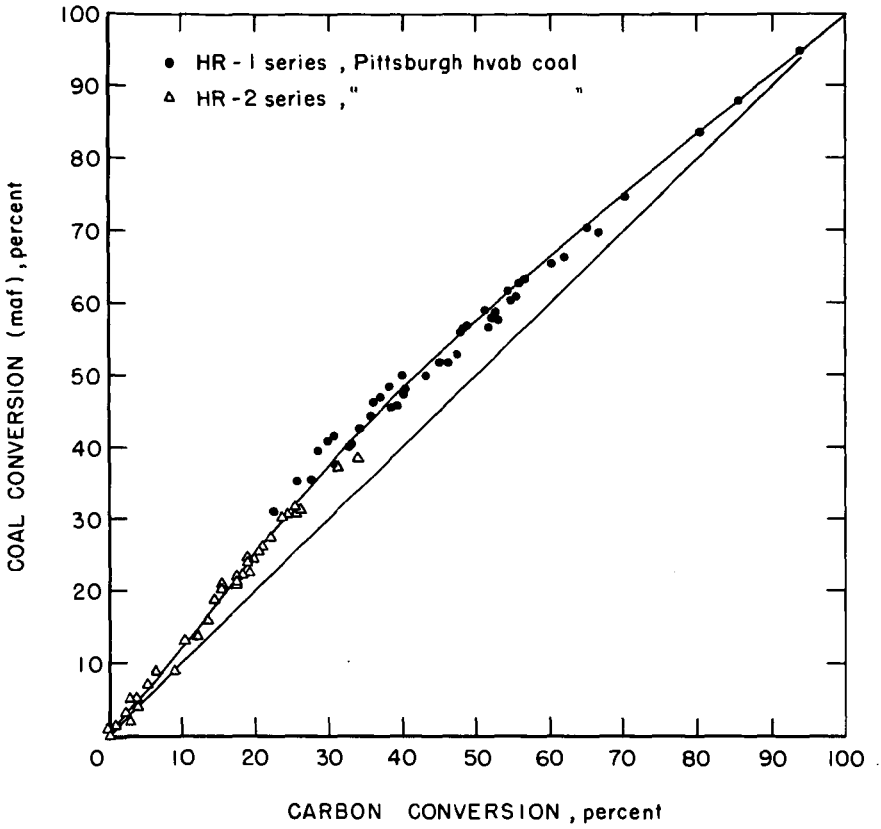


Figure 28 - Coal conversion (maf) as a function of carbon conversion during hydrogasification.

5-16-75

L-14306

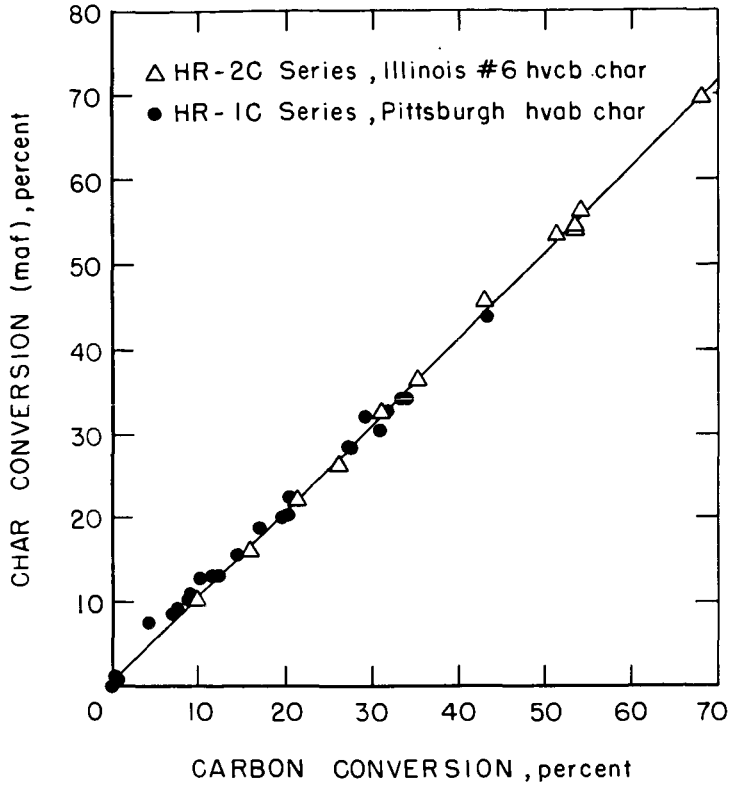


Figure 29- Char conversion (maf) as a function of carbon conversion during hydrogasification.

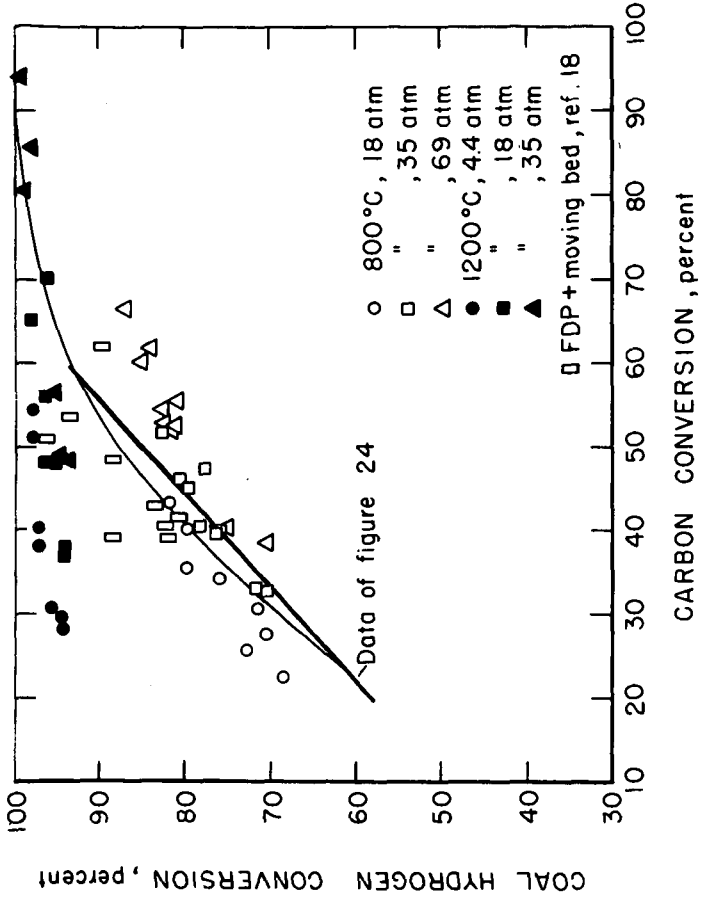


Figure 30-Conversion of coal hydrogen in HR-I tests.

5-20-75 L-14302

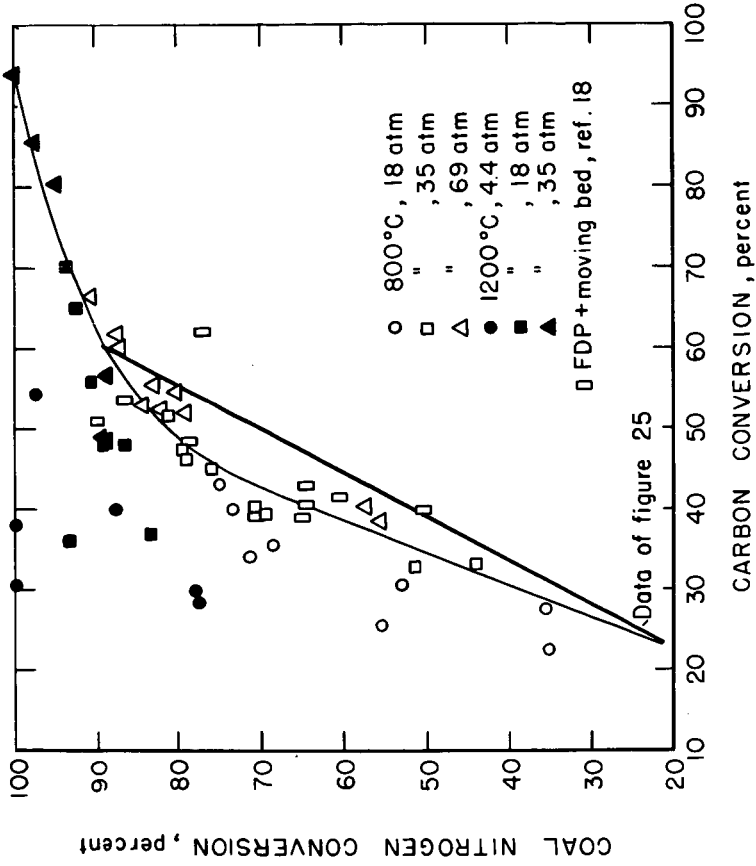


Figure 31- Conversion of coal nitrogen in HR-I tests

5-21-75

L-14303

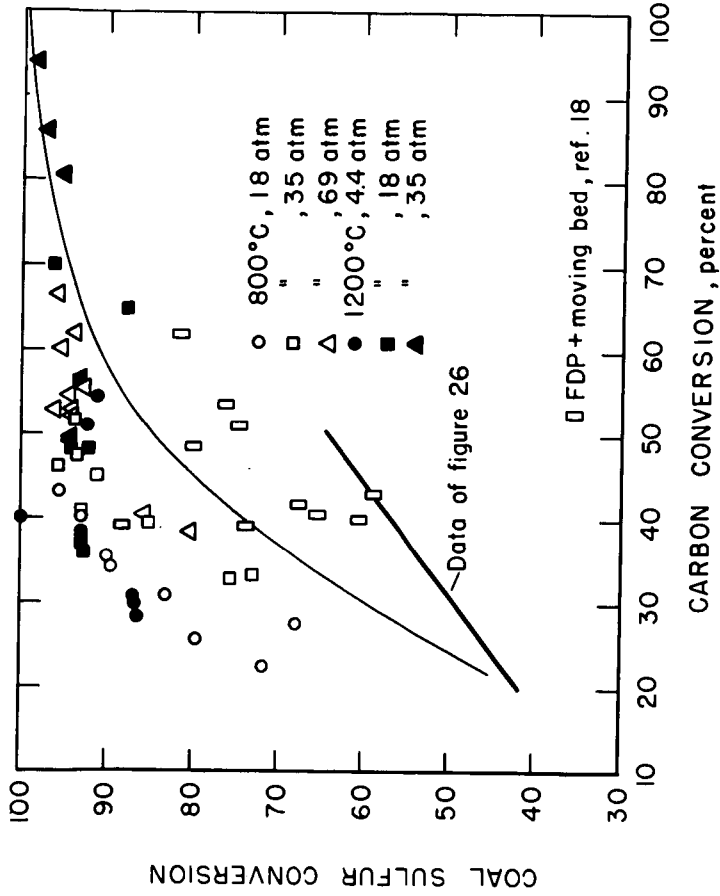
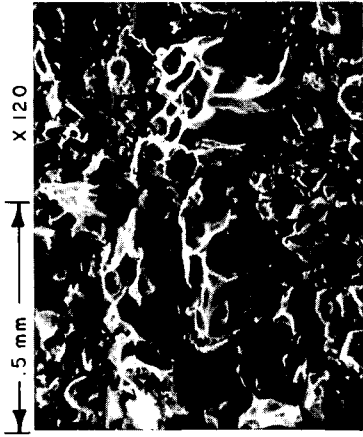


Figure 32 - Conversion of coal sulfur in HR-1 tests

5-20-75

L-14304



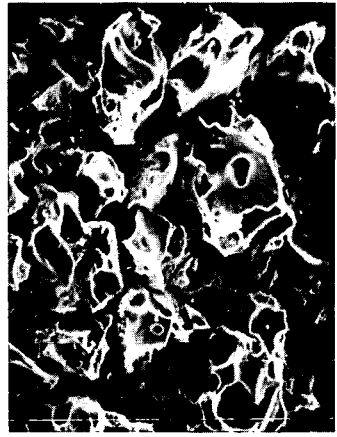
800°C- 2 min.



800°C- 10 min.



600°C- 2 min.

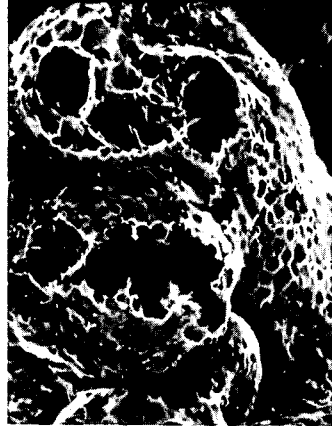


600°C- 10 min.

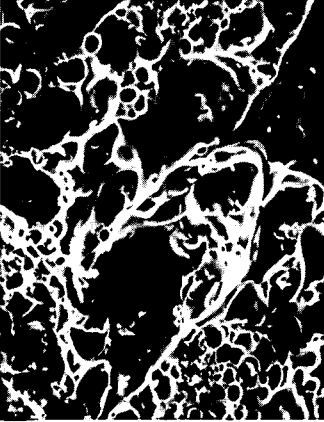
Figure 20 - SEM PHOTOGRAPHS OF 'HOT' ROD CHAR AT VARIOUS TEMPERATURES
(69 atm) X 120



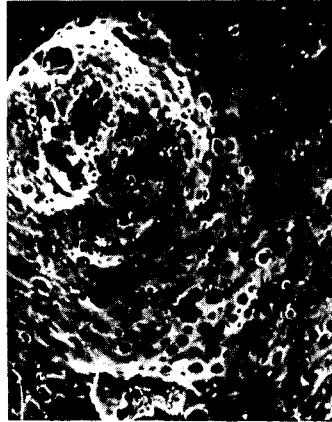
850°C- 137 atm



900°C- 35 atm



725°C- 205 atm



850°C- 69 atm

Figure 19 - SEM PHOTOGRAPHS OF FDP CHAR AT VARIOUS PRESSURES , X 120

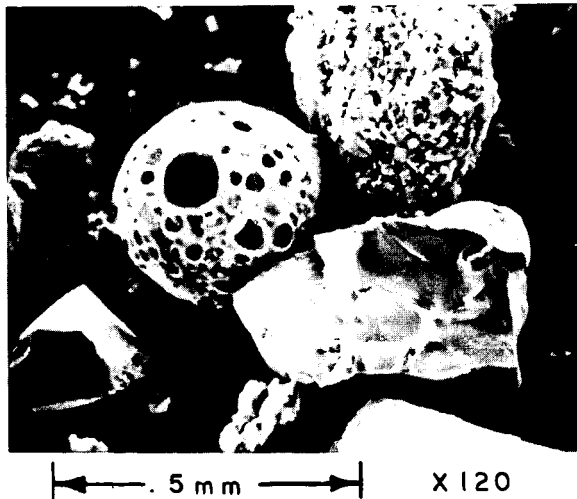
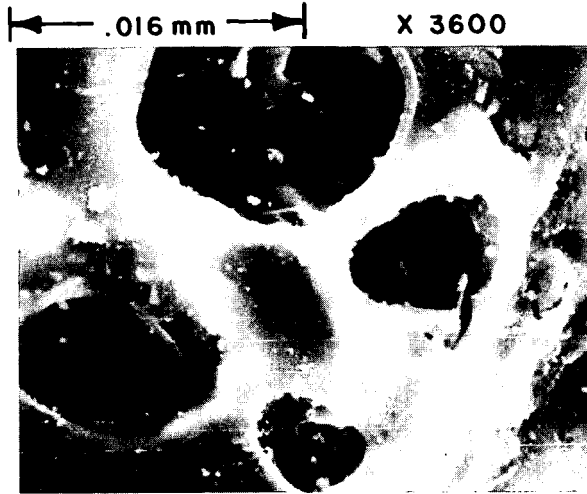


**Figure 21 - SEM PHOTOGRAPHS OF FDP CHAR (LIGNITE) ,
(850°C, 69 atm)**

HYDROGASIFICATION OF HYDRANE CHAR IN FLUIDIZED AND
MOVING BEDSC. Y. Wen,* S. Mori,* J. A. Gray,** and P. M. Yavorsky***West Virginia University
Morgantown, West Virginia**U.S. Bureau of Mines
Pittsburgh Energy Research Center
Pittsburgh, Pa. 15213ABSTRACT

To satisfy future pipeline gas requirements, considerable process development work is being aimed at gasifying coal to produce substitute natural gas (SNG). The heart of many of the gasification processes being developed is a fluid-bed gasifier in which char is reacted with steam/oxygen or hydrogen. In the HYDRANE process, being developed at the U.S. Bureau of Mines, Pittsburgh Energy Research Center, char is reacted directly with hydrogen in the fluid-bed stage of the hydrogasifier. In order to scale-up the fluid-bed reactor to pilot plant or commercial size with confidence, a fluid-bed reactor model has been developed using the bubble-assemblage concept and has been shown to fit existing data reasonably well. Data from moving-bed reactor experiments and the corresponding model were compared to the fluid-bed results and illustrate the differences between plug-flow and well-mixed solid-gas reactors.

INTRODUCTION

In order to satisfy future pipeline gas requirements and alleviate current shortages, considerable process development work is underway for gasifying coal to produce substitute natural gas (SNG). The heart of many of the gasification processes under development is a fluid-bed gasifier in which char is reacted with steam/oxygen or hydrogen. In the HYDRANE process (figure 1), being developed at the U.S. Bureau of Mines, Pittsburgh Energy Research Center, raw coal of bituminous or lower rank is reacted directly with hydrogen in a two-stage hydrogasifier to produce 95% of the product methane. The lower stage of the hydrogasifier is a fluidized bed of char in which hydrogen is the fluidizing gas. Conceptually,

the gas exiting the bed contains about 46% methane, and the char leaving the fluid bed contains about half the carbon initially fed to the hydrogasifier in the raw coal. Prevention of agglomeration is of great importance because most of the eastern and midwestern American coals soften, swell, and become sticky at temperatures above 400° C., especially in the presence of hydrogen, and are therefore impossible to process in a fluid bed without some pretreatment or dilution. Thus, the top stage of the hydrogasifier is a dilute-phase, free-fall reactor in which the raw pulverized coal is fed in a dilute cloud concurrently with the gas produced in the bottom stage, rendering the particles nonagglomerating and producing a very porous, reactive char. Approximately 20% to 30% carbon conversion occurs in this stage, and the product gas contains about 70% methane.

Experimental data have been obtained from a 12 lb./hr. process development unit in which the bottom stage of the hydrogasifier has been operated as either a fluidized bed or a moving bed reactor. In designing a scaled-up version of the fluid-bed reactor, a model describing the movement of gas and solids in the reactor and a reaction rate model is needed. The reactor model is then integrated with the reaction rate equation yielding reactor size and product gas composition. In this paper a fluid-bed reactor model has been developed using the bubble-assemblage concept originally developed by Kato and Wen (1) and is shown to describe some experimental data reasonably well. A moving-bed reactor model is also developed and used to model experimental data as well as illustrate the differences between plug-flow and well mixed solid-gas reactors.

Apparatus and Procedure

The two-stage laboratory hydrogasifier is shown in figure 2. It consists of a dilute-phase reactor integrated with a second stage which can be operated as either a moving-bed or fluid-bed reactor. The dilute-phase reactor is a 3-inch-diameter, schedule 10, type 304, stainless steel pipe 6-feet long. The pipe is heated in three 2-foot-long sections containing six 1,000-watt strip heaters

mounted directly on the pipe wall. The pipe is wrapped in fiberfrax insulation and is contained in a 10-inch-diameter, schedule 160, carbon steel pipe which acts as the pressure shell. Pulverized coal is fed into the reactor by gravity via a 1/4-inch nozzle which protrudes one foot into the reactor. When the second stage was operated as a fluid bed, the char leaving the dilute-phase reactor was crushed to reduce the particle size to a level acceptable for fluidization. The average diameter of char particles leaving the dilute-phase reactor can be as much as six times the average diameter of the pulverized feed coal particles owing to swelling and particle agglomeration and consequently, prevent adequate fluidization unless the particles are crushed. An example of particle swelling is shown in table 1. The second stage reactor is also a 3-inch-diameter pipe, but is 10-feet long and has five heated zones. A sleeve having a 2-inch inside diameter is inserted into the 3-inch-diameter pipe for fluidized-bed experiments. Temperatures reported for the dilute-phase and fluid-bed reactors correspond to reactor pipe wall thermocouple measurements. In the moving-bed experiments, reported temperatures correspond to thermocouples suspended directly into the char bed.

Two fluid-bed reactor schemes were used and are shown in figure 3. In scheme A, hydrogen was fed without preheating into the bottom of the bed by two gas nozzles, and residual char was removed at the bottom of the bed. A small amount of fines was carried over in the interstage gas. The bed level was measured by three pressure differential probes which were continually purged with a nitrogen flow of about 6 s.c.f.h. Some typical temperature profiles are shown in figure 4 and indicate that about 30 cm. of the fluid bed is required to heat up the hydrogen feed gas and attain a uniform bed temperature. In scheme B, the hydrogen was preheated to reactor temperature and was fed through a distributor plate at the bottom of the reactor. The preheater temperature and hence hydrogen feed temperature was controlled closely by a cooling water coil inside the preheater itself and extending the full length of the preheat zone.

TABLE 1.- Typical Particle Data for Dilute-Phase Char
(Illinois #6 h.v.C.b.) Before Crushing*

Run No.	162	163	164
<u>U.S. Mesh Size</u>	<u>Wt. %</u>	<u>Wt. %</u>	<u>Wt. %</u>
On 1/4"	0.05	0.03	0.05
1/4" x 4	1.16	0.57	0.49
4 x 6	8.96	4.89	5.62
6 x 8	17.35	14.77	10.27
8 x 10	12.09	12.09	10.81
10 x 12	8.47	8.91	8.51
12 x 14	8.34	8.89	9.40
14 x 20	17.35	19.34	20.00
20 x 30	13.27	13.78	17.76
30 x 50	9.52	10.52	14.31
50 x 100	3.11	5.47	2.45
100 x 200	0.18	0.47	0.18
Thru 200	0.15	0.25	0.18
\bar{d}_p , mm.	1.031	0.866	0.897
ρ_b , gm./cm ³	0.109	0.141	0.111

*Feed Coal 50- x 100-mesh (U.S. Sieve Size), \bar{d}_p = 0.223 mm.

The residual char was carried out of the reactor with the product gas via an overflow pipe and was separated from the gas. A baffle was inserted at the top of the reactor to prevent short-circuiting of feed char directly to the overflow pipe. Typical temperature profiles for this mode of operation are illustrated in figure 5. Again about 30 cm. of bed was needed to achieve a uniform temperature because too much cooling water was circulated through the preheater.

The reactor scheme for the moving-bed experiments is shown in figure 6. The char from the dilute-phase reactor dropped into the second-stage reactor which consisted of a free-fall zone and a moving-bed zone. Hydrogen was fed into the bottom of the moving-bed zone and flowed countercurrent to the movement of char. Char was removed from the bottom of the reactor by a starwheel crusher and the residence time was varied by changing the char bed height. Typical temperature profiles for this scheme are shown in figure 7.

In all experiments except HY-3, the carbon conversion was determined from an ultimate analysis of the char product and the composition of the initial coal assuming 100% ash recovery. In some experiments, the recovery of carbon, ash, and hydrogen were checked and were usually better than 95%. The moving-bed product gas composition was not known accurately because product gas from the dilute-phase reactor, containing about 70% methane, mixed with the moving-bed product gas near the sampling point. This yielded inflated values of methane concentration. Therefore, methane yields based on the moving-bed product gas analysis were not used. The mixing effect is shown in figure 8 where actual and calculated methane concentrations are shown. Carbon conversion for the overall two-stage unit based on the solids analysis was checked by calculating carbon conversion based on the total product gas and oil yields.

The ultimate analyses for the Illinois #6 h.v.c.b. coal and the char product for the fluid-bed tests and the char particle data are tabulated in table 2. The

TABLE 2.- Ultimate Analysis (As-received) of Illinois #6 h.v.c.b. Coal and Char,
and Char Particle Data for Fluid-Bed Tests

Run No.	2		3		5		11		12		13		14	
	Coal	Char	Coal	Char	Coal	Char	Coal	Char	Coal	Char	Coal	Char	Coal	Char
C	70.8	75.1	71.8	67.7	70.9	66.0	63.8	53.7	62.4	54.8	64.7	61.6	63.8	59.7
H	5.1	2.0	5.1	2.1	4.8	1.6	4.3	0.7	4.3	0.9	4.4	0.8	4.3	0.9
N	1.7	0.8	1.6	1.1	1.7	0.9	1.4	0.5	1.4	0.4	1.4	0.4	1.4	0.5
S	1.4	0.4	1.2	0.7	1.3	0.7	1.4	0.6	1.3	0.6	1.3	0.6	1.4	0.5
O	12.8	2.3	11.7	9.7	10.0	7.0	8.9	1.1	9.4	1.8	12.0	1.9	10.4	0.6
Ash	8.2	19.4	8.6	18.7	11.3	23.8	20.2	43.4	21.2	41.5	16.2	34.7	18.7	37.8
VM	34.7	6.1	34.4	6.6	34.4	3.8	30.8	3.1	30.4	1.1	30.5	2.8	36.8	1.5
Moisture	3.0	6.0	2.5	5.7	1.0	5.3	1.1	0.4	0.7	0.4	1.4	2.3	1.7	0.7
U.S. Mesh Size														
6 x 12														
12 x 20	0.5		0.7		0.2		8.3		2.7		10.0		4.7	
20 x 30			3.4		2.8		26.8		20.9		31.4		22.7	
30 x 50			26.5		23.7		19.3		18.6		16.3		17.4	
50 x 80			27.4		27.1		22.6		29.8		22.7		30.8	
80 x 100			8.5		8.2		13.1		17.8		9.7		16.2	
100 x 140			4.8		5.5		4.0		4.3		2.4		3.8	
140 x 200			3.1		2.3		3.3		3.5		2.0		2.5	
-200			25.6		30.3		1.0		0.9		0.9		0.9	
d., mm.			0.135		0.124		0.406		1.6		4.8		0.9	
ρ_p , gm./cm. ³			0.179		0.160		0.131		0.356		0.442		0.401	
									0.112		0.123		0.188	

corresponding run conditions and conversion data are listed in table 3. The carbon conversion in the dilute-phase reactor for tests HY-2, 3, 13, and 14 was assumed to be about 28% based on previous dilute-phase data with Illinois #6 coal (2), and the remaining conversion occurred in the fluid bed. For tests HY-5, 11, and 12, essentially pure hydrogen was used as the feed gas instead of a hydrogen-methane mixture so that an additional 4.5 to 5% carbon conversion occurred bringing the dilute-phase value to 33%. The conversion of the other coal constituents in the dilute-phase reactor can be calculated using the correlations given in figures 9-12, which are based on 95 coal hydrogasification experiments in the HYDRANE PDU. The data for sulfur removal are scattered because of the error in determining changes in small amounts of sulfur in the coal and char samples. Oxygen removal, which usually exceeds 90% for carbon conversions above 20%, can be considered to be complete. The calculated constituent conversions in the dilute-phase reactor for 28% and 33% carbon conversion are shown in table 4.

The ultimate analyses for the Illinois #6 h.v.C.b. coal used in the moving-bed tests and the analyses of the char product are shown in table 5. These data are presented on a dry basis for convenience in calculating conversions.

Reaction Rate of Coal-Char Hydrogasification

It has been demonstrated by a number of investigators (3,4,5,6,7,8) that coal consists roughly of two portions greatly differing in reactivity: a highly reactive portion relating to the volatile hydrocarbons present in coal, and a relatively low reactivity residual carbonaceous matter, coke. In the presence of hydrogen, the initial phase of extremely rapid reaction is presumably due to pyrolysis followed by hydrogenolysis of the intermediates that are derived from essentially aliphatic hydrocarbon side chains and oxygenated functional groups. The remainder of the carbon in the char is converted to methane much more slowly, apparently at the char surface almost stoichiometrically according to the graphite-hydrogen reaction.

TABLE 3.- Solids Conversion For Fluid-Bed Tests, 50- x 100-Mesh
Illinois #6 h.v.C.b. Coal, 1,000 p.s.i.g.

Run	2	3	5	11	12	13	14
Coal Rate, gms./hr. (Dry)	2270	2724	4631	5448	3087	2951	3042
<u>Dilute-Phase Reactor</u>							
Temp., ° C	850	850	850	850	900	900	900
Feed Gas, s.c.f.h.	234	185	260	167	108	110	110
% H ₂	45	56	94.5	93	92.6	53.4	47.8
CH ₄	48	35	0.2	0	0	38.0	39.0
Ar(He*)	6	8	4.3	7	7.4	7.3*	11.0*
N ₂	1	1	1.0	0	0	1.2	1.2
<u>Fluid-Bed Reactor</u>							
Feed Gas, s.c.f.h.	310	215	320	330	249	240	240
% H ₂	97	94	99	91	91.1	88	88
N ₂	3	6	1	9	8.6	12	12
<u>Total Conversion</u>							
C	55.2	53.6**	55.8	60.8	55.1	55.6	53.7
H	88.2	79.9	89.8	92.7	89.6	94.0	90.1
S	87.9	71.8	74.4	80.1	76.4	78.4	82.3
N	80.1	66.3	74.9	83.4	85.4	86.7	82.3
O	97.2	77.8	88.1	95.6	91.6	100	100
Fluid-Bed Height, cm.	143	143	143	122	122	122	122
Char Yield, gm./gm. dry coal	0.436	0.499	0.480	0.471	0.514	0.473	0.503

**Calculated based on char recovered.

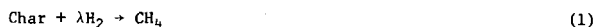
TABLE 4.- Calculated Constituent Conversion in
the Dilute-Phase Reactor

<u>Conversion, %</u>		
C	28.0	33.0
H	65.2	69.6
S	47.5	51.2
N	29.6	38.7
O	92.5*	93.0*
<u>Char Yield, gm./gm. dry coal</u>	<u>0.677</u>	<u>0.639</u>

*Estimated from Figure 13.

During the initial phase of the coal-hydrogen reaction, the coal particles are quickly softened, become metaplastic giving off volatile matter, and erupt in a manner somewhat similar to popping of popcorn. Wen and Huebler (7) presented a kinetic model for this initial rapid reaction of coal hydrogasification. In the free-fall reactor of the HYDRANE process, the initial phase of hydrogasification of coal takes place leaving a small portion of volatile matter in the char. This char is then reacted with hydrogen in a fluidized-bed reactor in the HYDRANE process. The reaction rate in this second phase of hydrogasification has been described elsewhere (7,9,10).

For the second phase reaction,



where λ is a stoichiometric coefficient obtained by an empirical correlation (9,11)

$$\lambda = \begin{cases} 1.0 & \text{for } X < 0.45 \\ 8X - 2.6 & \text{for } 0.45 \leq X \leq 0.55 \\ 1.8 & \text{for } 0.55 < X \end{cases} \quad (2)$$

and the average value of λ is obtained as follows:

$$\bar{\lambda} = \int \lambda \, dX / \int dX \quad (3)$$

The rate of hydrogasification of char is given by

$$\frac{dZ}{dt} = k(1-Z)P_{\text{H}_2} \quad (4)$$

where Z is the carbon conversion in the second phase reaction and is equal to $(X - X_0)/(1 - X_0)$. Here X is the carbon conversion based on the raw coal, X_0 is the carbon converted in the first phase reaction or in the pretreatment, P_{H_2} is the partial pressure of hydrogen and k is the reaction rate constant.

The above equation can be written in the following form as

$$\frac{dZ}{dt} = K(1-Z) Y_{\text{H}} \quad (5)$$

where $Y_{\text{H}} = P_{\text{H}_2} / P_{\text{H}_2}^{\circ}$, $K = k P_{\text{H}_2}^{\circ}$ and $P_{\text{H}_2}^{\circ}$ is the partial pressure of hydrogen at the inlet.

Feldmann et al (12) presented the following correlation for the reaction rate constant:

$$\ln k = -10.45 \times 10^3 \left(\frac{1}{T}\right) + 7.08, \quad k: \text{atm.}^{-1}\text{hr.}^{-1}, \quad T: K$$

As will be shown later, the values of k and activation energy calculated from experimental carbon conversions using the Bubble Assemblage model or moving bed model developed are significantly smaller than those calculated from the above equation.

Simulation of Fluidized-Bed Hydrogasifier

1. Minimum Fluidization Velocity

It has been shown by Feldmann et al (12,13) that the minimum fluidization velocity of coal chars with popcorn-like structure is greater than that calculated from the Wen-Yu correlation (14) which is applicable only to nonvesicular particles. The empirical correlation proposed by Feldmann et al (13) has the following form:

$$\frac{u_{mf} \rho_f d_p}{\mu} = 0.0135 \left[d_p^3 \frac{\rho_f (\rho_s - \rho_f)}{\mu^2} g \right]^{0.73} \quad (6)$$

where d_p is particle diameter,

ρ_f is gas density,

ρ_s is particle density,

μ is gas viscosity

g is gravitational acceleration, and

u_{mf} is the minimum fluidization velocity.

2. Fluidized-Bed Model

In the fluidized bed hydrogasifier, the second-phase reaction takes place either countercurrently, concurrently, or with overflow as schematically described in figure 13. The Bubble Assemblage model (1,15,16,17,18) is used to simulate the hydrogasification of coal char. The essential features of the Bubble Assemblage model are summarized as follows:

- The fluidized bed is divided into a number of compartments, each of which has a height that is uniquely determined by the diameter of the bubble at the corresponding height.
- Each compartment is composed of the bubble phase and the emulsion phase. The solids and gas in the emulsion phase and the bubble phase of each compartment are completely mixed with some exchange of gas between the two phases.
- The volume of the bubble phase is assumed to be equal to the volume of the bubbles in this paper. It is also assumed that no solids exist in the bubble phase.

Figure 14 depicts the Bubble Assemblage Model under various modes of flow arrangement. P_c is an index of solid flow arrangement and is equal to unity when solids flow countercurrent to the gas. Under this condition, $q_1 = 1 + q_2$, where q_1 and q_2 are the ratio of solids downflow rate and solids upflow rate to the solid feed rate, respectively.

When solids are fed from the top and withdrawn from the top of the bed (overflow type), P_c is 0 and $q_1 = q_2$.

From the material balance of H_2 around the n -th compartment in the bed, the following equations can be written for the bubble phase and emulsion phase.

$$W_{HO} (Y_{Bn-1} - Y_{Bn}) + V_{Bn} Y_{HO} F_{On} (Y_{en} - Y_{Bn}) = 0 \quad (7)$$

$$V_{Bn} Y_{HO} F_{On} (Y_{Bn} - Y_{en}) - V_{en} k_b Y_{en} (1 - Z_n) = 0 \quad (8)$$

where k_b is an apparent reaction rate constant for H_2 consumption in the emulsion phase and can be written as

$$k_b = \alpha_c (1 - \epsilon_{mf}) \rho_{CO} Y_{CO} K \quad (9)$$

α_c is the number of moles of H_2 reacted with one gram of carbon in char and is related to $\bar{\lambda}$ as $\alpha_c = \bar{\lambda}/12$.

From a material balance of carbon in the char around the n -th compartment, excluding $n=1$ and N , the following equation can be obtained,

$$q_1 W_{SO} Y_{CO} (Z_{n+1} - Z_n) + q_2 W_{SO} Y_{CO} (Z_{n-1} - Z_n) = -v_{en} k_b Y_{en} (1-Z_n) / \alpha_c \quad (10)$$

For the top compartment of the bed ($n=N$), we get $Z_{N+1} = 0.0$ and the following equation is obtained:

$$-q_1 W_{SO} Y_{CO} Z_N + W_{SO} Y_{CO} \left[q_2 Z_{N-1} - (1-P_c) Z_N \right] = -v_{eN} k_b Y_{eN} (1-Z_N) / \alpha_c \quad (11)$$

For the first compartment ($n=1$), the following equation can be written for the overflow type and the countercurrent type:

$$W_{SO} Y_{CO} (q_1 Z_2 - P_c Z_1) - q_2 W_{SO} Y_{CO} Z_1 = -v_{e1} k_b Y_{e1} (1-Z_1) / \alpha_c \quad (12)$$

From equations (7) and (8) we obtain:

$$Y_{Bn} = Y_{Bn-1} \left[1 - \frac{\alpha_2 (1-Z_n)}{1 + (1+\alpha_1) \alpha_2 (1-Z_n)} \right] \quad (13)$$

$$Y_{en} = -(Y_{Bn} - Y_{Bn-1}) / \alpha_2 (1-Z_n) \quad (14)$$

where $\alpha_1 \equiv F_t / V_{Bn} F_{on}$ and $\alpha_2 \equiv v_{en} k_b / W_{HO}$.

From equations (10), (11), (12), and (14) we get:

$$Z_{n+1} = \left[(q_{11} + q_{21}) Z_n - q_{22} Z_{n-1} + \alpha_3 (Y_{Bn} - Y_{Bn-1}) / \alpha_2 \right] / q_{12} \quad (15)$$

where $Z_0 = Z_{N+1} = 0.0$, $\alpha_3 \equiv v_{en} k_b / \alpha_c W_{SO} Y_{CO}$ and the values of q_{ij} are given in table 6.

If the solid particles in the bed are assumed to be completely mixed, the basic equation can be simplified as follows:

$$Z_n = Z_{1F} = \text{constant}$$

$$Y_{BN} = \prod_{j=1}^n \left[1 - \frac{\alpha_2 (1-Z_{1F})}{1 + (1+\alpha_1) \alpha_2 (1-Z_{1F})} \right] \quad (16)$$

where Z_{1F} is the conversion in the bed and at the outlet.

From an overall material balance, another equation relating Y_{BN} and Z_{1F} can be obtained as follows:

TABLE 6.- q_{ij} in equation (15)

	q_{11}	q_{12}	q_{21}	q_{22}
$n \neq 1, N$	q_1	q_1	q_2	q_2
$n = 1$	P_c	q_1	q_2	0.0
$n = N$	q_1	1.0	$1 - P_c$	q_2

$$Z_{1F} = \alpha_3 (1 - Y_{BN}) / \alpha_2 \quad (17)$$

From Hovmand and Davidson (19), if the value of $G_f \equiv (u_o - u_{mf}) / 0.35 \sqrt{g D_t}$ is less than 0.2, the bed can be kept in freely bubbling condition. When the value of G_f is greater than 0.5, the bed is in a slug flow condition. When G_f is between 0.2 to 0.5, the bed is in a transition condition between bubbling flow and slug flow.

Recently, Mori and Wen (17,18) presented a new correlation of bubble growth for a bubbling bed as follows:

$$D_B = D_{BM} - (D_{BM} - D_{BO}) \exp(-0.3 h / D_t) \quad (18)$$

where D_{BM} is the maximum bubble diameter, D_{BO} is the initial bubble diameter and h is the elevation above the distributor.

Since the fluidized gasification unit used has a large bed height to diameter ratio ($L_f \gg D_t$), equation (18) can be simplified as follows:

$$D_B \sim D_{BM} = 0.652 \{A_t (u_o - u_{mf})\}^{0.4} \quad (19)$$

Then, the height of each compartment in the bed, Δh_n , also can be approximated as:

$$\Delta h_n = D_B = D_{BM} \quad (20)$$

From Kato and Wen (1), the gas interchange coefficient, F_{on} , is given by

$$F_{on} = 11 / D_B \quad (21)$$

Based on the two-phase theory, volume fractions of bubble phase and emulsion phase in each compartment are given as follows, respectively:

$$\epsilon_{Bn} = V_{Bn} / \Delta h_n A_t = (u_o - u_{mf}) / u_B \quad (22)$$

$$V_{en} = (1 - \epsilon_{Bn}) \Delta h_n A_t \quad (23)$$

Since the solid particles may be assumed to be transferred upward in the wakes behind the bubbles, the volumetric flow rate of solids upward can be written as $f_w (u_o - u_{mf}) (1 - \epsilon_{mf}) A_t$, where f_w is the volume ratio of the wake and the bubble.

Thus, q_2 can be rewritten as,

$$q_2 = \frac{(u_o - u_{mf}) f_w (1 - \epsilon_{mf}) A_t}{W_{so}/\rho_{co}}$$

Using equations (19), (20), (21), (22), (23) and (24) the values of V_{Bn} , V_{en} , F_{on} , q_2 and Δh_n can be calculated for a set of operating conditions. Thus, numerical solutions of equations (13), (14), and (15) are obtained simultaneously by an iterative method. A computer logic diagram is shown in figure 15.

Results of Fluidized-Bed Performance Simulation

In table 7, the calculated reaction rate constants are shown based on the experimental carbon conversions. The values of reaction rate constants from the Bubble Assemblage Model and those from the simplified Bubble Assemblage Model with complete mixing of solids are compared. As for the axial solids mixing, the large height to diameter ratio of the experimental reactor used results in a relatively small degree of solid mixing. The following equation derived by Miyauchi (20) for a backflow mixing model is used to estimate the Peclet number for counterflow case,

$$\frac{1}{N_{Pe}} = \frac{E_{zp}}{(W_{so}/\rho_{co}) A_t} L_f = \frac{1}{2N} + \frac{q_2}{N} \quad (25)$$

where N is the total number of compartments. For the overflow case, an analogy of equation (25) is used to calculate the Peclet number:

$$\frac{1}{N_{Pe}} = \frac{q_2}{N} \quad (26)$$

In table 8, the values of $\frac{1}{N_{Pe}}$ are tabulated and vary between 0.3 to 1.2, considerably different from the large values obtained for complete mixing. As can be seen from table 7, the k values of countercurrent operation calculated from the Bubble Assemblage model with partial mixing of solids differ very little from the Bubble Assemblage model with complete mixing of solids indicating that the solid mixing does not affect carbon conversion significantly. The reaction rate constants are plotted on an Arrhenius Plot shown in figure 16 based on

TABLE 7.- Comparison of Reaction Rate Constants Calculated
from Bubble Assemblage Models

Run No.	Solid Flow	X_{1F} observed	Z_{1F} observed	Bed temp. K	$k_{cal.}, atm^{-1} hr^{-1}$	
					Solid partial mixed	Solid complete mixed
11		0.608	0.419	1073	0.0450	0.0515
12	counter current	0.551	0.335	1118	0.0202	0.0220
13		0.556	0.383	1113	0.0218	0.0248
14		0.537	0.357	1183	0.0139	0.0152
2		0.552	0.378	1158	0.0145	0.0123
3	over- flow	0.536	0.356	1158	0.0284	0.0140
5		0.558	0.345	1158	0.0316	0.0223

TABLE 8.- Estimated Solid Mixing in Fluidized-Bed Hydrogasifier in Terms of Peclet Number

Run No.	N	q_2	$1/N_{pe}$
11	32	19.9	0.64
12	34	25.1	0.76
13	39	20.3	0.53
14	41	25.8	0.64
2	38	46.4	1.22
3	54	16.0	0.30
5	40	20.5	0.51

N = total number of compartments.

N_{pe} = Peclet number of axial solid mixing in the fluidized bed.

the average temperatures of the bed. The data include the results of I.G.T. experiments (7) shown in table 9 for countercurrent and concurrent fluidized-bed hydrogasification experiments. The complete mixing model is used for calculation of the reaction rate constants for the I.G.T. experiments. The reaction rate constants calculated from moving-bed data are also plotted in figure 16.

An empirical relation for the temperature effect on the rate constant can be expressed as,

$$\ln k = -4.36 \left(\frac{1}{T} \right) \times 10^3 + 0.28 \quad (27)$$

where k : $\text{atm.}^{-1} \text{ hr.}^{-1}$, and T : K .

An activation energy of 8.63 Kcal/mole is estimated which is very much smaller than 15-16 and 21 Kcal/mole reported by Feldmann et al (12).

The rate constants calculated from the moving-bed data are considerably larger than those from the fluidized bed, particularly in the low temperature region. An explanation of the deviation is presented in the moving-bed section. In figure 17, the carbon conversions calculated using equation (27) are compared with experimental conversions. The scatters of the points shown in figures 16 and 17 are partly due to the nonuniformity and time dependency of temperature along the bed axis.

Moving-Bed-Reactor Model

In this model the gas and solid are assumed to move in a plug flow manner and the temperature profile of the bed is averaged to approximate an isothermal reactor. The movement of char through the moving bed, $V_s = \frac{dh}{dt}$, is assumed to be constant and can be combined with equation (3) to yield an equation describing the carbon conversion in terms of position in the moving bed ($h = 0$ at top of bed),

$$V_s \frac{dZ}{dh} = k P_{H_2} (1-Z) \quad (28)$$

The carbon conversion in the countercurrent moving bed can be related to the change in methane content of the gas by the carbon balance equation,

TABLE 9.- Operating Condition of I.G.T. Experiments
[Wen and Huebler (1965)]

Operation	Countercurrent	Concurrent
Char.	Consolidation Coal Co. Bituminous coal char	
d_p	60/325 mesh	
D_t , cm.	4.88	4.3(equivalent)
T, K	905 - 958	992 - 1189
U_{mf} , cm./sec.	1.83	
W_{CO} , g./sec.	0.61 - 1.07	0.28 - 1.05
F_t , cm ³ /sec.	57 - 111	29 - 54
P_T , atm.	137 - 141	
L_f , cm.	214	143, 225

$$Y_{co} W_{so} \frac{dZ}{dh} = - \frac{d}{dh} (W_g Y_M) \quad (29)$$

where W_{so} is the dry coal feed rate to the dilute-phase reactor (gm./hr.), X_o fractional carbon conversion in the dilute-phase reactor, Y_{co} the gm. moles of carbon per gram of dry coal, W_g the molar gas rate (gm.-moles/hr.), and Y_M the mole fraction of methane in the gas. We have made the assumption that the conversion of carbon to CO or CO₂ in the moving bed will be negligible. Previous work with char appears to support this assumption (6,21). The partial pressure of hydrogen is given by

$$P_{H_2} = (n - Y_M) P_T \quad (30)$$

where P_T is the total pressure and n is the combined mole fraction of hydrogen and methane in the gas. The difference of n from unity represents the mole fraction of inerts in the gas. The net change in the molar gas rate is

$$\frac{dW_g}{dh} = (\lambda - 1) Y_{co} W_{so} \frac{dZ}{dh} \quad (31)$$

Equations (29) and (31) may be integrated over an arbitrary distance h starting at the top of the moving bed resulting in the equations

$$W_{go} Y_{Mo} - W_g Y_M = Y_{co} W_{so} Z \quad (32)$$

$$W_g - W_{go} = Y_{co} W_{so} \int_0^Z (\lambda - 1) dZ \quad (33)$$

Evaluation of equations (32) and (33) using the boundary conditions $Z = Z_H$, $Y_M = 0$ and $W_g = W_{gH}$ at $h = H$ yields values for W_{go} and Y_{Mo} . Once W_{go} and Y_{Mo} are known, Y_M and W_g can be evaluated at any point in the moving bed. Thus, the mole fraction of methane at any position h is given in terms of the carbon conversion as

$$Y_M = \frac{W_{go} Y_{Mo} - Y_{co} W_{so} Z}{W_{go} + Y_{co} W_{so} \int_0^Z (\lambda - 1) dZ} \quad (34)$$

Henceforth the integral in the denominator will be written as $F(Z)$. Substitution of equations (30) and (34) into equation (28) and integrating over the length of the bed, H , yields the following relationship for the reaction rate constant k :

$$k = \frac{1}{P_T \theta} \int_0^{Z_H} \frac{[1 - BF(Z)] dZ}{[A + B(1-Z) - nBF(Z)][1-Z]} \quad (35)$$

where $\theta = v_s/H$

$$A = n - Y_{Mo} - B$$

$$B = - \frac{Y_{co} W_{so}}{W_{go}}$$

Equation (35) can be solved analytically in one, two, or three parts, depending on the evaluation of λ in equation (1). The solution of equation (35) is shown in Appendix A.

Moving-Bed Results

The conversion of the coal constituents are plotted in figure 18 versus residence time in the moving bed. Zero residence time corresponds to solid material free-falling through the dilute-phase reactor followed by free-fall through the empty moving-bed reactor. Such a condition should approximate the conversion in the dilute-phase reactor plus that in the free-fall portion of the moving-bed reactor when a char bed level is maintained. Char conversion in the free-fall section of the moving-bed reactor is probably low because the reactivity is much lower compared to the starting coal and the residence time is less than a second. Zero residence time tests yielded a carbon conversion of 30%, and this value is used as X_o in the moving-bed model calculations. These results are summarized in table 10 and the rate constants are shown on figure 16 as an Arrhenius plot. The effect of temperature on the moving-bed rate constant values can be described by the

TABLE 10.- Countercurrent Moving-Bed Kinetic Data, Illinois #6

Run	Total C** Conv.	Moving Bed C Conv.	Z _H	W _{SO}	Dry Coal Rate, gm./hr.	Feed Gas Rate, mole/hr.	W _{GH}	Product Gas Rate, mole/hr.	W _{GO}	Total Pressure, atm.	Residence Time, min.	Rate Const. atm. ⁻¹ hr. ⁻¹	Temp. °C
33*	.620	.457		3178	133.9	173.5	116.0	69.0	20	.0573	905		
37	.392	.131		6497	173.5	173.5	161.8	68.7	3.8	.0360	900		
38	.485	.264		5262	163.2	161.8	191.9	68.7	7.3	.0396	875		
39	.617	.167		6170	191.9	191.9	177.9	68.4	4.0	.0449	645		
43b	.430	.186		4654	177.9	177.9	178.5	68.4	5.1	.0395	765		
44b	.391	.130		4985	178.5	178.5	174.9	68.7	5.1	.0260	650		
45b	.406	.151		4998	176.9	176.9	173.6	68.7	5.1	.0307	660		
46a	.399	.151		4772	173.6	173.6	173.6	68.7	5.1	.0305	684		
48	.511	.301		4540	177.0	177.0	173.3	68.7	10.5	.0299	800		
49	.536	.337		4685	176.6	176.6	168.8	68.1	10.0	.0358	715		

*n = 0.67; other tests, n = 1

**X₀ = 0.300, Z = (X - X₀)/(1 - X₀)

equation

$$\ln k = -2.21 \left(\frac{1}{T}\right) \times 10^3 - 1.19 \quad (36)$$

The discrepancy between the moving-bed and fluid-bed data in figure 16 was first believed to be a result of hydrogen mass transfer resistance between the bulk gas and the char particle surface. The Reynolds number for the moving-bed tests ranged from 0.882 to 1.146 while the Schmidt number varied from 0.569 to 0.933. Using these values and available mass transfer correlations, the mass transfer coefficient, k_g , was estimated to be 0.119 to 0.132 moles $H_2/hr.cm.^2.atm$. Correction of these values to the same form as k yielded mass transfer coefficients in excess of $1,400 atm.^{-1}.hr.^{-1}$ confirming that particle film resistance was not a significant factor. The discrepancy is believed to be a result of heat transfer resistance from the char particles to the bulk gas phase resulting in the particle temperature being higher than the temperature of the gas and the measured bed temperature. This can be verified by a simple heat transfer model if we assume the reaction rate, the average particle temperature, and the average gas temperature in the bed are constant, and the heat generated by reaction is distributed uniformly within the particles. A heat balance around a particle gives the equation

$$\frac{dT_p}{d\eta} = \frac{h A \theta}{\rho_p \bar{C}_{ps}} (T_g - T_p) + \frac{A_T H}{\bar{C}_{ps} \bar{W}_s} Q_T \quad (37)$$

where the equation for the heat generation rate per unit volume of bed, Q_T is

$$Q_T = \frac{(-\Delta H) Z_1 Y_{CO} W_{SO}}{A_T H} \quad (38)$$

Using the boundary conditions $T_p = T_g$ when $\eta = 0$ ($t = 0$) and $T_p = T_{p1}$ when $\eta = 1$ ($t = \theta$) the solution of equation (37) is,

$$\frac{T_{p1}}{T_g} = \left(1 + \frac{\beta}{\delta}\right) - \left(\frac{\beta}{\delta}\right)e^{-\delta} \quad (39)$$

$$\text{where } \delta = \frac{6h_f(1-\epsilon)\theta}{\rho_b T_{ps}^2 d_p}$$

$$\beta = \left[\frac{Z_1 Y_{CO} (-\Delta H)}{T_g T_{ps}} \right] \frac{W_{so}}{W_s}$$

Evaluation of equation (39) using the parameter values listed in table 11 yields

$T_{p1}/T_g = 1.2$ and $T_{p1} = 1120$ K. This means the temperature of the particles at $t = \theta = 30.6$ sec. is 187 K above the temperature of the gas, which is 933 K.

The log-mean average temperature of the particles is 990° K, so that on the average the difference in temperature between the gas and particles is 57 K for this case. Thus, the moving-bed k values at the lower temperatures in figure 16 should be more toward the left since the particle temperature was probably higher than the gas temperature. The measured temperature approximates the gas temperature since the gas channels along the thermocouple sheath sweeping its surface to a large extent. The contact area between the char particles and the thermocouple sheath is small compared to the area swept by the gas.

CONCLUSIONS

Hydrogasification reaction rate constant values were calculated using partial mixing and complete mixing versions of the Bubble Assemblage model of the fluidized bed. These results indicated that solid mixing did not have a significant effect on the carbon conversion. This was not unexpected because the carbon conversions in the bed were under 40%. Thus, the reactor was operating in a regime where changes in axial mixing exhibit only a minor influence on conversion. The k values for the complete mixing model with countercurrent operation are slightly higher than the values for the partial mixing model because the carbon content in the

TABLE 11.- Parameter Values Used in Equation 39

u_o	2.5 cm./sec.	C_{pf}	3.5 cal./gm. K
T_g	933 K	Z_1	0.10
θ	30.6 sec.	Y_{co}	0.68
d_p	0.04 cm.	Pr	12.6
ρ_b	0.15 gm./cm. ³	Re	1.11
\bar{C}_{ps}	0.4 cal./gm. K	Nu	0.01
ρ_f	4×10^{-3} gm./cm. ³	h_f	2.5×10^{-5} cal./cm ² sec. K
μ_f	3.6×10^{-4} poise	δ	1.0
k_f	1.0×10^{-4} cal./cm.sec. K	β	$0.3 \frac{w_{so}}{w_s} \sim 0.3$
$-\Delta H$	1.5×10^3 cal./gm. carbon reacted		

completely mixed bed is lower than in most locations in the partial mixed bed, thus, requiring a larger rate constant in order to obtain the same amount of conversion. In the case of overflow operation of the fluid bed, larger k values are obtained for the partial mixing case than for complete mixing because some of the char particles have a very short retention time in the bed before overflowing out. The k values must then be larger in order to obtain the same conversion as the complete mixing case.

Mixing was important, however, from the standpoint of heat removal from the char particles and maintaining an approximately isothermal bed. The importance of heat removal was very evident in the moving-bed results where heat transfer from the char particles was apparently poor, causing the particle temperature to be higher than the measured temperature. This effect was dominant in the low-temperature region where moving-bed k values were significantly larger than fluid-bed k values. This heat transfer problem may be the reason why Feldmann, et al (12) obtained large values of k and a large activation energy when they fit the kinetic model given by equation (3) to the moving-bed data of Lewis, et al (21). Obviously, hydrogasification data is best obtained in a fluidized bed or in a thermobalance such as that used by Johnson (22) where the reaction heat can be removed so the char temperature is equivalent to the gas temperature and is isothermal.

NOMENCLATURE

A_p	specific surface area, $A_p \approx (1-\epsilon) \frac{6}{d_p}$, cm^2/cm^3
A_t	cross sectional area of the bed, cm^2
\bar{C}_{pf}	average heat capacity of gas, $\text{cal}/\text{gm} \cdot \text{K}$
\bar{C}_{ps}	average char heat capacity, $\text{cal}/\text{gm} \cdot \text{K}$
d_p	particle diameter, cm .
E_{zp}	axial solid dispersion coefficient, cm^2/sec .

F_{on}	gas interchange coefficient per unit volume of bubble phase in n -th compartment, sec.^{-1}
F_t	volumetric gas flow rate in the bed, $\text{cm.}^3/\text{sec.}$
h	axial distance along bed, cm.
H	moving-bed height, cm.
h_f	heat transfer coefficient, $\text{cal./cm.}^2 \text{ K. sec.}$
Δh_n	length of the n -th compartment, cm.
$-\Delta H$	heat of reaction, cal./gm. carbon
k	reaction rate constant of carbon, $\text{atm.}^{-1} \text{ hr.}^{-1}$
L_f	fluid-bed height, cm.
N	total number of compartments
n	n -th compartment or one minus inerts mole fraction
P_{H_2}	hydrogen partial pressure, atm.
q_1, q_2	ratio of solid downflow rate and solid upflow rate to the solid feed rate, respectively
Q_T	heat generated in the moving bed, cal./sec. cm.^3
t	time, sec.
T	average bed temperature, K.
T_g	average gas temperature, K.
T_p	average particle temperature, K.
u_o	superficial gas velocity, cm./sec.
u_B	bubble rising velocity, cm./sec.
u_{mf}	superficial gas velocity at minimum fluidization, cm./sec.
V_{Bn}, V_{en}	volume of the bubble and emulsion phase at the n -th compartment, cm.^3
V_s	downward char rate in moving bed, cm./sec.
W_g, W_{gO}, W_{gH}	total gas rate through the bed, moles/sec.
W_{Ho}	feed rate of hydrogen gas, moles/sec.

W_{so}	coal feed rate, gm./sec.
\bar{W}_s	average char rate in moving bed, gm./sec.
X	total fractional carbon conversion
Y_{Bn}, Y_{en}	nondimensional partial pressure of hydrogen in bubble and emulsion phase at n -th compartment, respectively
Y_{Ho}	hydrogen concentration in feed gas, mole/cm. ³
Y'_{co}	initial carbon content in feed coal, $Y'_{co} = Y'_{co}(1-X_o)$
Y_M	methane concentration, mole/cm. ³
Z	carbon conversion based on the feed char, $Z \equiv (X-X_o)/(1-X_o)$
Z_1, Z_{1F}	outlet carbon conversion from moving bed and fluidized bed, respectively
α_c	number of moles of hydrogen reacted with one gram of carbon, mole/gm.
ϵ_{mf}	void fraction in emulsion phase
n	nondimensional time
θ	residence time in moving bed, sec.
λ	number of moles of hydrogen reacted with one mole of carbon, mole/mole
ρ_b	char bulk density, gm./cm. ³
ρ_p	char particle density, gm./cm. ³
ρ_{co}	density of feed coal, gm./cm. ³

Subscript

O	inlet
1	outlet
B	bubble phase
e	emulsion phase
n	n -th compartment

BIBLIOGRAPHY

1. Kato, K. and C. Y. Wen. Chem. Engrg. Sci. 24, 1351 (1969).
2. Feldmann, H. F., J. A. Mima and P. M. Yavorsky. Coal Gasification. Advances in Chemistry Series, 131, A.C.S., Wash., D.C., p. 108 (1974).
3. Chermin, H. A. G. and D. W. VanKrevelen. Fuel, 36, 85 (1957).
4. Van Krevelen, D.W., C. Van Heerden and F. J. Huntjens. Fuel, 30, 253 (1951).
5. Pitt, G. J. Fuel, 41, 267 (1962).
6. Feldkirchner, H. L. and H. R. Linden. I. & E.C. Process Design and Development, 21, 153 (1963).
7. Wen, C. Y. and J. Huebler. I. & E.C. Process Design and Development, 4, 142 and 149 (1965).
8. Wen, C. Y., R. C. Bailie, C. Y. Lin, and W. S. O'Brien. Coal Gasification, Advances in Chemistry Series, 131, A.C.S., Wash., D.C., p. 9 (1974).
9. Feldmann, H. F., W. H. Simons, J. A. Mima and R. W. Hiteshue. A.C.S. Div. of Fuel Chem. Preprints, v. 14, No. 4, Part II, p. 1, Sept. 1970.
10. Feldmann, H. F. and P. M. Yavorsky. Paper presented at the 5th A.G.A./O.C.R. Synthetic Pipeline Gas Symposium, Chicago, Ill., Oct. 1973.
11. Feldmann, H. F., W. H. Simons, C. Y. Wen and P. M. Yavorsky. Paper presented at the 4th International Congress of Chem. Engrg., Chemical Equipment, Design and Automation, Marianske Laxne, Czechoslovakia, Sept. 1972.
12. Feldmann, H. F., C. Y. Wen, W. H. Simons and P. M. Yavorsky. Paper presented at the 71st National Meeting, A.I.Ch.E., Dallas, Tex., 1972.
13. Feldmann, H. F., K. D. Kiang and P. M. Yavorsky. A.C.S. Div. of Fuel Chem. Preprints, v. 15, No. 3, p. 62, Sept. 1971.
14. Wen, C. Y. and Y. H. Yu. A.I.Ch.E. J., 6, 220 (1960).
15. Yoshida, K. and C. Y. Wen. Chem. Engrg. Sci., 25, 1395 (1970).
16. Ishida, M. and C. Y. Wen. Chem. Engrg. Sci., 23, 125 (1968).
17. Mori, S. and C. Y. Wen. Paper presented at the 67th A.I.Ch.E. Annual Meeting,

- Wash., D.C., Dec. (1974).
18. Mori, S. and C. Y. Wen. Paper submitted in I. & E.C. Process Design and Development (1974).
 19. Hovmand, S. and J. F. Davidson. Fluidization, Chapt. 5, Academic Press (1971).
 20. Miyauchi, T. Chem. Engrg., Tokyo, 26, 999 (1962).
 21. Lewis, P. S., S. Friedman and R. W. Hiteshue. Fuel Gasification, Advances in Chemistry Series, 69, A.C.S., Wash., D.C., p. 50, (1967).
 22. Johnson, J. L. Coal Gasification, Advances in Chemistry Series, 131, A.C.S., Wash., D.C., p. 145 (1974).

APPENDIX A

Solution of Equation (35)

The function $F(Z)$ in equation (35) has three different forms as defined by equations (2) and (34) depending upon the total fractional carbon conversion. When the total fractional carbon conversion, X , is less than 0.45, λ has the constant value 1.0 and $F(Z) = 0$. The integral for this case is then very simple. When X is between 0.45 and 0.55, λ has a value that varies linearly with X and $F(Z)$ turns out to be a parabolic function. For this case the integral of equation (35) is evaluated in two steps: first, for X up to 0.45 and $F(Z) = 0$; and second, for 0.45 up to the measured value of X and $F(Z)$ as a parabolic function. Thus k_1 and k_2 correspond to the values of the first and second parts of the integral. When X is larger than 0.55, λ has the constant value 1.8 and $F(Z)$ is a linear function of Z . For this case the same procedure as used previously results in three parts for the integral corresponding to k_1 , k_2 , and k_3 . These results are summarized by the following equations.

Case 1: $X < 0.45$
 $F(Z) = 0$

$$k = \frac{1}{P_T \theta A} \ln \left[\frac{1 - \frac{BZ_H}{A+B}}{1 - \frac{Z_H}{Z_1}} \right] \quad (A1)$$

Case 2: $0.45 \leq X \leq 0.55$
 $F(Z) = aZ^2 + bZ + C$

where $a = 4(1-X_0)$
 $b = 8X_0 - 3.6$
 $c = 4(0.45 - X_0)^2 / (1 - X_0)$
 $k = k_1 + k_2$

$$k_2 = \frac{1}{P_T \theta} \left\{ -\frac{1}{2n} \ln \left[\frac{\bar{Z}}{\bar{Z}_1} \right] - \left(\frac{1 - BC'}{2\bar{C}} \right) \ln \left[\frac{(1-Z_H)^2}{(1-Z_1)^2} \left(\frac{\bar{Z}_1}{\bar{Z}} \right) \right] + \left[\frac{\bar{b}}{2n} + Bb' + \frac{B(1-BC')}{2\bar{C}} \right] \frac{2}{\sqrt{q}} \left[\tan^{-1} \left(\frac{2\bar{a}(1-Z_H) + \bar{b}}{\sqrt{q}} \right) - \tan^{-1} \left(\frac{2\bar{a}(1-Z_1) + \bar{b}}{\sqrt{q}} \right) \right] \right\} \quad (A2)$$

where $\bar{a} = -4nB(1-X_0)$
 $\bar{b} = B(1-nb')$
 $\bar{C} = A - nBC'$
 $q = 4\bar{a}\bar{C} - \bar{b}^2, q > 0$
 $b' = -(2a + b)$
 $C' = (a + b + C)$
 $\bar{Z} = \bar{a}(1-Z_H)^2 + \bar{b}(1-Z_H) + \bar{C}$

$$\bar{z}_1 = \bar{a}(1 - z_1)^2 + \bar{b}(1 - z_1) + \bar{c}$$

$$z_1 = 1 - (0.45 - X_0)/(1 - X_0)$$

Case 3:

$$X > 0.45$$

$$F(Z) = 0.8Z + (0.8X_0 - 0.40)/(1 - X_0)$$

$$k = k_1 + k_2 + k_3$$

$$k_3 = \frac{1}{P_{r\theta}} \left\{ \frac{D}{G} \ln \left[\frac{J + G(1 - Z_H)}{J + G(1 - Z_2)} \right] + \frac{E}{J} \ln \left[\frac{J + G(1 - Z_H)}{J + G(1 - Z_2)} \cdot \frac{1 - Z_2}{1 - Z_H} \right] \right\} \quad (A3)$$

where $D = 0.80B$

$$E = 0.8B - B(0.8X_0 - 0.40)/(1 - X_0)$$

$$G = (1 + 0.8n)B$$

$$J = A + n(E - 1)$$

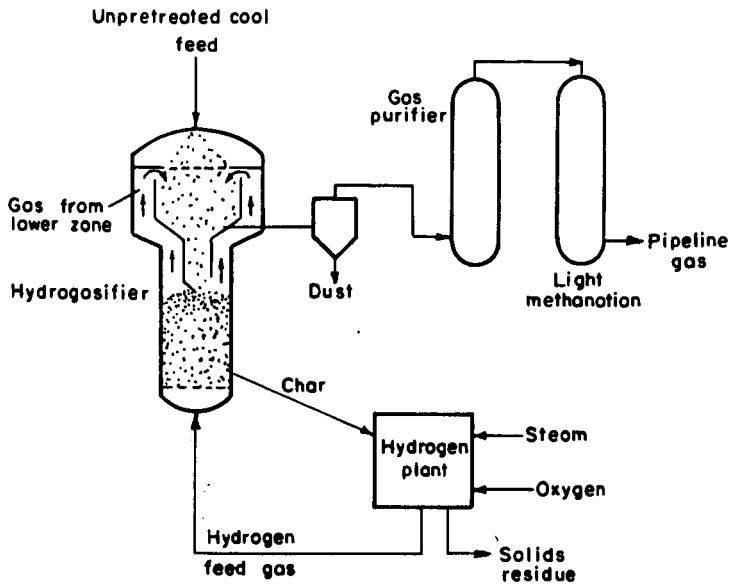


FIGURE 1 - The hydrane process for producing high BTU gas by the direct reaction of coal with hydrogen .

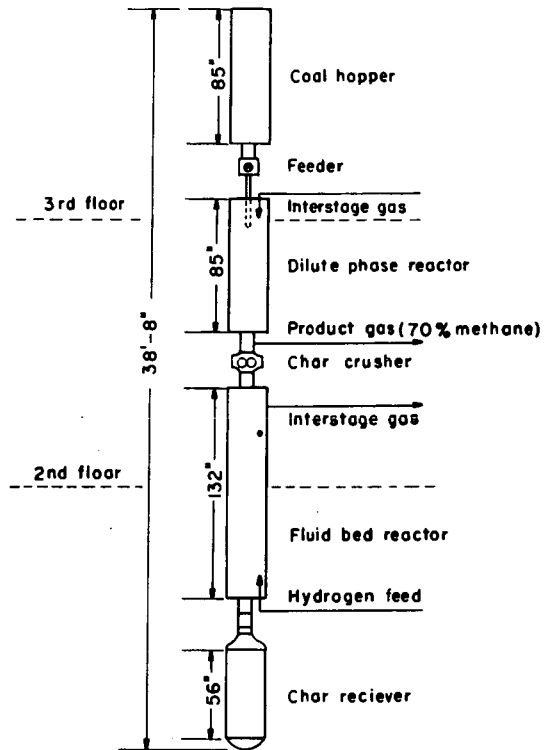


Figure 2 - Integrated hydrogasification unit.

L-12914

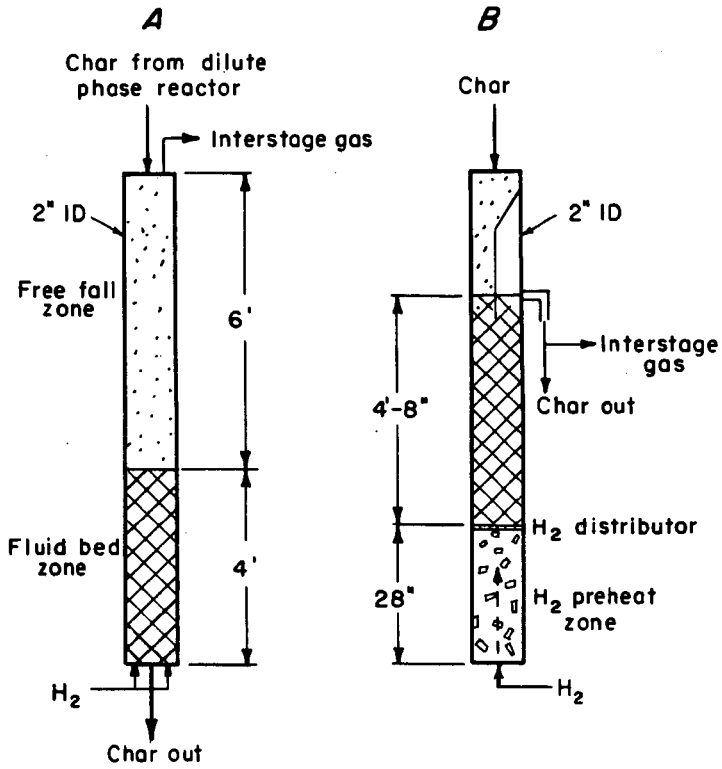


Figure 3—Schematics of fluid bed reactors

L-14051

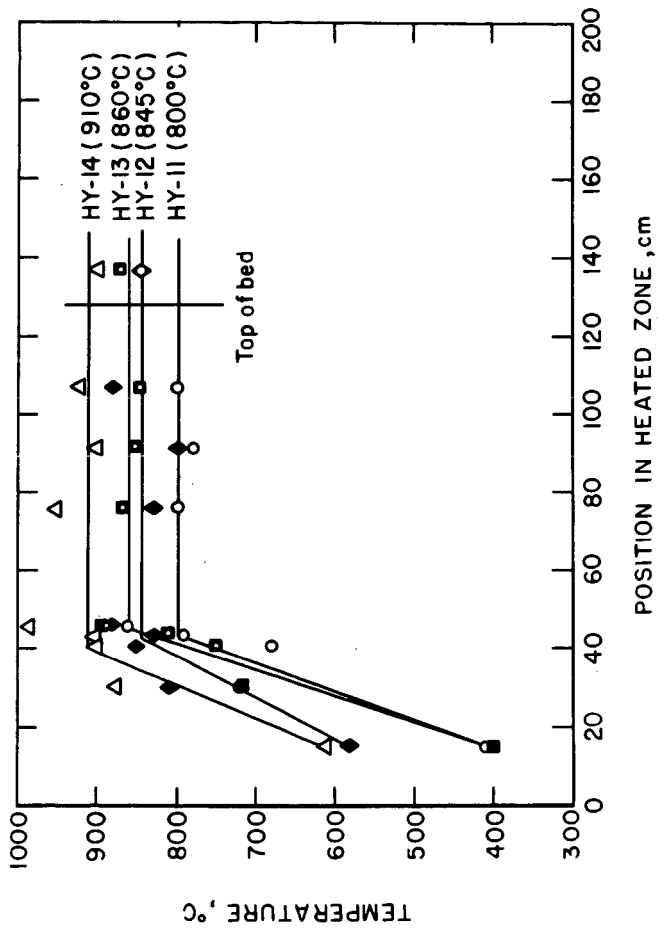


FIGURE 4 - Temperature profiles for scheme A fluid bed reactor.

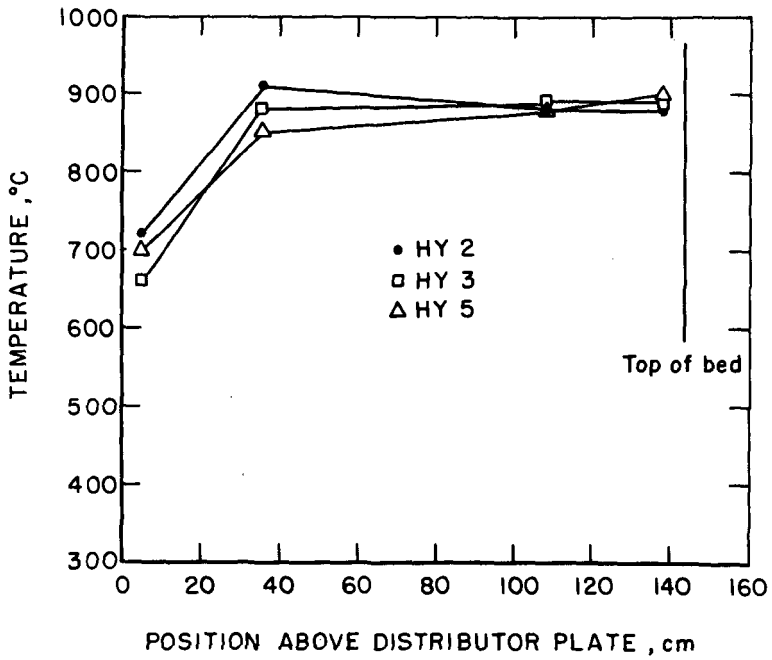


FIGURE 5 - Temperature profiles for scheme B fluid bed reactor.

L-14043

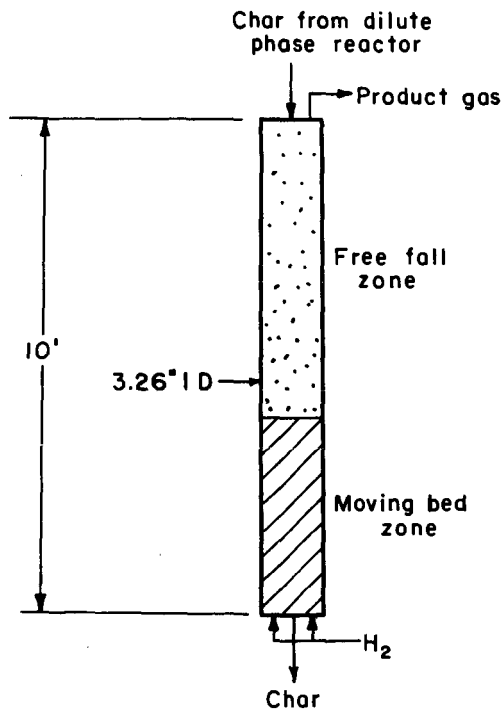


Figure 6—Schematic of moving bed reactor

L-14056

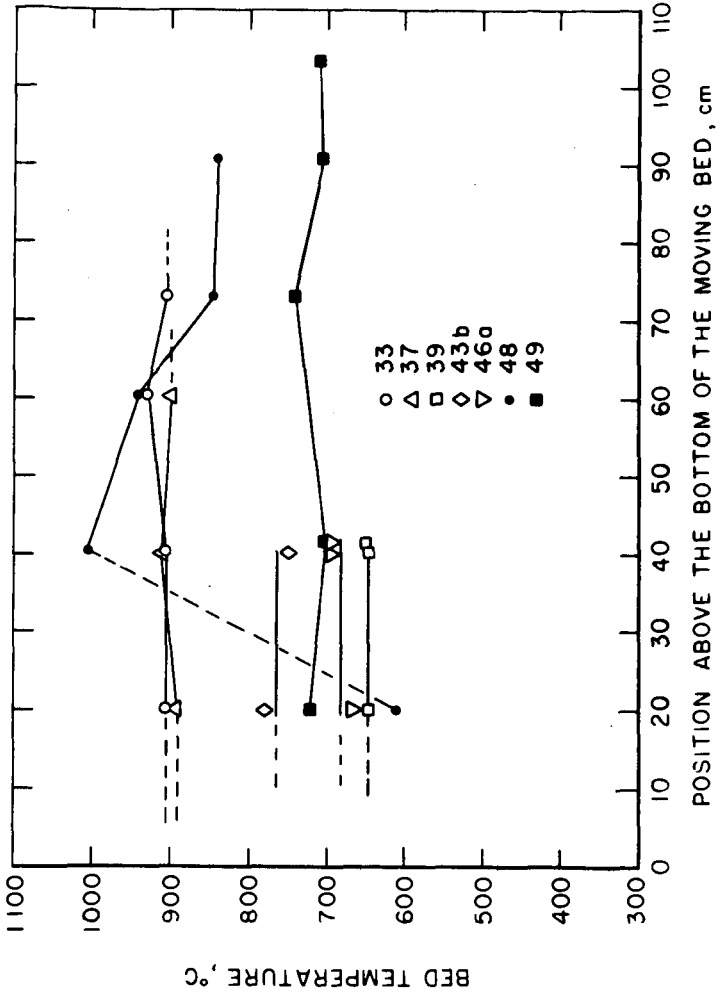


FIGURE 7 - Temperature profiles for the moving bed reactor

L-14044

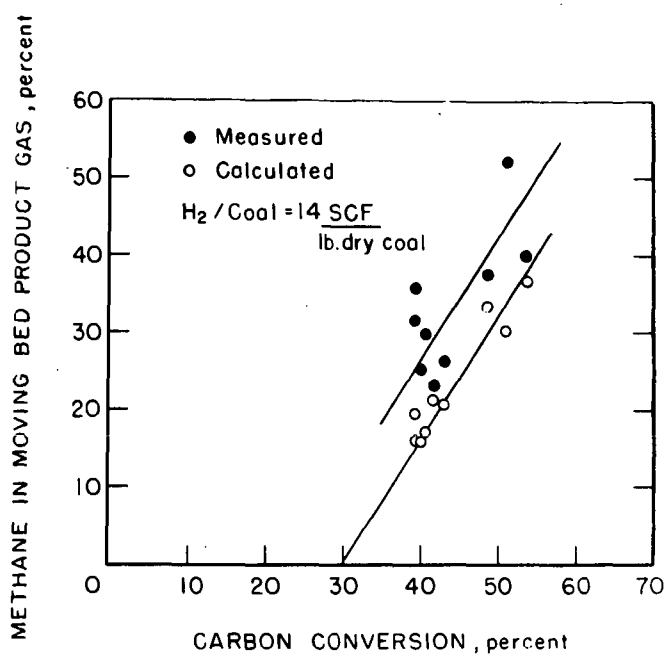


FIGURE 8 - Mixing effect on the moving bed product gas near the sampling point.

L-14042

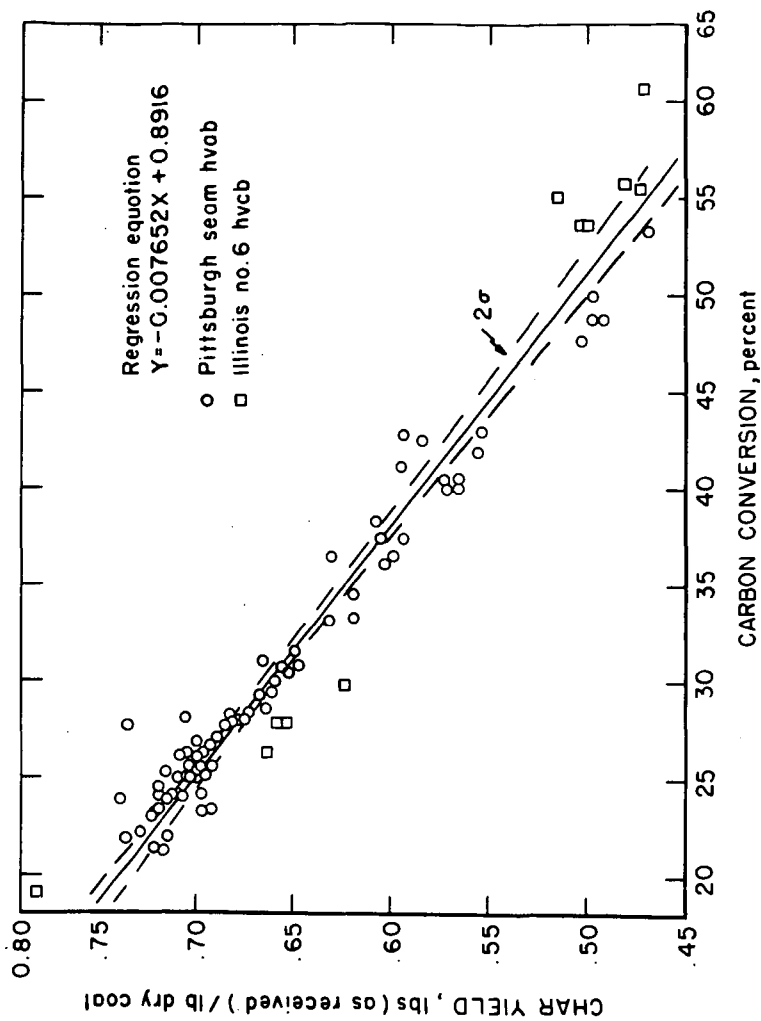


FIGURE 9 - Char yield as a function of carbon conversion during hydrogasification.

L-13708

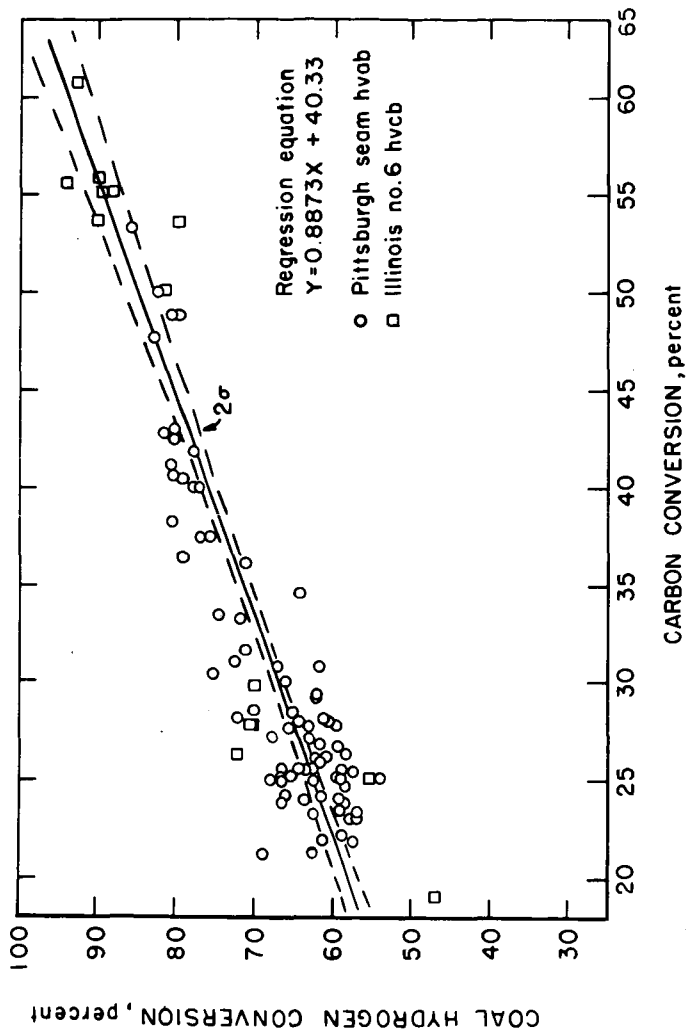


FIGURE 10 - Coal hydrogen conversion as a function of carbon conversion during hydrogasification.

L-13709

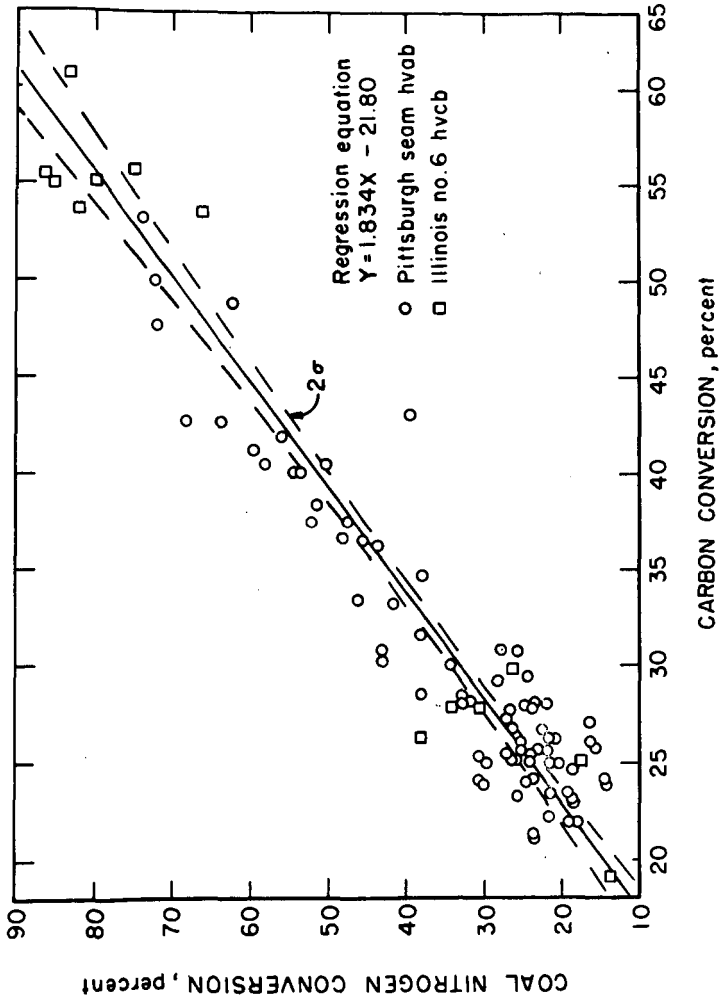


FIGURE II - Coal nitrogen conversion as a function of carbon conversion during hydrogasification.

L-13712

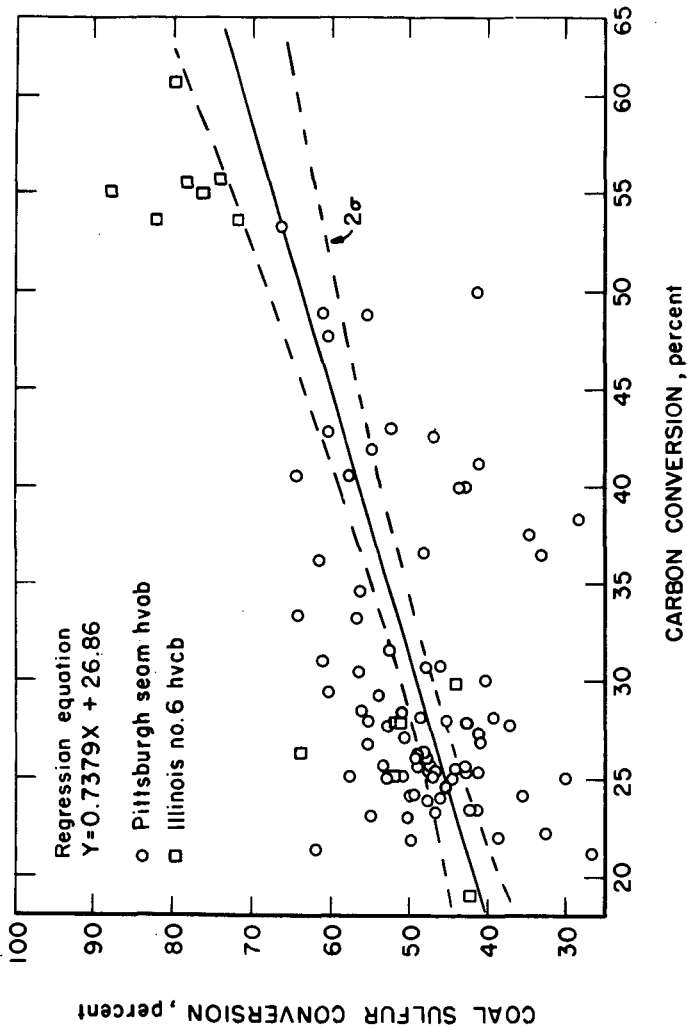


FIGURE 12 - Sulfur conversion as a function of carbon conversion during hydrogossification.

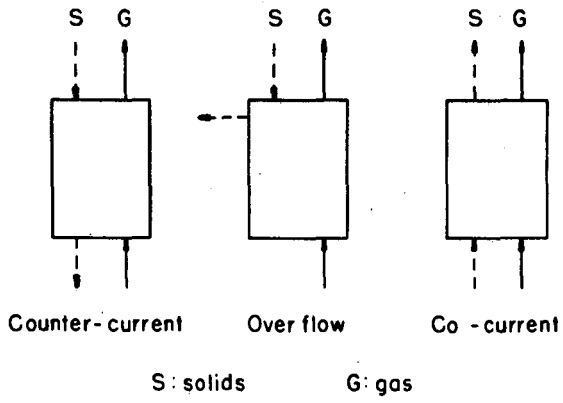


FIGURE 13- Modes of the fluidized bed operations.

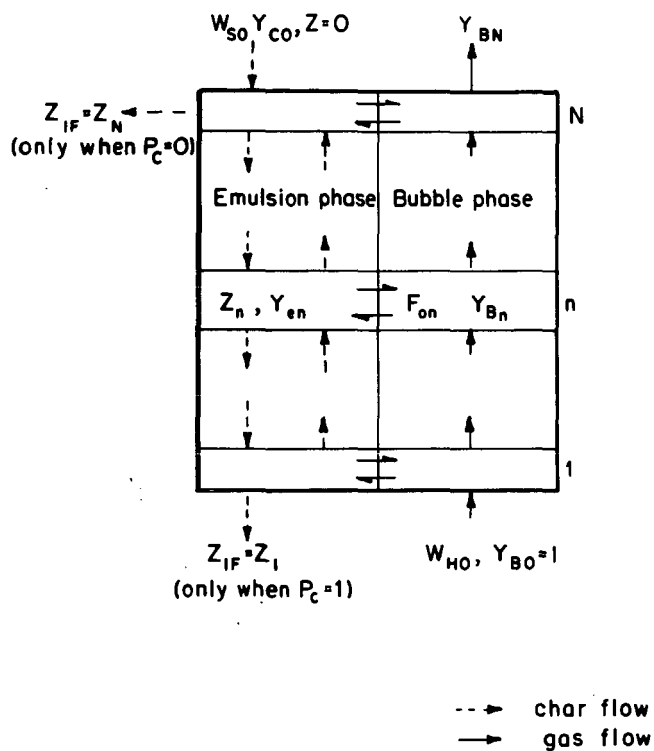


Figure 14 —Bubble assemblage model for fluidized char gasification

L-14046

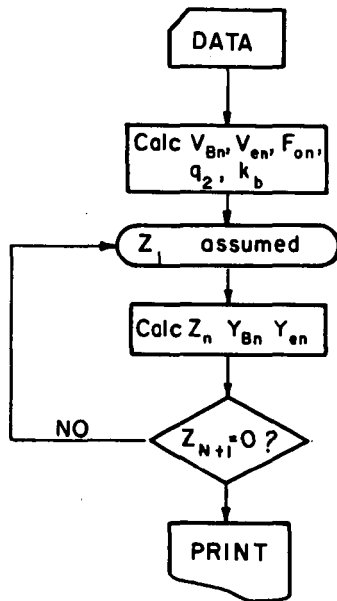


Figure 15 - Computer logic diagram

L-14049

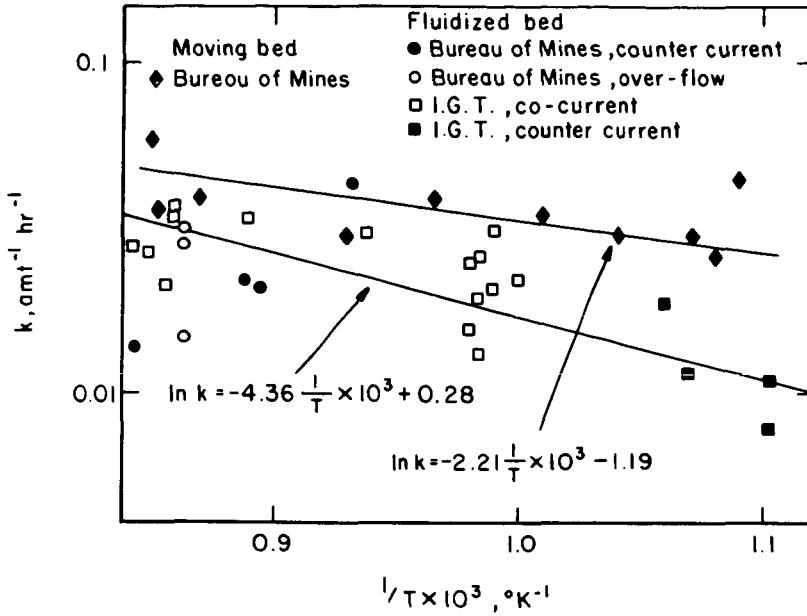


FIGURE 16 - Effect of average bed temperatures on rate constants for char hydrogasification

L-14047

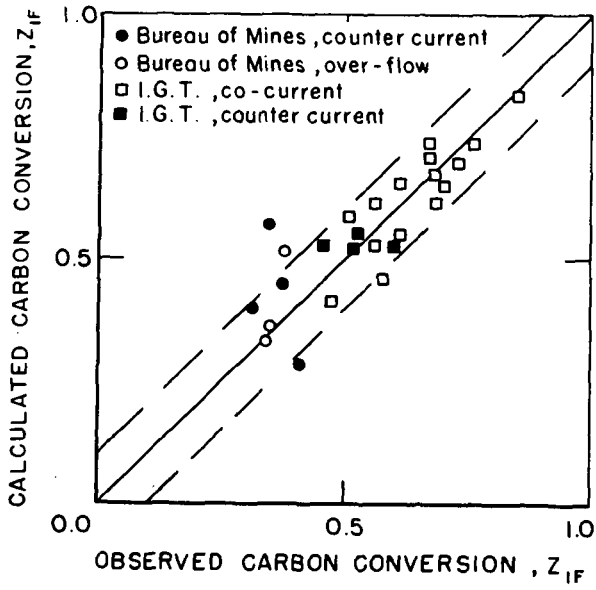


FIGURE 17- Comparison of calculated and observed carbon conversions in fluidized char hydrogasification experiments .

L-14048

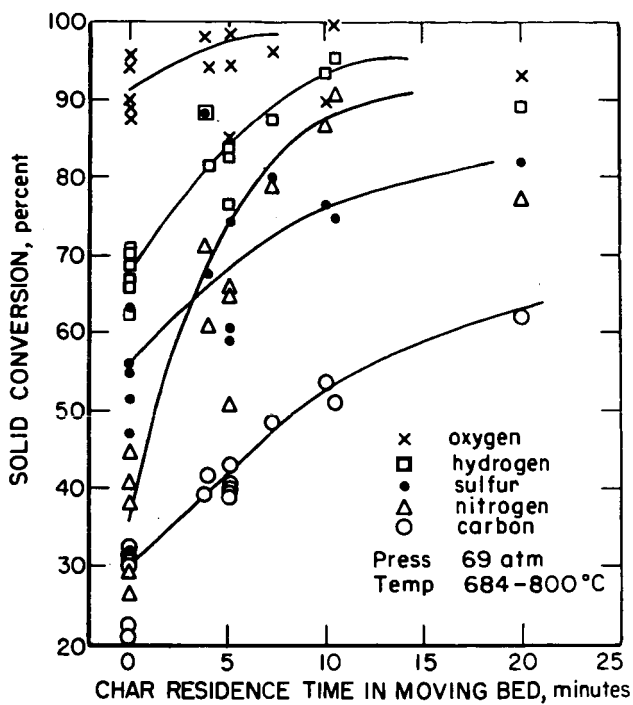


Figure 18 - Cool constituent conversion as function of residence time

L-13954

(HYDRO) GASIFICATION OF BATTELLE TREATED COAL (BTC)

S. P. Chauhan, H. F. Feldmann, E. P. Stambaugh,
and J. H. Oxley

Battelle Columbus Laboratories
505 King Avenue, Columbus, Ohio 43201

INTRODUCTION

Conversion of coal to SNG is one of the options available for alleviating the critical supply shortage of natural gas. This gas supply problem is most extreme in our eastern industrial areas. However, the only commercial SNG plants using coal as a feed stock proposed thus far have been planned for the western states. A primary reason for using western coal is that the only commercially available technology that is being considered for SNG is Lurgi technology which works best with the western noncaking coals. Rapid expansion of a coal-based SNG industry in the west is limited by factors other than finding cooperative coal. For example, the issues of reclamation of strip-mined land in arid regions, potential water supply problems, as well as the reluctance of the residents to have these areas undergo rapid industrialization can be expected to have a retarding effect on the construction of coal-conversion plants.

Availability of water, large reserves of high-sulfur coals which cannot be burned without exceeding allowable SO₂ emission levels, proximity to areas where gas shortages are most severe, the availability of an existing industrial and mining base and adequate rainfall to insure reclamation of strip-mined land are all factors that should encourage the utilization of eastern coals as SNG feedstocks. However, the utilization of eastern coals is complicated by its highly agglomerating nature.

Another constraint on the development of an SNG from coal industry whether it is located East or West is the capital required to build these plants. Recent estimates place the investment required for building a plant that will produce approximately 280 x 10⁹ SCF/day of pipeline gas from coal in the neighborhood of \$800 million.

Thus, there is a strong driving force to develop technology that will allow both the economic solution to the agglomeration problems that complicate the utilization of eastern coal and that allows the investment required to build these plants to be reduced.

One approach to lowering investment costs is by catalysis of the coal-steam-hydrogen reactions to allow the coal-steam reaction to occur at lower temperatures and the coal-hydrogen reaction at lower pressures. Numerous attempts have been made since the beginning of this century to catalyze the reaction of coal and other carbonaceous matter with steam (1-9). A few attempts have been made recently to catalyze the reaction of coal and other carbonaceous matter with hydrogen--called hydrogasification (8-12). However, it is of considerable importance to develop even better catalyst systems to promote both the hydrogasification and the steam-carbon reactions.

In this paper, we discuss the preliminary results of a novel treatment process that, in addition to enhancing the reactivity of coal to steam and hydrogen, eliminates the swelling and caking properties of even the most highly caking Eastern U.S. coals.

PROCESS DESCRIPTION

Battelle's process involves the chemical and physical incorporation of a suitable catalyst in coal.* This process is the outgrowth of a development effort to reduce the sulfur content of coal by chemical extraction that has been supported by the Battelle Energy Program. Gasification tests of the BTC showed that it had a reactivity far greater than that predictable from the results of ongoing investigations described in the literature. In addition, BTC was found to be nonswelling and noncaking. Because of these promising results, a separate effort was undertaken to develop gasification concepts and to conduct experimental feasibility studies to establish the technical and economic feasibility of this approach for the production of SNG. The results of this study have exceeded our expectations and, we believe, provide the basis for a breakthrough in SNG technology.

The catalyst usually consists of a conventional gasification catalyst and a reagent that reacts with coal to alter and open up the structure of coal facilitating the penetration of the catalyst throughout the volume of coal. During the treatment, a significant amount of catalyst (normally 1 to 3 weight percent) chemically binds to the coal while a controlled quantity of catalyst is physically incorporated into the coal. The reagent used to alter the structure of coal can be reclaimed by washing of treated coal.

EXPERIMENTAL RESULTS

A large number of gasification experiments were conducted with hydrogen and steam to determine the effects of catalyst incorporation, using the Battelle process, on the reactivity and caking properties of coal, on the gas analysis, and on the physical and chemical characteristics of the char.

Most of the experiments were conducted on 70 percent minus 200 U.S. mesh coal from the Eastern United States, containing about 30 percent volatile matter. The process was found to be applicable to coarser coals, e.g., plus 25 U.S. mesh, also. In this paper, we discuss the results with lime (CaO) as a gasification catalyst using coal from the Montour mine (Pittsburgh Seam No. 8) sized to 70 percent minus 200 U.S. mesh. The reagent and the conditions for treatment will be disclosed at a later date*. The BTC was washed prior to gasification to remove the reagent used during treatment.

The experiments were conducted in a thermobalance reactor, designed for high-pressure (1500 psig) and high-temperature (1200°C) operation, shown schematically in Figure 1. The reactor system is very similar to the one described by Gardner, et al (9). The use of the thermobalance reactor allows the monitoring of the mass of a sample as a function of time during reaction. In this manner, precise differential rate data can be obtained. The catalyst-impregnated coal was formed into 3/16-inch-diameter by 1/16-inch-long cylindrical pellets, without using a binder, since the sample container was made of 100-mesh stainless steel screen. During a run, a 2-gram sample of coal was lowered into the preheated reactor zone from the loading zone in a few seconds using a motor-operated windlass. Thus, the reaction time was precisely known. The gasification system included a steam condenser, a water trap, flowmeters, a methane-analyzer (IR), and a gas chromatograph (GC).

Prevention of Caking and Swelling

The Battelle treatment makes even the highly caking coals, e.g., coals with a free swelling index (FSI) greater than 6, completely noncaking. Figure 2 is a photograph comparing the swelling and caking of BTC with both raw coal and coal

* Coal treated by the Battelle process is abbreviated in this paper as BTC. This process is described more fully in another paper titled "The Battelle Hydrothermal Coal Process" to be presented by E. P. Stambaugh at the 80th AIChE Meeting.

treated by impregnating it with CaO as is conventionally done. As can be seen, BTC containing 7.5 percent calcium (some of which was present as an oxide with the rest chemically bound to coal) did not swell, cake, or fuse together during hydrogasification or steam gasification while the conventionally-impregnated coal containing 14.5 weight percent calcium (20.3 percent CaO) swelled, caked, and severely fused together on steam gasification. The swelling and agglomeration of the conventionally-treated coal would have been even more extreme under hydrogasification conditions. The scanning electron micrographs of raw coal and BTC coal before and after gasification are compared in Figure 3. It can be seen that BTC does not expand or swell during hydrogasification while raw coal expands and swells severely.

The use of the Battelle process to make the coal noncaking is much more attractive than the existing state of the art which involves the preoxidation of coal or the use of rather complicated gasifiers to eliminate the need for preoxidation of coal which results in the loss of volatile matter, a reduction in the reactivity of coal, and subsequently a lowering of the efficiency of the SNG process. The Battelle process, on the other hand, involves no loss of volatile matter and substantially simpler reactor systems.

Hydrogasification Rates

The reactivities of BTC under various conditions relative to raw (untreated) coal were determined from the fractional conversion versus time data obtained from the pressurized thermobalance. The fractional conversion of coal on an ash-free basis can be defined as

$$x = 1 - \frac{(\text{mass of coal at any time}) - (\text{mass of the ash})}{(\text{initial mass of coal}) - (\text{mass of the ash})} \quad 1)$$

For the purpose of determining the effect of Battelle treatment on the reactivity of coal, relative to raw coal, one can define an average relative reactivity, R_x , for a given fractional conversion, x , as

$$R_x = \frac{t_{x, \text{raw}}}{t_{x, \text{BTC}}} \quad 2)$$

where $t_{x, \text{raw}}$ and $t_{x, \text{BTC}}$ are the time required for a fractional conversion, x , of raw and Battelle-treated coal, respectively.

BTC was found to have a much higher hydrogasification reactivity than raw coal. The data in Figure 4 show that the average rate of gasification at 850°C and 500 psig hydrogen pressure based on 70 percent conversion (moisture-free basis) of BTC containing 7.5 weight percent calcium, was about 40 times faster than the raw coal.

The BTC was found to be more than an order of magnitude more reactive than coal that was impregnated with catalyst by the conventional slurry mixing at room temperature, as shown in Figure 5.

The importance of the increased hydrogasification reactivity is that high concentrations of methane should be achievable in the raw product gas thereby reducing the amount of methane that has to be produced by methanation.

One of the most important results of this work from a process economics point of view is the reduced pressure at which the BTC can be hydrogasified compared to raw coal. Figure 4 shows that even at pressures of 150 psig the BTC is much more reactive than raw coal at 500 psig. Furthermore, comparison of methane yields by graphical integration of gas analysis data (Figure 6) indicate that the methane yield, defined as the ratio of the carbon converted to methane to the total carbon

gasified, of BTC at 250 psig is the same as for the raw coal at 500 psig.

Thus, because coal can be converted to methane at pressures much lower than had been previously thought possible, investment costs for SNG plants using BTC can be substantially reduced. In addition, the reliability of the plant should be significantly increased because of the lower pressure operation.

Steam Gasification Rates

Providing heat for the endothermic steam-carbon reaction is one of the factors that contributes substantially to the cost of SNG from coal. The reason for the costliness of this step is primarily that oxygen is usually used to combust part of the carbon to provide the heat. Thus, anything that can lower the temperature required for gasifying coal with steam will reduce oxygen requirements and, thereby, the SNG costs.

Experimental data show that the Battelle catalyst incorporation process allows a substantial reduction in gasification temperature over that required for either raw coal gasification or coal that contains alkali catalysts that are impregnated into the coal by conventional means. For example, Figure 7 compares the time required to achieve various gasification conversion levels for BTC, coal conventionally impregnated with CaO and raw coal all at 825°C. Clearly, the reactivity of BTC is substantially better than either of the others even though the BTC contains only about half the concentration of Ca as in the conventionally impregnated coal.

The effect of temperature on gasification rate is shown in Figure 8. Interpolation indicates that, with BTC, gasification rates at approximately 675°C are equivalent to those at 825°C with raw coal.

More important in reducing oxygen consumption than the lowering of sensible heat requirements is the higher methane yield that one expects from lower temperature operation and the catalysis of the carbon-hydrogen reaction. The higher ratio of methane to carbon oxides achievable at the lower temperature substantially reduces the endothermicity of the carbon-steam reaction.

Reactor Systems for (Hydro) Gasification)

BTC's important advantages (i.e., low temperature and pressure operability, and no swelling or caking) will have a very important impact not only on the reactor system that is developed for integration with the coal treatment step but also on other supporting operations. Obviously, BTC could be used in any of the reactor systems currently being developed. However, because of the noncaking nature of the BTC and its high reactivity a much simpler reactor system than more currently being developed for handling eastern coals should suffice.

CONCLUSIONS

The Battelle-treated coal (BTC) is a potentially superior gasification feedstock than raw (untreated) coal or coal impregnated in a conventional manner with catalysts.

The specific advantages of BTC demonstrated by this gasification study are:

1. The prevention of caking and swelling of coal during hydrogasification and steam gasification
2. High rates of steam gasification allowing steam gasification to proceed at substantially lower temperatures than with raw coal or coal treated with catalysts in a conventional manner

3. Rates of hydrogasification as high as 40 times those of raw coal and the maintenance of this high reactivity even at pressures as low as 250 psig.

Because of these advantages we believe that the development of a (hydro) gasification process based upon the use of BTC will result in a substantial lowering of both investment and operating costs as well as allow the reliable utilization of our large eastern U.S. coal reserves for the production of clean gaseous fuels.

ACKNOWLEDGMENTS

This work was supported by the Battelle Energy Program. The technical assistance provided by Dr. John F. Foster is greatly appreciated.

REFERENCES

- (1) Elliott, M. A., Preprints of Fuel Division, American Chemical Society Meeting, 19 (3), 140 (1974).
- (2) Kroger, C., Melhorn, Gunter, Brennstoff-Chem., 19, 257 (1938).
- (3) Kroger, C., Angew. Chem., 52, 129 (1939).
- (4) Lewis, W. K., Gilliland, E. R., Hipkin, H., Ind. Eng. Chem., 45, 1697 (1953).
- (5) Kislykh, V. I., Shishakov, N. V., Gaz. Prom., 5, 15 (1960).
- (6) Willson, W. G., et al., Coal Gasification, Advances in Chemistry Series 131, Edited by L. G. Massey, American Chemical Society, Washington, D.C., 1974, p. 203.
- (7) Haynes, W. P., Gasior, S. J., Forney, A. J., Coal Gasification, Advances in Chemistry Series 131, Edited by L. G. Massey, American Chemical Society, Washington, D.C., 1974, p. 179.
- (8) Renwick, R. T., Wentrcek, P. R., Wise, H., Fuels, 53, 274 (October 1974).
- (9) Gardner, N., Samuels, E., Wilks, K., Coal Gasification, Advances in Chemistry Series 131, Edited by L. G. Massey, American Chemical Society, Washington, D.C., 1974, p. 217.
- (10) Wood, R. E., Hill, G. R., Preprints of Fuel Division, American Chemical Society Meeting, 17 (1), August, 1972.
- (11) Dent, F. J., Blackburn, W. M. Millet, H. C., Trans. Inst. Gas Engrs., 87, 231 (1937).
- (12) Dent, F. J., Blackburn, W. M., Millet, H. C., Inst. Gas Engrs., Commun., 190, 69 (1938).

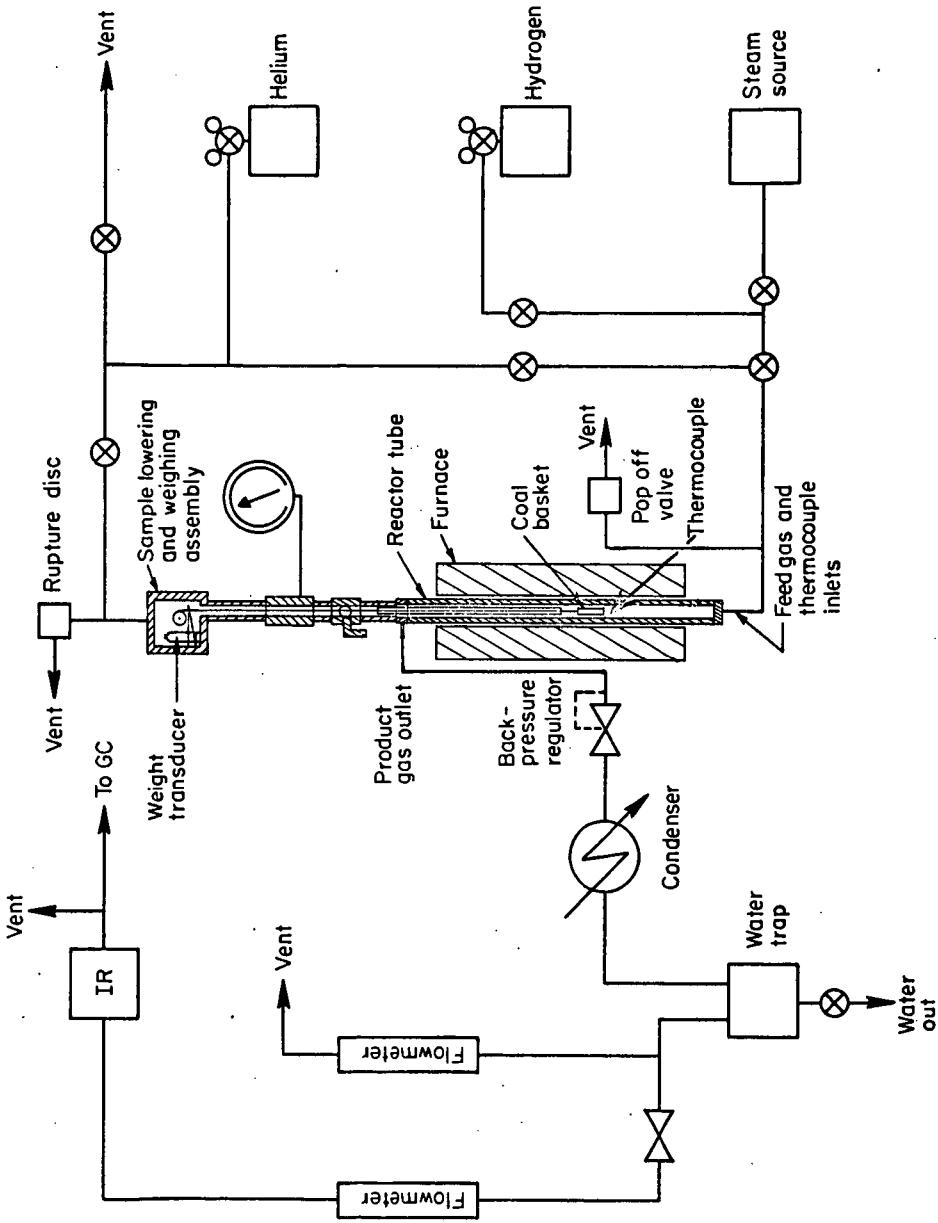


FIGURE 1. SCHEMATIC OF COAL GASIFICATION SYSTEM

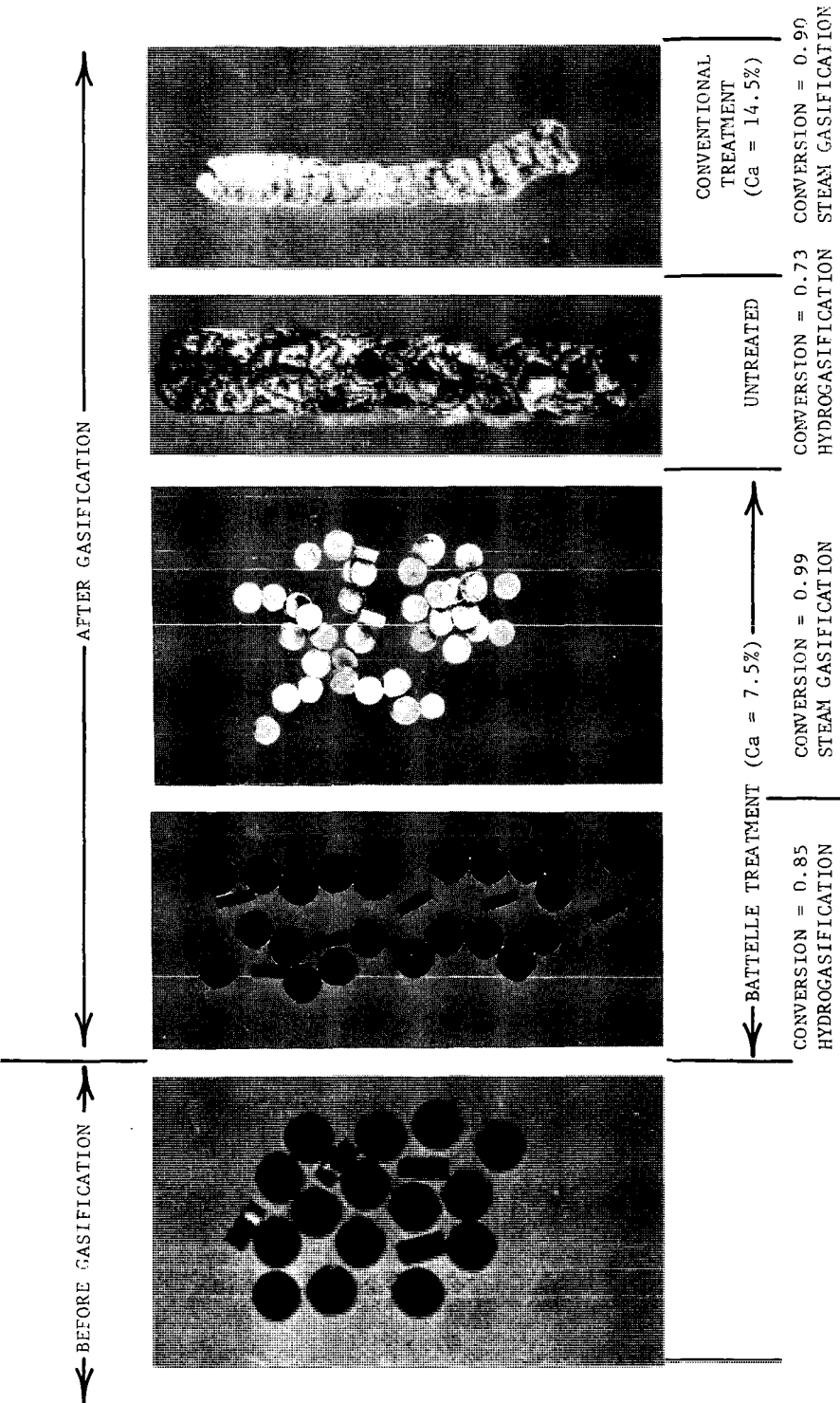
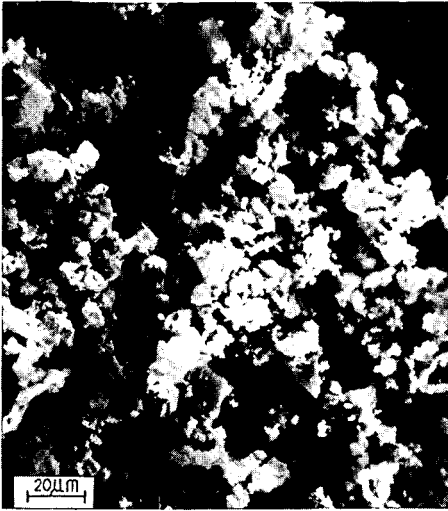


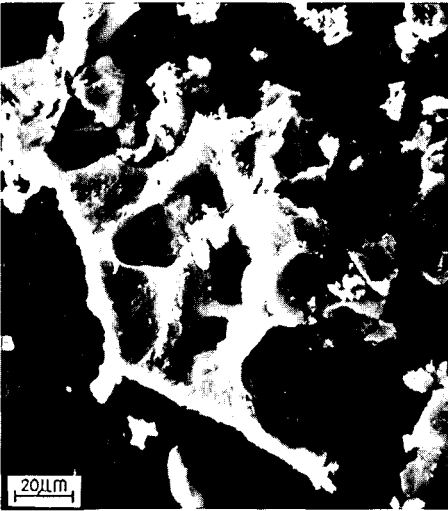
FIGURE 2. PHOTOGRAPHS OF TREATED AND UNTREATED COALS BEFORE AND AFTER GASIFICATION



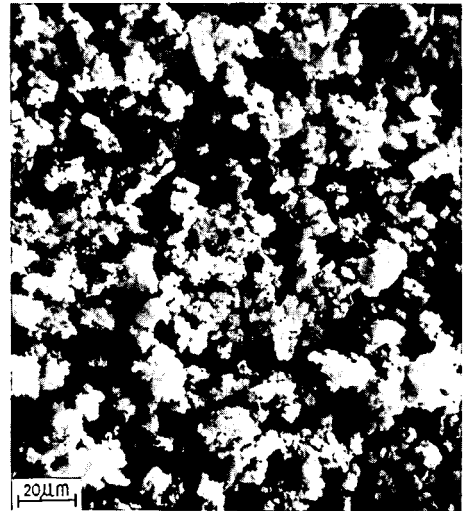
Raw Coal, Before Hydrogasification



BTC, Before Hydrogasification



Raw Coal, After Hydrogasification



BTC, After Hydrogasification

FIGURE 3. SCANNING ELECTRON MICROGRAPHS OF RAW COAL AND BTC BEFORE AND AFTER HYDROGASIFICATION

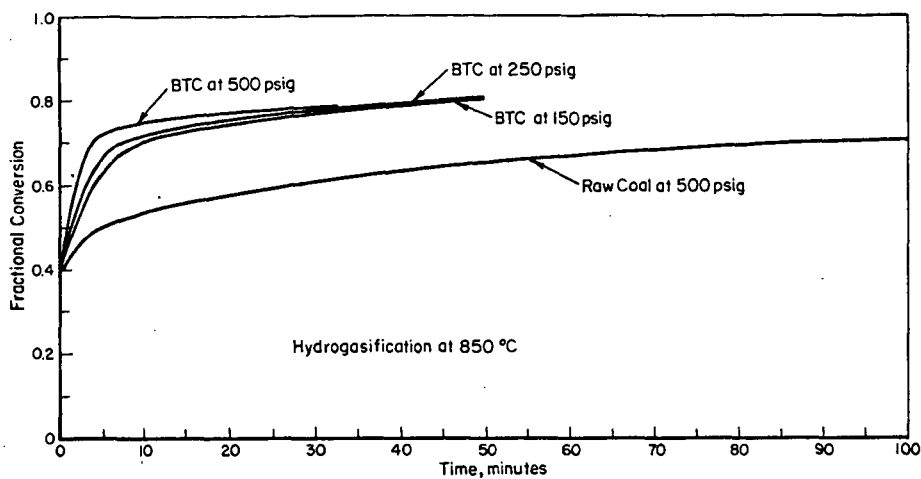


FIGURE 4. DEPENDENCE OF THE RATE OF HYDROGASIFICATION OF BTC ON PRESSURE

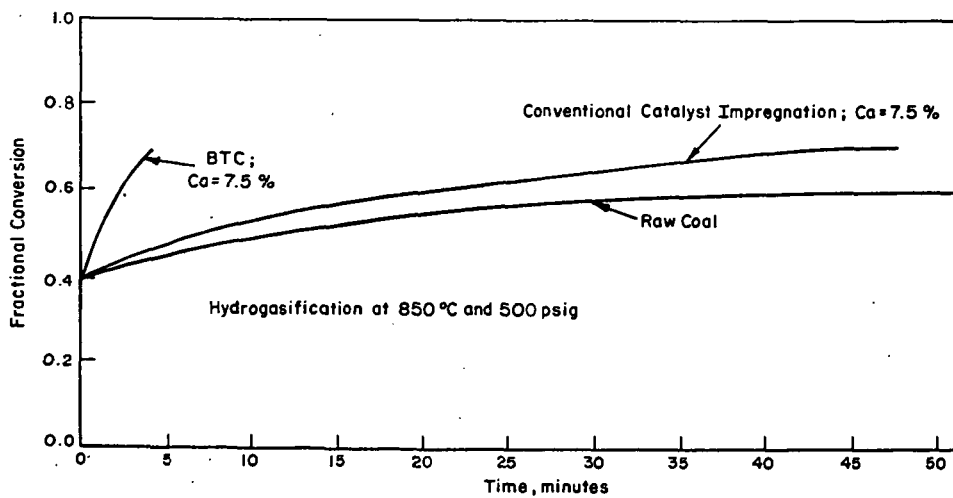


FIGURE 5. COMPARISON OF THE REACTIVITY OF BTC WITH RAW COAL AND A COAL THAT WAS CONVENTIONALLY IMPREGNATED WITH CATALYST

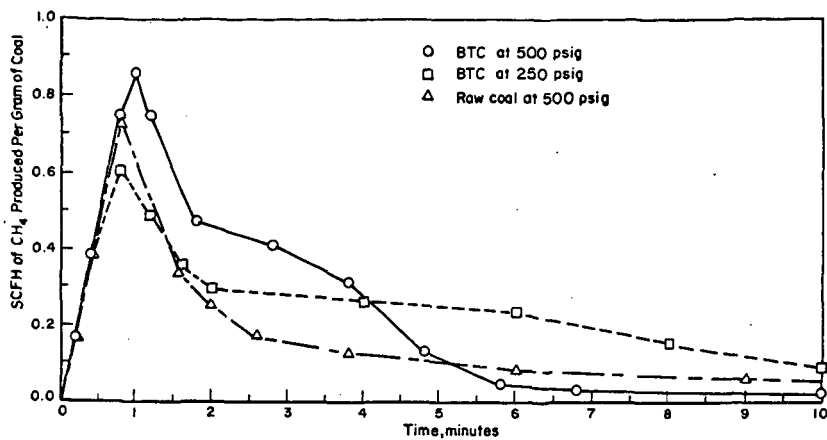


FIGURE 6. RATE OF METHANE PRODUCTION DURING HYDROGASIFICATION AT 850°C FOR COAL WEIGHING ONE GRAM (ASH-FREE) BEFORE GASIFICATION

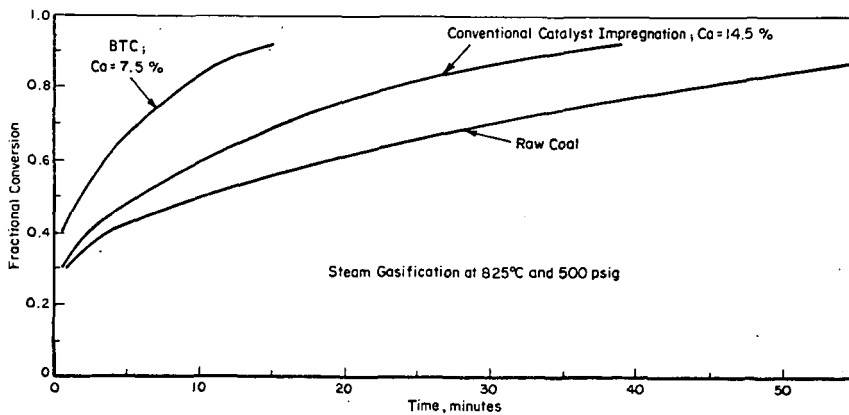


FIGURE 7. COMPARISON OF THE REACTIVITY OF BTC WITH RAW COAL AND A COAL THAT WAS CONVENTIONALLY IMPREGNATED WITH CATALYST

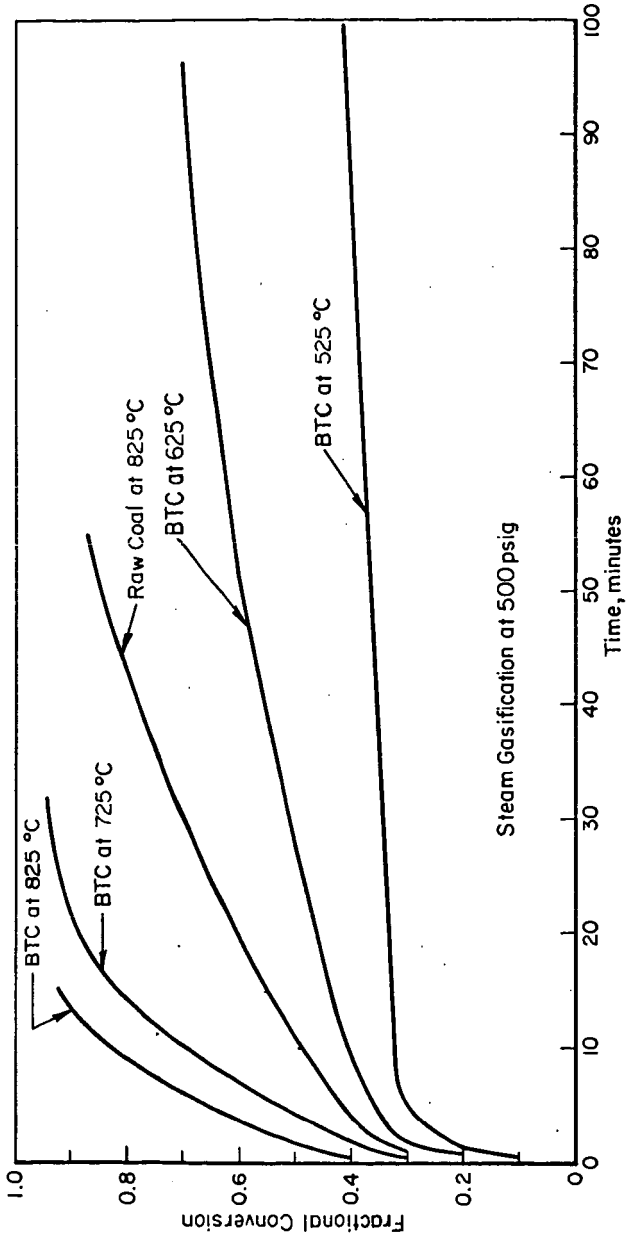


FIGURE 8. DEPENDENCE OF STEAM GASIFICATION RATE ON TEMPERATURE

FACTORS AFFECTING THE THERMAL EFFICIENCY OF A GASIFICATION PROCESS

C. Y. Wen, P. R. Desai and C. Y. Lin

Department of Chemical Engineering, West Virginia University, Morgantown, WV 26506

Abstract - Two main factors affecting the thermal efficiency of the gasification process are the amount of methane formed in the gasifier and the kind of coal used. Thermal efficiencies are calculated for the various coal gasification processes having potential for commercialization. Another way of comparing different processes, based on the second law of thermodynamics considerations in terms of available work is introduced.

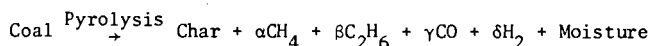
The results show that higher amounts of methane formed by direct methanation in the gasifier will result in higher thermal efficiency of the process. Thermal efficiency of Lurgi Process decreases considerably when higher ranking coals are used. The available work efficiency can be used not only for comparison but also to pinpoint inefficiencies inherent in certain process steps.

Introduction

Coal gasification processes for production of SNG can be divided into several individual sub-systems, such as coal preparation, pretreatment gasification, shift conversion, gas purification and methanation which may be followed by compression to desired pipeline gas pressure if necessary. As the products of gasification affect the overall thermal efficiency of the process greatly, gasification sub-system is described briefly in the following section.

Gasification

In gasification, coal is converted into gases that can be converted later into a pipeline quality gas having a heating value of more than 900 Btu/SCF. In a gasifier, following reactions take place:



Steam-char reaction is highly endothermic while water gas and hydrogasification reactions are exothermic. Heat required in reaction 1) can be supplied directly by coal-oxidation or indirectly by heating. (13)

The major factor affecting the thermal efficiency is the amount of methane formed in the gasifier. Amount of methane produced depends on pressure, temperature and the kind of gasifier used.

Effect of Methane Concentration in Gas from Gasifier on the Thermal Efficiency of the Process:

In Figure 1, heating value of the gas at the gasifier exit is plotted against the calculated values of overall thermal efficiency for various processes (2), (6). The results clearly show that when the amount of methane produced in the gasifier is higher, the thermal efficiency of the process is consistently higher. The reason for this is that the amount of hydrogen required to produce methane is less if hydrogen reacts with carbon in coal rather than with carbon in carbon monoxide or

dioxide as it occurs in methanator later on. Also the heat generated in the gasifier because of hydrogasification reaction can be utilized to carry out the carbon-steam endothermic reaction in the gasifier. This heat utilization is more efficient than utilization of heat recovered in the form of high pressure steam in methanation. In addition, heat generated due to hydrogasification reaction reduces the oxygen requirements reducing the consumption of energy in the oxygen plant. Coal contains certain amounts of aliphatic compounds and hydrogen in the form of volatile matter. This volatile matter decomposes into low hydrocarbon compounds such as methane, ethane, etc., by reacting with hydrogen during the pyrolysis and the initial stage of gasification. For example, in Lurgi Process using moving bed gasifier, coal and gas flows are countercurrent and hence, large amounts of hydrogen is contacted with coal in the devolatilization zone (top of the reactor) producing methane.

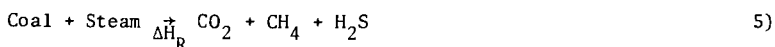
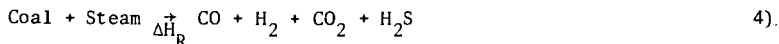
Effect of Temperature and Pressure on Methane Production:

Amount of methane produced decreases with increase in temperature, e.g., in Koppers-Totzek Process, due to high temperature (3200°F) very little methane is produced (3). And, therefore, intensive methanation is required. However, due to high temperature, tar and higher hydrocarbons decomposes into carbon monoxide and hydrogen eliminating complications in the purification section found in other lower temperature processes. Amount of methane produced increases with the increase in pressure. This increase in methane concentration continues at pressures above 400 psig. (used in Lurgi gasifiers) and quantitative data on this phenomenon have been reported by B.C.R.(4).

The other factor affecting the thermal efficiency is the kind of coal gasified. Coal can be classified into peat, lignite, sub-bituminous, bituminous, semi-bituminous and anthracite. Lignite and sub-bituminous coals are usually caking coals and form non-porous coke on heating.

Effect of Coal on the Efficiency of the Gasification Process:

In coal-steam reaction, theoretically the following two forms of reactions can take place.



Even though reaction 4 and 5 are extremes, they take place simultaneously in a gasifier with few exceptions. For example, in Koppers-Totzek gasifier reaction 4 occurs while in Hydrane gasifier reaction 5 occurs to large extent. Both of the above reactions are endothermic. Endothermicity of the reaction represents the amount of heat required to complete the reaction and in gasification, this heat is supplied by oxidation of coal with oxygen. The endothermicity of the reaction is different for different coal and since heat is supplied by oxidation of coal, it may be expected to be directly related to the efficiency of the process.

For three different coals, data shown in Table 1 were reported by Koppers company (3). These data show that the amount of oxygen and steam required for gasification increases with the increase in volatile matter. The data also show that the composition and the heating value of the gasifier product are almost similar in all cases and thus are nearly independent of kind of coal used. Carbon conversion is a function of reactivity of coal. Lignite and sub-bituminous coals can be converted almost completely while conversion of high volatile coals approaches 95%-97% (3). The same kind of data collected from trials at Westfield, Scotland, were reported by Lurgi for Montana, Illinois 5, Illinois 6 and Pittsburgh 8 coals.(1),(11)

TABLE 1 Effect of Coal on Gasifier Products, Koppers-Totzek Process (3)

Coal	Sub-bituminous Western	High Volatile B-Bituminous Illinois	High Volatile A-Bituminous Eastern
<u>Composition (wt. %)</u>			
C	56.76	61.94	69.88
H	4.24	4.36	4.90
O	13.18	6.73	7.05
N	1.01	0.97	1.37
S	0.67	4.88	1.08
Ash	22.14	19.12	13.72
Moisture	2.00	2.00	2.00
Heating Value BTU/lb.	9,888.	11,388.	12,696.
<u>Gasification</u>			
Oxygen required T/T of coal	0.649	0.704	0.817
Steam required T/T of coal	0.136	0.27	0.294
<u>Gas Composition</u> Dry Basis (Vol %)			
CO	58.68	55.38	55.90
CO ₂	7.04	7.04	7.18
H ₂	32.86	34.62	35.39
N ₂	1.12	1.01	1.14
H ₂ S	0.28	1.83	0.35
COS	0.02	0.12	0.04
	<u>100.00</u>	<u>100.00</u>	<u>100.00</u>
Gas Heating value BTU/SCF	295.1	290.2	294.4
No. of moles/ton of coal	136.4	156.6	174.8
<u>Efficiency %</u>			
Heating value of gas/ Heating value of coal	77.3	75.8	77.0
Heating value of gas/ Heating value of coal + + coal used for pro- duction of steam and power required.	69.7	67.9	68.7

These data are shown in Table 2. It can be concluded that higher operating temperature is necessary with decreasing coal reactivity. Oxygen and steam consumptions increase with the decrease in coal rank. However, yield of methane remains fairly constant for different kinds of coal. It also shows that efficiency of gasification, allowing for the coal equivalent of steam and oxygen supplies, decreases substantially with the increase in coal rank.

The type of coal processes also affects the amount of water required in a gasification process. The factors affecting the water requirements are:

- a) Moisture content
- b) Reactivity of coal
- and c) Sulfur content of coal.

For a plant producing 250 MMSCF of pipeline gas, the total water requirement is roughly about 19,000 gpm. when lignite coal is used while for bituminous coal water required is about 22,500 gpm.

Thermal efficiency calculations done on the basis of first law of thermodynamics are useful for comparison of coal gasification processes. Another way of comparing different alternatives is to calculate energy utilization efficiency based on the second law of thermodynamics, which is defined as the ratio of total output of work equivalent in all outgoing streams to the total input. The main advantage of this approach is its ability to compare energy utilization efficiency of different processing schemes and alternatives, which may start from different energy resources and may produce different products, in a consistent way. It also pinpoints the inefficiencies inherent in certain process steps.

From second law of thermodynamics, the available work, de , can be expressed in terms of enthalpy change (dH) and entropy change (ds) as:

$$de = dH - T_0 ds$$

where T_0 is the temperature of the surrounding.

For a closed system in equilibrium at T_0 , when no work can be obtained from it in the given surroundings,

$$e = H - H_0 - T(S - S_0)$$

is the maximum amount of work which can become available from the system if it can exchange heat only with a heat reservoir at T_0 . A process stream carrying \dot{n} moles of i per unit of time and performing work \dot{w} in the same time is equivalent to a flux of available work

$$\dot{e} = \sum_i \dot{n}_i e_i + \dot{w}$$

At steady state, for any system, the available work \dot{e}_{in} entering the system is always greater than or equal to that leaving the system.

$$\dot{e}_{in} \geq \dot{e}_{out}$$

Then, the available work efficiency η can be defined as

$$\eta = \dot{e}_{out} / \dot{e}_{in}$$

The fraction $(1-\eta)$ is being lost due to irreversible processes causing an entropy production σ

$$(1-n) \frac{Q}{T_{in}} = T_0 \sigma = I$$

Where I is the irreversible work associated with the entropy change.

The datum level used in available work efficiency calculations, is defined as one in which an existing substance, when in equilibrium with the surrounding, will have zero available work.

The bases used for calculations are air and water at 1 atm. and 25°C. Under these conditions, it may be assumed that available work from CO₂ and SO₂ is zero.

Table 2 Effect of coal on Gasifier Products
Lurgi Process (1)

Coal	Rosebud Montana	Illinois #5	Illinois #6	Pittsburgh #8
Composition wt %				
C	50.56	64.11	64.16	74.15
H	3.18	4.36	4.34	5.04
O	9.80	7.04	8.10	4.52
N	0.91	1.22	1.21	1.35
S	1.09	3.13	2.80	2.52
Ash	9.76	8.20	9.16	7.84
Moisture	24.70	11.94	10.23	4.58
	100.00	100.00	100.00	100.00
Heating value Btu/lb	8611.	11456.	11464.	13442.
Gasification				
Oxygen required T/T of coal	0.24	0.46	0.45	0.59
Steam required T/T of coal	1.25	2.25	2.51	3.24
Gas composition Dry Basis (%)				
CO	15.1	17.6	17.3	16.9
CO ₂	30.4	31.0	31.2	31.5
H ₂	41.1	38.8	39.1	39.4
N ₂	1.2	1.5	1.2	1.6
H ₂ S	0.5	1.1	1.1	0.8
CH ₄	11.2	9.2	9.4	9.0
C ₂ H ₆	0.5	0.5	0.7	0.7
C ₂ H ₄	-	0.3	-	0.1
	100.0	100.0	100.0	100.0
Gas heating value excluding H ₂ S Btu/SCF	239.	291.	290.	285.
No. of moles/ton of coal	212.6	160.6	158.	187.
Efficiency %				
Heating value of gas/ heating value of coal	79.9	77.5	75.8	75.3
Heating value of gas/ (Heating value of coal gasi-58.7 fied + coal used for produc- tion of steam and power re- quired)		52.8	50.9	48.8

Based on above datum level, the corresponding work equivalent of the chemical elements are calculated and are shown in Table 3.

Table 3 Available Work of Chemical Elements

Substance	State	ϵ at 25°C & 1 atm. Btu/mole
Coal*	Solid	224,460 (Btu/mole-C)
C	Solid	168,000'
S	Solid	127,560
O ₂	Gas	1,670
N ₂	Gas	250
H ₂	Gas	101,210
H ₂ O	Gas	3,700
CO	Gas	109,780
CO ₂	Gas	0
CH ₄	Gas	348,570

*Pittsburgh seam coal is used. Entropy of coal is about 4 cal/gmole-carbon °K.

Energy utilization efficiency based on available work and percentage distribution of irreversibility for different process steps of Lurgi, Koppers-Totzek and Hydrane Processes were calculated. The results are shown in Table 4.

Table 4 Evaluation of irreversible work distribution in the coal gasification processes to produce pipeline gas.

(Feed Coal = 1 ton basis, Pittsburgh seam)

	Lurgi-Gasifier	Koppers-Totzek Gasifier	Hydrane Process
Feed coal, available work x 10 ⁶ Btu	25.74	25.74	25.74
Product pipeline gas, available work x 10 ⁶ Btu	15.30	13.49	16.72
Irreversible lost work x 10 ⁶ Btu	10.44	12.25	9.02
Thermal eff.	64%	54%	72%
Available work eff.	59%	52%	65%
Irreversible lost work distribution, x 10 ⁶ Btu			
Gasifier	3.82	4.03	4.16
Heat exchanger and spray tower	0.96	1.06	0.81
Shift converter	0.33	1.41	0.30
Purification unit	1.16	1.28	1.05
Methanation unit	1.09	1.80	0.13
Oxygen plant	1.34	2.06	0.86
Steam and power plant	1.74	0.61	1.71

Acknowledgment

This work was supported partially by National Science Foundation and partially by ERDA.

References

1. Elgin, D. C., "Results of Trials of American Coals in Lurgi Pressure-Gasification Plant at Westfield, Scotland", proceedings of Sixth Synthetic Pipeline Gas Symposium, Chicago, Illinois, October 1974.
2. Feldmann, H. F., Wen, C. Y., Simon, W. H., Yavorsky, P. M., "Supplemental Pipeline Gas from Coal by the Hydrane Process", paper presented at the 71st National AIChE Meeting, Dallas, Texas, February 20-23, 1972.
3. Fransworth, J. F., Mitsak, D. M., Kamody, J. F., "The Production of Gas from Coal Through a Commercially Proven Process", Koppers Company, Inc., Pittsburgh, August, 1973.
4. Hendrickson, T. A., "Synthetic Fuels Data Handbook", pp. 168-182, Cameron Engineers, Inc., 1975.
5. Howard, H. C., Ind. & Eng. Chem. Vol. 44, No. 5, p. 1083, 1952.
6. Huebler, J., Lee, B. S., and Schora, F. C., Jr., "Hygas Coal Gasification Process", For Publication in the Handbook of Energy Technology, June, 1974.
7. Lowry, H. H., Chemistry of Coal Utilization, p. 208, p. 250-260.
8. Mazumdar, B. K., Coal Science, p. 475, 1966.
9. Mudge, L. K., Schietelbein, G. F., Li, C. T., and Moore, R. H., "The Gasification of Coal, A Batelle Energy Program Report, July, 1974.
10. Riekert, L., Chem. Eng. Sci., Vol. 29, p. 1613, 1974.
11. Rudolph, R. F. H., "Processing of American Coals in a Lurgi Gasifier", Proceedings of Sixth Synthetic Pipeline Gas Symposium, Chicago, Illinois, October, 1974.
12. University of Michigan, "Evaluation of Coal Conversion Processes to Provide Clean Fuels", Final Report, p. 376-379, Feb. 1974.
13. Wen, C. Y., "Optimization of Coal Gasification Processes", Interim Report to Office of Coal Research, 1972.

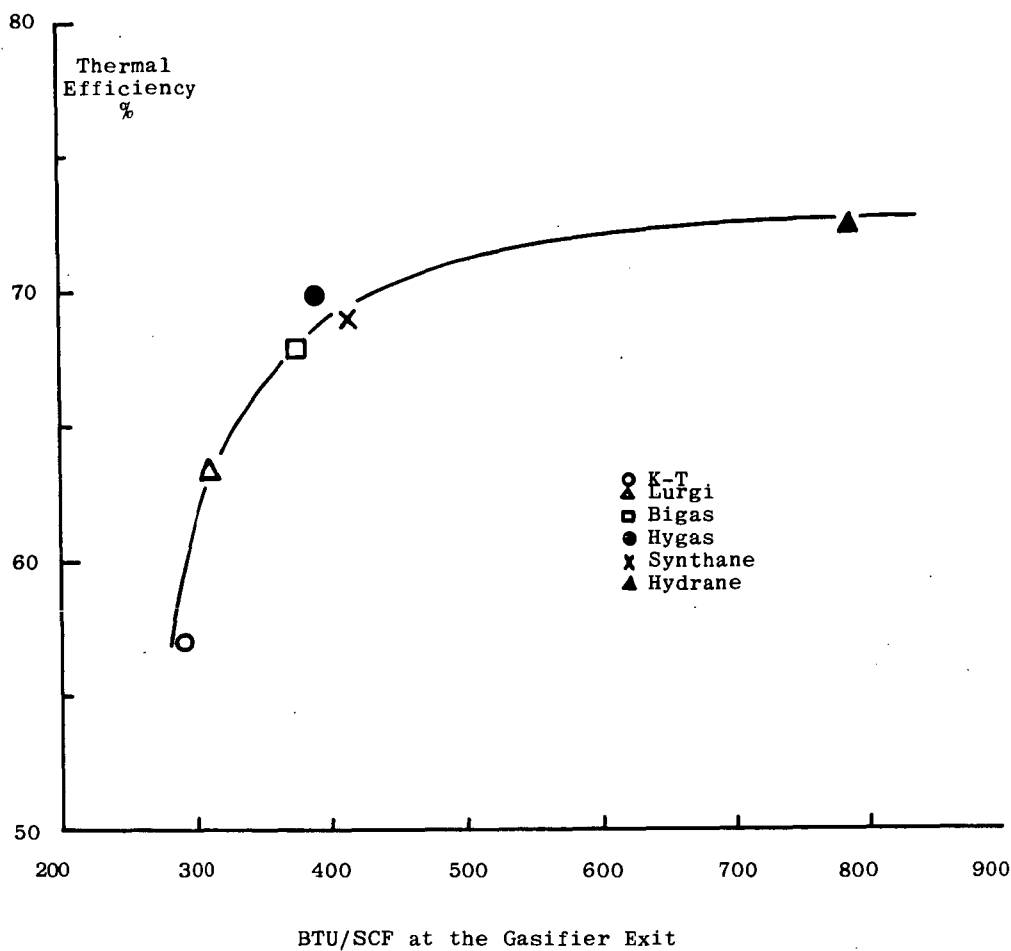


Figure 1 Effect of Amount of Methane Produced in the Gasifier on the Thermal Efficiency of the Process.

LABORATORY EVALUATION OF PROPERTIES
OF FLY ASH-IRON OXIDE ABSORBENTS FOR H₂S
REMOVAL FROM HOT LOW-BTU GAS

E. C. Oldaker, A. M. Poston, Jr., and W. L. Farris, Jr.

U.S. Energy Research and Development Administration
Morgantown Energy Research Center
Morgantown, West Virginia

INTRODUCTION

The Morgantown Energy Research Center is conducting research on solid, regenerable absorbents to remove H₂S from hot (1,000°-1,500°F) low-Btu fuel gas made by gasifying coal with air and steam. The heating value of low-Btu gas ranges from 100 to 150 Btu per cubic foot, which makes it uneconomical for long distance transport but is suitable for "on-site" utilization to fire powerplant or industrial boilers. Removal of the sulfur (largely H₂S) from the gas while still hot affords two benefits for the utilization of low-Btu gas as a fuel. First, the gas can be directly fired in boilers and meet environmental standards concerning sulfur emissions to the atmosphere. Second, the sensible heat of the gas is retained, thereby increasing the overall thermal efficiency of the fuel.

The use of iron oxide to remove H₂S from industrial gases has been practiced for many years. Coke oven gases have been desulfurized by fixed or fluid beds of iron oxide at temperatures up to 752°F (1). Abel et al. (2) and Shultz (3) reported the results of laboratory studies in which solid absorbents were used to remove H₂S from hot, simulated and actual producer gas. Clay and Lynn (4) described the use of iron oxide supported on alumina to remove NO_x and SO_x from powerplant stack gases at temperatures approaching 1,000°F. They injected a stream of synthesis gas (CO + H₂) to reduce the SO₂ to H₂S and NO to N₂ before passing the flue gases over the catalyst.

Laboratory investigations are being directed toward developing a solid, regenerable absorbent composed of iron oxide supported on a matrix of fly ash which has both the absorption capacity and physical strength believed to be required for a commercial application in removing H₂S from low-Btu fuel gases at temperatures above 1,000°F.

Mechanical problems involving attrition of the iron oxide leading to unacceptable carry-over and absorbent replacement, and plugging or fouling of system components were some of the shortcomings of previous work using iron oxide to remove H₂S from various type gases. By supporting the iron oxide upon a matrix of fly ash, these problems are overcome. The development of a solid, pellet-sized absorbent having adequate surface area or pore volume which effectively removes H₂S eliminates the need for fluidization and/or the use of very small iron oxide particles. Another advantage is the lower capital and operational costs when using a fixed bed for absorbing, in which continuous recycling and replacement of iron oxide is not required.

The process described herein is designed to remove H₂S from raw producer gas above 1,100°F by passing it through a fixed bed of fly ash-iron oxide absorbents. The H₂S reacts with the Fe₂O₃ to form FeS and FeS₂. When the absorbents are fully sulfided, the FeS+FeS₂ is easily returned to Fe₂O₃ by passing air through the bed for a short period.

MATERIAL, EQUIPMENT AND PROCEDURES

Fly ash from a coal-fired powerplant near Morgantown, West Virginia, was used exclusively as supporting material for the fly ash-iron oxide absorbents. This fly ash was similar to the fly ash from three other local sources. A typical analysis

of the fly ash was: SiO_2 -51.7%, Al_2O_3 -24.6%, Fe_2O_3 -15.9%, CaO -3.06%, K_2O -2.38%, MgO -0.94%, TiO_2 -0.84%, Na_2O -0.66%, and P_2O_5 -0.34%. The BET surface area was 0.95 m^2/gm . The fly ash was dried and screened to remove agglomerates but was not otherwise processed.

The iron oxides used were Fisher Certified or MCB Technical Grade with BET surface areas of 10 and 8.5 m^2/gm respectively. (These iron oxides were used to maintain consistent data throughout the investigations. Commercial iron oxides will be used for later tests.)

Laboratory grade, high-swelling bentonite (2 grams to 24 milliliters) of 63% SiO_2 and 19% Al_2O_3 content, and technical grade 40-42° Baume (3.22 $\text{SiO}_2/\text{Na}_2\text{O}$) sodium silicate solution, were used as additives to improve physical strength.

The dry ingredients were thoroughly mixed using a split-sleeve mixer, then transferred to a small portable-type cement mixer. Water was added to the mixture to obtain correct consistency for extrusion. The extrusion apparatus produced 3/16-inch diameter by 3/4-inch long extrudates through a multiple die arrangement at the end of a 2-inch diameter by 6-inch long barrel and auger. The solid extrudates were dried, then sintered at temperatures and times required. The crush strength (force applied across the diameter) was measured on a Tinius-Olsen testing machine.

Figure 1 is a flowsheet of the equipment used to conduct absorption and regeneration experiments with the iron oxide-fly ash absorbents. An entrainment carbonizer, used in previous coal carbonization research (5) was adapted to simulate on a small scale the production of hot, raw producer gas (containing coal-related tars and particulates) or clean, hot producer gas. Various gases to make up the producer gas were supplied from bottled gases metered into a manifold and into the gas preheater. Water was metered and injected into the gas preheater to simulate the amount of steam in actual producer gas.

When tars and particulates were required in the experiment, coal was fed into the carbonizer by a screw-type feeder. The coal entered the top of the carbonizer, 4-inch diameter by 18-inches high which was electrically heated, and was charred as it fell through; char and ash were removed through a lock hopper at the bottom. The outlet gas contained tars, light oils, and particulates and the gas make up was similar to actual producer gas. Eighty percent of the total gas passed through the absorption bed; the other 20% provided a sample of the input for analysis. The absorption vessel was 2-inches inside diameter by 45-inches long. A stainless steel screen 31-inches down from the top supported the absorbent bed. The vessel was externally heated by high temperature heating tapes. Both the vessel and heating tapes were covered with insulation to prevent excessive heat losses. Five internal thermocouples were used to monitor bed temperatures.

The input gas sample system consisted of a heated dust filter, an electrostatic precipitator, a water-cooled condenser, a silica gel trap and a dry gas meter. The input gas was analyzed for H_2S only using the Tutwiler method (6). The gas sample system following the absorption bed was identical to the input sample system except the gas stream passed through a bank of infra-red gas analyzers and was analyzed for CO , CO_2 , CH_4 and H_2 . H_2S was again analyzed by the Tutwiler method.

On start-up, the preheater was heated to 950°F and the carbonizer chamber preheated to 1,300°F. The absorbent bed was heated to 1,100°F before starting the absorption period. The gas flow was allowed to proceed until a predetermined amount of H_2S was found in the gas passing through the absorption bed, usually 400 grains H_2S per 100 standard cubic feet of gas. The input H_2S concentration, as near as possible, was maintained at a level decided upon before the start of the experiment. H_2S concentrations much higher than normal producer gas were used to shorten the time required to complete an experiment. Results have been cross checked with those

made with producer gas H_2S concentrations and no major differences in results were obtained. Total gas flow through the system varied with the experiment and ranged from 25 to 35 scfh. When the predetermined H_2S concentration was reached, the input gases were turned off and a nitrogen purge started. The system was purged for 30 minutes with nitrogen to prepare the system for the regeneration cycle.

Figure 2 is a flow diagram for the absorption tests made using a 1,500 scfh side stream from the MERC stirred, fixed-bed gasifier (7). The gas was maintained at its exit temperature of $1,100^{\circ}F$ by means of electric heaters and insulation surrounding the pipe. The hot gas was brought into contact with the iron oxide-fly ash absorbents in a 6-inch diameter, 4 foot high stainless steel absorber equipped with electric shell heaters and insulated for temperature control. The sulfided absorbents were regenerated by introducing air at $70^{\circ}F$ into the 1-inch inlet of the absorber and piping the SO_2 -rich gas to the stack through the 1-inch exit line. Inert gas was also piped into the absorber inlet for bed temperature control during regeneration. The complete system was maintained above $1,000^{\circ}F$ to prevent condensation of the tar which would affect the absorbents or plug the lines to and from the absorber. The absorber contained 73 pounds of 3/16-inch diameter absorbents, composed of 25% iron oxide and 75% fly ash with 3%, by weight, of bentonite added as a binder. A space velocity (scfh gas/cu.ft. absorbent) of 1,900 was maintained throughout the tests.

EXPERIMENTAL RESULTS

Four important criteria must be met before an absorbent can be considered optimum for process consideration. The absorbent must be physically strong to withstand handling, loading and cyclic thermal degradation. The absorbent must have the necessary surface area containing iron oxide particles to effectively react with H_2S and provide enough absorptive capacity for economical operations. The absorbent should be regenerable so that material and replacement costs are at a minimum. Finally, and equally important, the absorbent should have a satisfactory life expectancy.

Absorbents containing additives such as bentonite, sodium silicate and magnesium sulfate were prepared and tested for their effect on physical strength. The addition of bentonite greatly increased both hardness and crushing strength. However, the addition of 3% bentonite caused a sharp decrease in H_2S absorption capacities. The data, as shown in Table 1, indicate that bentonite does not adversely effect absorption capacity until 1.5% is added and the lesser amounts are effective in providing strength to the absorbent. Sodium silicate also produced an extrudate having a crush strength of approximately 70 pounds per one centimeter length, as opposed to around 16 pounds for an untreated extrudate, without appreciable loss in absorption capacity. On the other hand, the addition of magnesium sulfate decreased the absorption capacity without benefiting the physical strength of the absorbent.

The variables effecting absorption capacity that were tested included porosity, amount of iron oxide contained in the absorbent and steam concentrations of the hot gas being desulfurized. Ten percent, by weight, of ordinary starch was added to and burned out from the fly ash-iron oxide absorbent mixture to determine if additional porosity could be obtained. This absorbent showed nearly twice the absorption capacity of the untreated absorbent; however, it did not develop the crush strength observed earlier with a similar absorbent containing 1% bentonite. After sintering for 2 hours, the absorbent showed a decrease in absorption capacity with very little increase in physical strength.

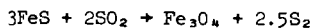
By adding varying amounts of iron oxide mixed with fly ash in preparing an absorbent mixture, it was found that 25% iron oxide with 75% fly ash showed the better absorption capacity. When 33% iron oxide was used, a significant decrease in absorption capacity was noted (2). When 13% iron oxide was used, the same significant decrease was observed. It is believed that particle size distribution of the iron

oxide and fly ash controls this phenomenon. Another disadvantage of higher amounts of iron oxide was the lesser physical strength indicated by noticeable amounts of absorbent degradation during testing while those at lesser percent were quite resistant to degradation.

Abel (2) reported that producer gas containing steam reduced the capacity of the absorbent to react with H_2S . At $1,500^{\circ}F$ the absorption capacity was reduced about 25% in wet (8%) simulated gas. This phenomenon is not surprising since steam is a product of reaction in the absorption of H_2S . Tests performed under the present investigations using improved absorbents also showed reduced capacity. The water-gas shift reaction, $CO + H_2O = CO_2 + H_2$, occurred with the iron oxide-fly ash absorbent bed catalyzing the reaction to show an approximate shift of 2% for H_2 and CO_2 . This effect may be beneficial when the end use is feed stock for a methanation plant since the H_2/CO ratio is brought closer to the desired 3 to 1 value for the dry CO_2 -free gas.

Regeneration of the sulfided absorbents was accomplished by using air or mixtures of air and nitrogen. Air regeneration at 12 scfh produced bed temperatures of $1,700^{\circ}$ to $1,900^{\circ}F$ in the zone of regeneration. Lower flow rates reduced temperatures 100° - $400^{\circ}F$. Dilution of air with nitrogen had a similar effect.

At $900^{\circ}F$ regeneration started immediately and proceeded rapidly, depending on the space velocity, to completion. The higher the rate of air introduction, that is, the greater the flow of oxygen, the higher the temperature of regeneration. The temperature increased and decreased rapidly as the zone of reaction passed through the bed and it was not known how much damage to the absorbent occurred at high temperatures for short durations. It was postulated to be around $1,800^{\circ}F$ but a safer long-term maximum temperature for the absorbents should be $1,500^{\circ}F$. The dilution of the air with nitrogen was one method of controlling the maximum bed temperature without losing time in regeneration at lower flow rates. Figure 4 shows a typical temperature profile on regeneration using 12 scfh air flow rate compared with using 12 scfh air and 12 scfh nitrogen or a total of 24 scfh flow rate. Number 1 thermocouple is near the inlet while No. 5 thermocouple is located near the exit from the bed. TC-5 was consistently lower in all regenerations. This was believed to have been caused by the partial regeneration of the bed by unreacted oxygen from the main zone of regeneration with possibly some credit given to the endothermic reaction between FeS and SO_2 . Elemental sulfur was found in the exit piping and valves. It would be produced according to the following reaction:



Sulfur balances calculated using the H_2S input versus SO_2 in the outlet gas averaged about 95% recovery as SO_2 . Several batches of regenerated absorbents were analyzed for total sulfur after several cycles of absorption and regeneration and the sulfur content was found to be less than 1%. This would indicate that very little sulfate was formed at the high regeneration temperatures used.

Regeneration was essentially completed in 120 minutes when the air flow rate was 12 scfh. At 6 scfh, regeneration required 190 minutes. A 1 to 1 mixture of air and nitrogen at 24 scfh flow rate required a regeneration time of 150 minutes. Since the normal absorption cycle required about 5 hours, enough time was available to use any of the above flow rates. Aside from critical temperature design criteria, another consideration was the SO_2 -enrichment that was needed for downstream conversion or reduction. The SO_2 concentration in the effluent gas approximated 11½-12% when using air for regeneration; however, when dilution gas was used, the SO_2 concentration was proportionate to the amount of diluent used, being around 5½-6% at 1 to 1 dilution of air with nitrogen. Typical regeneration curves, depicted by Figure 5, showed that maximum SO_2 concentration was reached in less than 5 minutes and dropped from maximum to base line in approximately 20 minutes. These time factors are noted for both air and diluted air regeneration schemes.

The life expectancy of a specific absorbent could only be determined with accuracy by continuous cycling until the absorption capacity dropped below acceptable limits or degradation and fusion caused operational problems. This was costly in terms of money and manpower. However, one absorbent bed has been through 30 absorption-regeneration cycles using simulated producer gas containing both coal-related tars and particulates to study the cyclic effect upon the absorbents. Absorbents used in this study were prepared by adding 10%, by weight, of starch to an absorbent mixture containing 25% iron oxide and 75% fly ash. The absorbent was sintered at 1,800°F for 30 minutes in an oxidizing atmosphere. The producer gas was maintained at 1,100°F throughout the absorption cycle at an average flow rate of 15 scfh. The H₂S concentration in the inlet gas stream was maintained at 2% and the steam content between 7 and 11%.

Regeneration after each absorption cycle was accomplished by using a 12 scfh air flow rate for approximately 2 hours. The average absorption cycle lasted 5 hours. Figure 3 indicates the absorption capacity of each cycle. The increasing absorption capacity through the first few cycles was believed due to the result of burn-out of the residual starch during regeneration where temperatures approached 1,300°F for short periods. The continuing starch-char burnout would open more pores for better gas penetration to the iron oxide particles in the absorbent. After 30 cycles, the absorbent was in good condition without visible signs of deterioration or caking. Table 2 lists 6 of the 30 runs which were representative of the typical information computed from the raw data obtained during operations.

Abel (2) earlier reported that sintered pellets containing 25% iron oxide and 75% fly ash underwent 174 absorption-regeneration cycles using hot (1,000°-1,500°F), clean simulated producer gas without visible damage to the pellets or appreciable loss in absorptive activity. The absorption capacity averaged 8% for those tests conducted at 1,100°F. The pore volume reached a constant value of 0.12 cubic centimeters per gram after 30 absorption-regeneration cycles.

Four 15-hour absorption runs were completed using a 1,500 scfh sidestream of hot (1,100°F) raw producer gas made by gasifying high volatile bituminous coal with air and steam in a 42-inch stirred, fixed-bed gasifier (7). These runs were made primarily to demonstrate the feasibility of the process at much higher gas flow rates and at actual process conditions. The four 15-hour runs were completed successfully with an average absorption capacity of 8.25 wt.-pct. Ninety to 94% of the H₂S was removed from the hot producer gas which averaged 0.5% H₂S entering the absorber. Table 3 shows the data and run conditions for the 4 periods. The absorbents remained in good condition for the duration of the tests and were not adversely affected by the tars and particulates in the effluent gas. The tars could be tolerated if the absorber bed temperature remained above 1,000°F. The fine carbonaceous particulate accumulated in the absorber bed during absorption was burned off during the regeneration cycle. An insignificant amount of ash residue remained in the bed after regeneration which was determined by visual inspection of the bed after completion of the 4 cycles. Pressure drop across the bed increased to 8-9 psig at the end of the absorption periods but returned to 1.5 psig after regeneration of the absorbent bed.

CONCLUSION

The laboratory tests conducted thus far indicate that the fly ash-iron oxide absorbent containing bentonite is an adequate absorbent for removing H₂S from raw producer gas at temperatures between 1,000°F and 1,500°F. The physical strength, expressed as the crush strength (measured across the diameter), of 50 to 100 pounds per one centimeter of length is considered adequate to withstand handling, transportation and placement of the absorbents. The absorbent is regenerable and has an average capacity of 10 wt.-pct. This amount of absorptive capacity coupled with an efficiency of 90-94% permits ample time "on line" and provides an effluent gas which meets the existing environmental air standards.

Thirty and 174 absorption-regeneration cycles were completed without visible deterioration or loss of absorptive capacity. Although not conclusive, these tests indicate that the absorbents could withstand many more cycles. Eventual pore closing by fusion due to long time thermal cycling and/or micron size particulate exposure needs to be investigated further. These two occurrences would be the most likely limiting factors on life expectancy of the absorbents.

Laboratory work is now being performed to find a suitable substitute for the fly ash so that higher temperatures and faster regeneration would be permissible. Finding cheaper sources of iron oxide and comparing results of these oxides should be investigated so that availability of iron oxide would be assured. Finally, a pilot plant hot gas cleanup facility should be operated so that its feasibility for commercial application would be demonstrated along with hardware development and scale-up design criteria established.

REFERENCES

1. Reeve, L. Desulfurization of Coke-Oven Gas at Appleby-Frodingham. *J. Inst. Fuel*, vol. 31, No. 210, July 1958; pp. 319-324.
2. Abel, W. T., F. G. Shultz, and P. F. Langdon. Removal of Hydrogen Sulfide from Hot Producer Gas by Solid Absorbents. BuMines RI 7947; 1974, 23 pp.
3. Shultz, F. G. Removal of Hydrogen Sulfide from Simulated Producer Gas at Elevated Temperatures and Pressures. Proc. 2d International Conf. on Fluidized-Bed Combustion, Hueston Woods State Park, College Corner, Ohio, Oct. 4-7, 1970. U.S. Environmental Protection Agency, Office of Air Programs, 1972, pp. III-5-1--III-5-5.
4. Clay, D. T. and Scott Lynn. Iron-Catalyzed Reduction of NO by CO + H₂ in Simulated Flue Gas. General Motors Symposium on NO Reduction, Oct. 7-8, 1974.
5. Belt, R. J. and M. M. Roder. "Low Sulfur Fuel by Pressure Entrainment Carbonization of Coal," Chap. 11, pp. 121-134, *Pollution Control and Energy Needs*, R. M. Jameson and R. S. Spindt, *Advances in Chemistry Series 127*, ACS, Washington, D. C., 1973.
6. Altieri, V. J. *Gas Analyses and Testing of Gaseous Materials*, American Gas Assoc., New York, 1st Edition, 1945, pp. 339-340.
7. Oldaker, E. C., A. M. Poston, and W. L. Farrior. Removal of Hydrogen Sulfide from Hot Low-Btu Gas with Iron Oxide-Fly Ash Sorbents. MERC/TPR-75/1, Feb. 1975.

TABLE 1. - Effect of Bentonite on Absorption Capacity of Fly Ash-Iron Oxide Absorbent Using Apparatus Shown in Figure 1

Bentonite, percent	Gas flow rate, std. cu.ft./hr.	Run duration, hr.	Space velocity, vol/vol/hr	H ₂ S absorption		
				Total, grains	Capacity wt.-pct.	Total absorbed, pct.
0.5	17.19	4.11	510	1290	11.94	96.3
1.0	15.30	5.75	454	1265	11.70	96.6
1.5	14.27	4.52	423	1134	10.5	97.2
3.0	17.58	3.15	521	678	6.28	94.1

Absorption temperature -- 1,100°F
 Saturation point -- 400 grains/100 scf
 Weight of absorbent -- 700 grams

TABLE 2. - Typical Data from Six of Thirty Absorption Capacity Tests (Figure 1) Using Same Fly Ash-Iron Oxide Absorbent Containing 10 Percent Starch

Gas flow rate, std. cu.ft./hr.	Run duration, hr.	Space velocity, vol/vol/hr	H ₂ S absorption			Total quantities through bed	
			Total grains	wt.-pct.	Efficiency pct.	Tar, gms	Dust, gms
14.27	6.28	501	1118	10.35	92.5	31.5	.2
15.97	5.75	563	1193	11.04	95.0	30.8	.6
16.37	5.75	570	1180	10.92	93.5	28.2	.4
16.38	5.50	587	1135	10.51	93.1	33.5	.5
15.23	6.00	529	1159	10.73	94.2	32.3	.5
15.09	7.25	549	1332	12.33	92.2	33.4	.5

Absorption temperature -- 1,100°F
 Saturation break-through point -- 400 gr/100 scf
 Weight of absorbent -- 700 grams

TABLE 3. - Run Data Obtained During Four Absorption Periods Using Raw Producer Gas from MERC Producer (Figure 2)

	Run 1	Run 2	Run 3	Run 4
Volume of bed, cubic feet	0.785	0.785	0.785	0.785
Weight of absorbents, pounds	73	73	73	73
Gas flow rate, scfh	1,500	1,500	1,500	1,500
Space velocity, $\frac{\text{scfh}}{\text{cu. ft. absorbent}}$	1,910	1,910	1,910	1,910
Duration of run, hours	15.87	9.78	14.50	10.75
Inlet steam concentration, percent	8.5	3.3	3.1	6.3
Bed temperature, °F	1,085	1,085	1,085	1,085
Absorption capacity, weight-percent	9.19	6.17	8.35	9.29
H ₂ S absorbed, grains	46,950	31,532	53,624	47,450
H ₂ S absorbed when 150 grains = point of saturation, percent	83	83	81	86
H ₂ S absorbed if 50 grains = point of saturation, percent	92.9	91.4	90.7	94.2

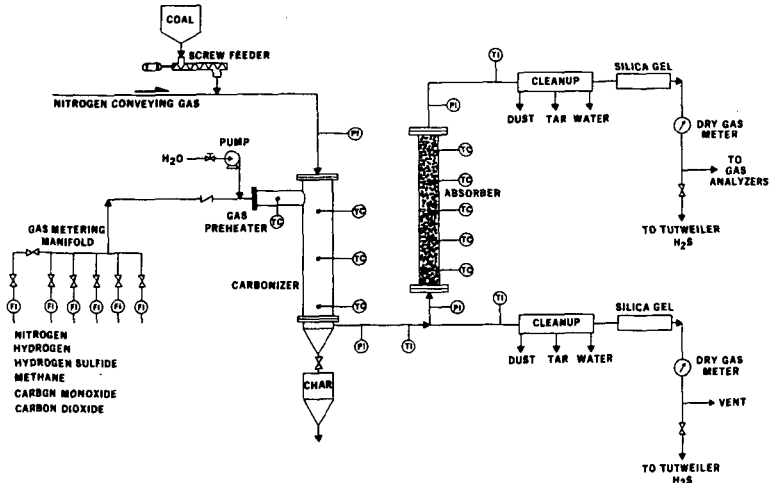


Figure 1. - Flow Diagram of Apparatus for Measuring Absorption Capacity

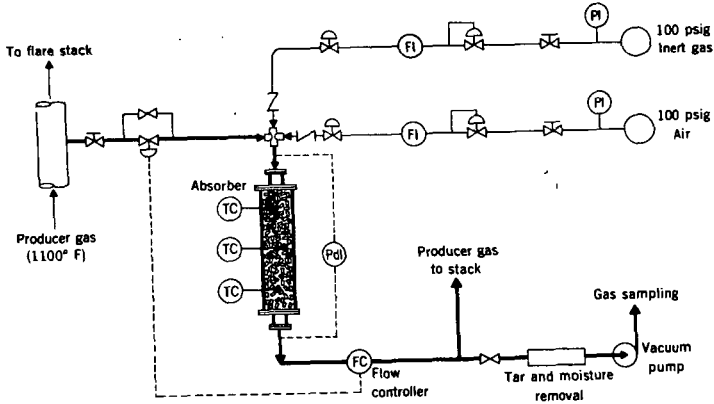


Figure 2. - Flow Diagram of Apparatus for Testing Solid Absorbents Using Hot Producer Gas

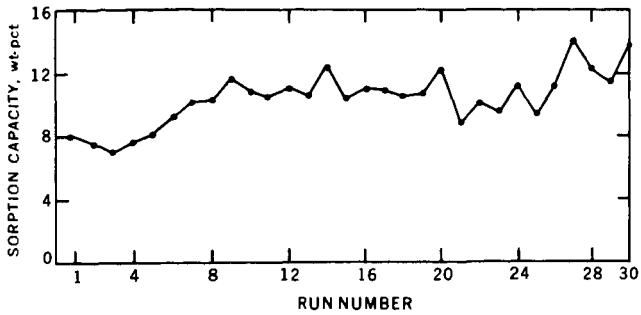


Figure 3. - Absorption Capacities Achieved During Thirty Absorption-Regeneration Test Runs Using the Same Absorbent, with Operating Conditions Listed in Table 2

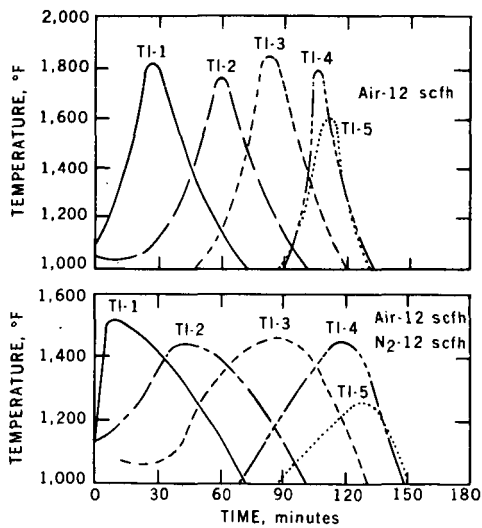


Figure 4. - Comparison of Bed Temperature Profiles With and Without Dilution Gas for Regeneration of Sulfided Absorbents

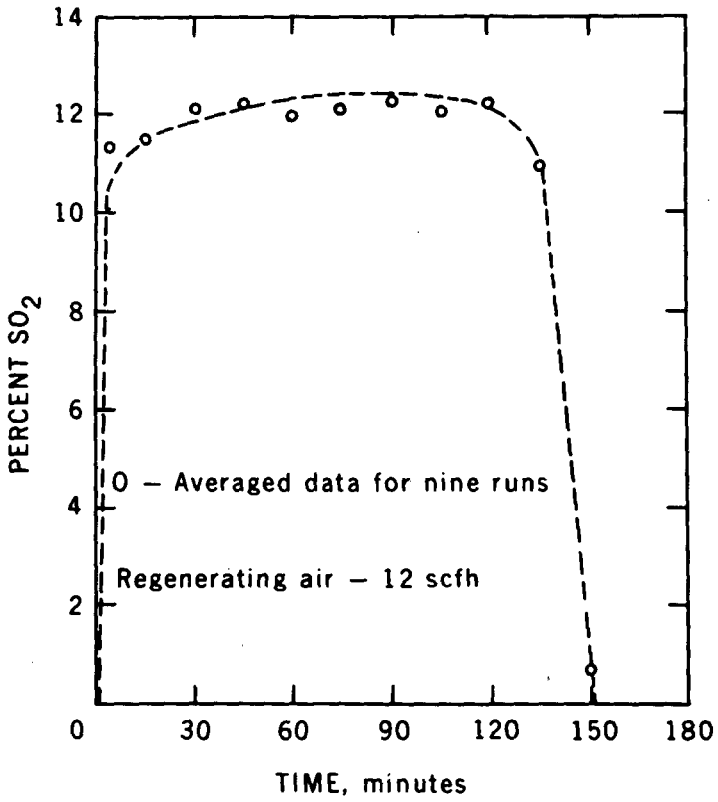


Figure 5. - Typical Curve Showing SO₂ Concentration in the Effluent Gas During Regeneration of the Sulfided Absorbents

INVESTIGATIONS ON THE REMOVAL OF HYDROGEN
SULFIDE AT HIGH TEMPERATURE FROM COAL GAS

Keshava S. Murthy

Battelle's Columbus Laboratories
505 King Avenue
Columbus, Ohio 43201WHY HOT-GAS CLEANUP?

At current consumption levels, proven U.S. natural gas reserves are estimated to last 8 years.^{(1)*} Gasification of oils with negligible sulfur content is not feasible since the U.S. oil supply, slowly dwindling, is sufficient for only 10 years.⁽¹⁾ Thus, if continued gas supply is desired, coal gasification may be the only immediately feasible alternative.

Lurgi and Kopper-Totzek (K-T) gasifiers are among the older commercially proven processes. The Lurgi process produces low- or medium-Btu gases contaminated with varying amounts of sulfur compounds such as hydrogen sulfide (H₂S) and carbonyl sulfide (COS). The Lurgi gas is at a higher pressure (350 psi) and lower temperature (750 to 1100 F depending on coal type) than K-T gas which is at 1 atmosphere and 2500 F. Both processes produce gas with a heating value (HHV) of 300 Btu/scf when using oxygen. The Lurgi process can also produce a 180 Btu/scf gas when air blown.

These medium- and low-Btu gases can be used in many ways. The high-pressure-low-temperature Lurgi gas, after removal of its H₂S, tar, and dust content is well suited for synthesis of methane to produce substitute natural gas (SNG). Also, because of its high pressure, the gas can be desulfurized by any of the established wet processes, although this requires cooling the gas to 200 F or -50 F, depending on the liquid scrubbing process chosen. In contrast, if the gas is desulfurized and cleaned until free of particulates at close to the gasifier exit temperature, the sensible heat of the gas can be utilized to efficiently generate electric power in a combined-cycle power plant or to avoid the large heat-exchange hardware requirements in a SNG production scheme.

The K-T gas, at atmospheric pressure and 2500 F, needs compression to 450 psig and cooling before the wet desulfurization and subsequent methanation steps if SNG is the desired product. The prior compression and cooling may be less attractive compared with the direct utilization of the K-T gas in a power plant boiler if a means can be found to desulfurize and clean the crude gas at near gasifier exit temperature. In the latter event, the sensible heat of the medium-Btu gas (45 Btu/scf or 15 percent of its heating value) could be usefully employed. The K-T gasifier can gasify any type of solid fuel (caking coals, chars, petroleum coke, tar, oils, and slurries) and has quick startup and shutdown capabilities. The K-T gasifier is expected to be a suitable source of fuel gas to many power plants in western United States now using natural gas; the retrofit difficulties are estimated to be minimal. If the electric utility industry and other industrial markets now using over 65 percent of the natural gas supply convert to low-Btu gas, about 5 trillion cu ft (35 percent) of natural gas would be freed for other uses.⁽¹⁾

Doubtless, the K-T gasifier--hot-gas-cleanup approach needs to compete with the emerging flue-gas desulfurization (FGD) processes which permit the use of sulfur containing coal. Currently, the FGD processes generate large volumes of secondary wastes, including sludges and liquid purge streams. A detailed evaluation of FGD versus the K-T gasifier--hot-gas-cleanup system may demonstrate the latter

* References are listed at the end.

approach to be favorable, since it does not produce significant secondary wastes; the choice could be largely site specific.

If hot-gas-cleanup systems can be developed to remove sulfur compounds in crude gases, to less than the 0.1-ppm level, they may also be applicable to the SNG production processes. Significant savings appear possible by eliminating the cooling step or minimizing the degree of cooling and heat exchange.

The above arguments suggest that the development of a hot desulfurization process has merit. Also, as evidenced in the development of FGD processes and their wide but slow acceptance, a factor that favors the development of new systems is that when a well-proven system exists, the best use will be made of it. The Energy Research and Development Administration (ERDA) has been investigating hot-gas H_2S -removal techniques since 1967.⁽²⁾ Others independently involved in the study are the University of Kentucky (since 1972), Air Products and Chemicals, Inc., and Conoco. Battelle's work began in 1974 as a result of funding under the Battelle Energy Program* initiated early in 1973. This paper describes the results of the Battelle investigations on the development of sorbents for removal of H_2S at high temperature from coal gases.

EXPERIMENTAL FACILITY

The Battelle experimental facility is presented in Figure 1. It consists of a gas-mixing section, a preheater, and a fixed-bed tubular glass reactor. Both the reactor and preheater operate in the range 100 to 1800 F, and precise control of temperature of the gas and sorbent bed is possible. The preheater and reactor used are made of clear quartz tube, 50-mm ID. Quartz was chosen after stainless steel reactors (Types 304 and 446) were found to react severely with H_2S . No particular hazard was observed with the operation of the unit when the gases were properly scrubbed and vented.

EXPERIMENTAL PROCEDURES

Certified standard gas mixtures** were used to obtain simulated coal gas of the following composition in volume percent: H_2 , 17; CO, 26.0; CO_2 , 5.0; N_2 , 50.5; and H_2S , 1.5. The large amount of nitrogen suggests simulation of a low-Btu gas obtained by air-blown process. The gas does not resemble any actual producer gas exactly; the H_2S content is rather high and also free of the usual moisture, tar, and dust present in actual coal gases. The rationale for choice of this composition was that Battelle studies were designed to generate data for comparison with the results of ERDA studies.⁽²⁾ A gas chromatographic analysis confirmed that actual gas composition was close to the desired values. Matheson flow controllers were helpful

* Research described here was supported by The Battelle Energy Program (BEP). The Program has been established to carry out major R&D efforts aimed at developing practical solutions to some of the extremely serious energy shortage and utilization problems expected to exist in the United States during 1975-1995. Battelle Memorial Institute has allocated millions of its own funds to support this effort because of the importance of the energy problem to the nation. The primary emphasis of BEP is on the development of coal as a clean fuel source since coal holds the greatest promise for filling the gap between the U.S. energy requirements and the ability to meet these requirements in the time period of interest. Additional energy sources being investigated under the program include solar energy.

** Matheson Gas Products, Joliet, Illinois, was the vendor.

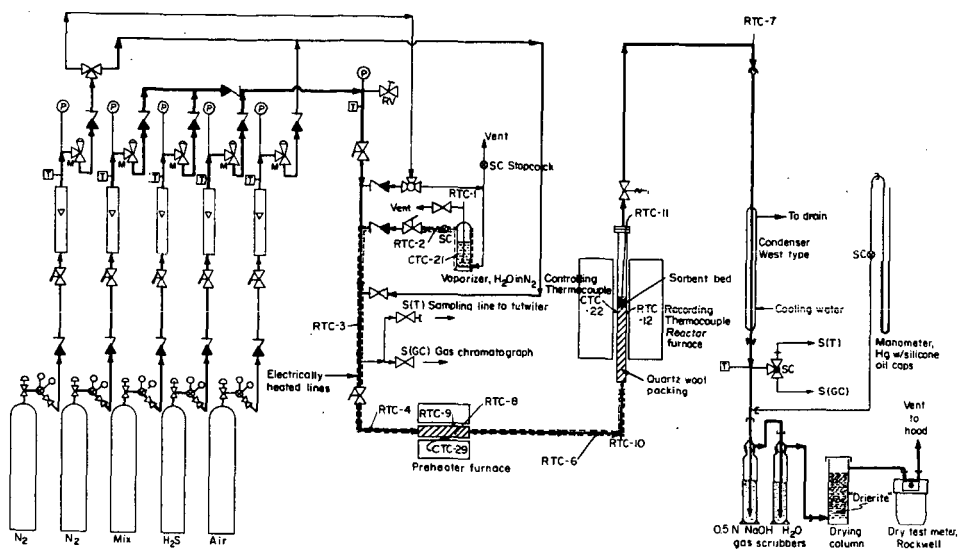


FIGURE 1. FLOW DIAGRAM OF THE HIGH-TEMPERATURE H₂S-REMOVAL ASSEMBLY

in maintaining flow accuracy and precision to within ± 3 percent on the total flow. H_2S was fed as a 25 percent gas mixture in nitrogen and the H_2S in test gas was 950 grains/100 scf with a precision of ± 10 grains.

H_2S in the inlet and outlet streams was measured by the Tutwiler method.⁽³⁾ The method consists of grab sampling 100 cc of the gas in a glass bulb connected to a burette containing standard iodine solution. The gas, collected over starch solution, is titrated with the iodine to a blue end point. Each milliliter of the iodine solution (prepared by diluting 13.5 ml of 0.1 N solution to 100 ml with distilled water) is equivalent to 100 grains of H_2S /100 scf of gas. The method can detect H_2S as low as 2 grains/100 scf of gas, or $3\frac{1}{2}$ ppm of H_2S .

The quartz preheater and reactor were packed with quartz wool to provide a heat-transfer surface. The test sorbent, 100-gram charge, was supported on a honeycomb structure made of quartz tube to provide even gas distribution. The sorbent bed was located ± 2 inches about the center of the reactor's length. The thermocouple tip was about 0.5 cm above the bed. The temperature profile through the bed indicated that the bed was nearly uniform in temperature, and the gas entered and exited the bed at nearly the reaction temperature. A 12-point recorder provided temperature read-out.

To insure a proper basis for comparison of results on sorbent performance, the experiments were performed at uniform operating conditions (1500 F reaction temperature, cold gas flow of 1 liter/min. at 70 F and 14.7 psia and 950 grains H_2S /100 scf). The cold-space velocity was 600 gas volumes per volume of bed per hour, equivalent to an operating GSV of 2000 V/V/hr varying slightly with bed volume. The acceptance run was terminated when the outlet-gas H_2S concentration approached 100 grains at an inlet-gas H_2S content of 950 grains. The regeneration run was ended when the sulfur dioxide in the regenerator gas dropped from 6 volume percent to 0.05 percent. Sulfur dioxide was also measured by the Tutwiler method. After one cycle of acceptance and regeneration, the sorbent was subjected to sieve analysis to determine attrition.

SORBENT PREPARATION

Sorbents were prepared utilizing CP or reagent-grade chemicals. These, as dry powder (-200 U.S. sieve), were weighed and mixed together with 1 gram each of starch, bentonite, and sodium silicate per 100 grams of the mixture. The resulting mix was made into a paste with distilled water. The paste was either pelletized or extruded. The pellets, after oven-drying at 250 F, were sintered at 1800 F (or 1600 F) for 2 hours. The sintered pellets were screened to -6 + 10 U.S. sieve mesh. The extrudates (1/8 inch in diameter and about 1/4 inch long) were also dried and sintered similarly and screened to remove all minus 10-mesh particles. The sorbent was free flowing and reasonably strong. The average density was about 0.9 cc/g.

EXPERIMENTAL RESULTS AND DISCUSSION

As a first step, five blank runs were performed with test gas. The reactor was not charged with sorbent. Results with Type 304 stainless steel and other reactor materials (Table 1) show that stainless steels are unsuitable as experimental reactors but that quartz resists H_2S attack satisfactorily. The steel reactor walls flaked off and thermocouple wells were damaged by corrosion.

TABLE 1. TEST RESULTS WITH BLANK REACTOR

Parameter	Stainless Steel		Quartz
	Type 304	Type 446	
Diameter (ID), inches	1.26	2.0	2.1
Length of Hot Zone, inches	16.0	16.0	16.0
Gas Flow Rate			
At 70F, 1 Atm, cm ³ /min	750	750	1000
H ₂ S absorbed, percent			
At 1000 F	15 ^(a)	8	0
At 1500 F	90	90	5
Test Duration, hours			
At 1000 F	15	8	3
At 1500 F	27	10	4

- (a) During the first 11 hours, the removal was 99.5 percent; a gradual drop to 15 percent occurred in the next 4 hours. At 1500 F, no significant reduction in removal was observed.

H₂S Acceptance Experiments

With the quartz reactor (using quartz thermocouple wells), 21 experiments were conducted to study the H₂S acceptance-regeneration characteristics of the 11 sorbents listed in Table 2. The USBM sorbent was provided by the Morgantown Energy Research Center (MERC).^{*} The fly ash used in the sorbent contained approximately 52 percent SiO₂, 25 percent Al₂O₃, 15 percent Fe₂O₃, with the remainder being CaO, MgO, K₂O, etc.⁽⁴⁾ This sorbent was studied in four experiments to establish baseline performance data at 1500 F, since the reported desulfacity^{**} results obtained with stainless steel reactors⁽²⁾ were suspected to be too high.

A comparison of data reported by USBM (now ERDA) with those obtained in BCL studies (Table 3) for three sorbents, including fly ash--iron oxide sorbent, indicates that the influence of H₂S uptake by the reactor at 1500 F is a significant factor in the reported desulfacity results. Contrary to a reported increase in desulfacity at higher temperature, the BCL data establish that a significantly higher H₂S removal occurs at 1000 F than at 1500 F. Thermodynamic considerations support these data in that the predicted equilibrium conversion is high (approaching 100 percent) at temperatures of 1000 F and higher. This is modified by the fact that the reaction is exothermic, hence lower temperatures permit actual realization of the predicted high conversion.⁽⁵⁾

The data in Table 3 also indicate a significantly low exit H₂S concentration for all sorbents containing component X (used in BCL sorbents) at all temperatures. Also, BCL experiments show that pure iron oxide at 1000 F permits a very low exit-H₂S concentration. In certain applications of coal gas, the low H₂S level may be an advantage. A graphical comparison of the low exit H₂S concentration of various sorbents is presented in Figure 2.

Regeneration Results

A comparative plot of the regeneration curves of various sorbents is presented in Figure 3. All of these experiments were performed at uniform conditions of 1 liter/minute of air inflow at 70 F, 1 atm, and 1000 F sorbent bed temperature. The data do not provide conclusive evidence on comparative regeneration characteristics of the sorbents. This indicates that the need for further experimentation is more pronounced in the area of regeneration than in the area of H₂S acceptance. The major ambiguity is in reference to Curves 5 and 6 for the regeneration of sorbent BCL 29 E. These two curves, which should have been closely similar because of replication of the same experiment, are obviously very different. However, while the sorbent in Curve 5 was regenerated immediately after the end of the acceptance run (with no overnight cooling of the sulfided sorbent), the sorbent in Curve 6 was cooled overnight between the acceptance and regeneration runs. Neither of these occurrences was deliberate.

Although the reasons for the superior regeneration characteristics of Curve 5 are not clear, this curve represents a desirable regeneration trend. The 3 percent SO₂ in exit gas for over 5 hours followed by a sudden concentration drop should help in further processing of the SO₂-bearing gas to either sulfuric acid or sulfur. The sulfur balance, based on 23.7 grams of H₂S absorbed by the sulfided

* Courtesy of Ernest Oldaker, MERC, ERDA, Morgantown, West Virginia.

** Desulfacity is defined as grams of H₂S removed from the gas by 100 grams of sorbent charge, or weight percent H₂S-removal capacity either at breakthrough or when exit gas H₂S concentration reaches 100 grains/100 scf.

TABLE 2. LIST OF SORBENTS STUDIED

Sor bent Designation	Size	
	Pellet -6+10 U.S. Sieve	Extrudate, 1/8" Diam., 1/4" Long
USBM #0074*		3/16" diam. x 1/2" long
BCL #8WB**	X	
BCL #20	X	
BCL #20E		X
BCL #21	X	
BCL #23	X	
BCL #25E		X
BCL #26E		X
BCL #27E		X
BCL #28E		X
BCL #29E		X

* U.S. Bureau of Mines Sorbent Batch No. 0074 contains 75 percent fly ash and balance iron oxide.

** BCL (Battelle Columbus Laboratories) Sorbents. The composition of these Sorbents are withheld for proprietary reasons.

TABLE 3. COMPARISON OF DATA ON DESULFURIZATION* (Weight Percent) AND CONCENTRATION OF H₂S IN REACTOR EXIT GAS

Sorbent	USBM Reported Data in Stainless Steel Reactor (2), weight percent	BCL Data From Quartz Reactor, weight percent	H ₂ S in Exit Gas, (BCL Data) grains/100 scf
USBM #0074			
At 1000 F	8.7	No data	No data
At 1500 F	41.1	19.0	22.5
BCL SWB			
At 1000 F	22	26.3	4.4
At 1500 F	Bed plugged	19.2	21.6
BCL 29E Extrudates**			
At 1000 F	Not studied	22.2	10.2
At 1500 F	Not studied	17.2	12.0
BCL 20			
Pellets, 1500F**	Not studied	21.9	8.3
Extrudates, 1500F	Not studied	21.0	10.0
BCL 21			
(Pure Component X), 1500 F	Not studied	21.0	8.0

Note: All the BCL experiments were conducted under nearly identical conditions: 1000 scf cm/min of gas flow at 70 F, atmosphere pressure, inlet H₂S of 950 grain/scf, 100 grams of sorbent charge, and excellent temperature control.

* Grams H₂S removed by 100-g sorbent charge; see full definition on Page 6.

** Both these sorbents contain Component X.

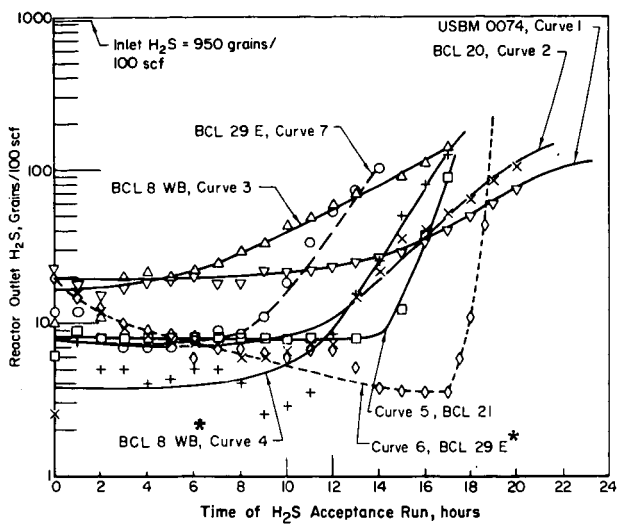
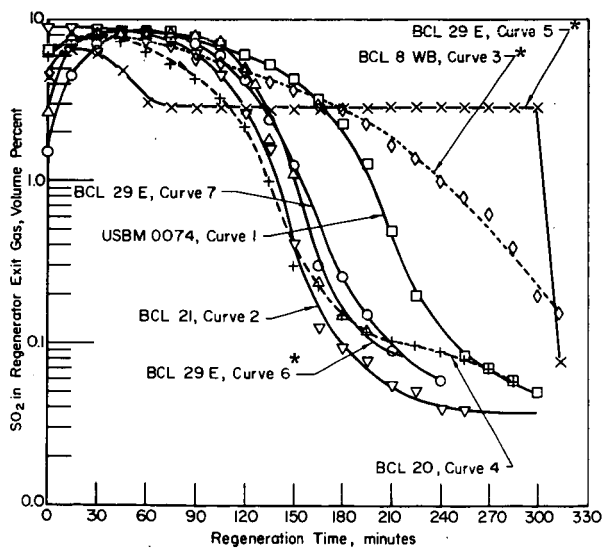
FIGURE 2. H_2S - ACCEPTANCE CURVES

FIGURE 3. SORBENT REGENERATION CURVES

* For these runs, H_2S acceptance temperature was 1000 F, while for the remaining, it was 1500 F. All regeneration runs were done at 1000 F. Gas and air flow rates and all other conditions were the same for all runs shown here. Also, Regeneration Curves 5 and 6 are discussed on Page 6.

sorbent, indicates that 80 percent of the sulfur absorbed is accountable in the regenerator exit gas as SO_2 . Also about 0.25 gram of sulfur was formed during regeneration, thus accounting for another 1 percent of the sulfur.

Sulfur balance calculations for Curve 1 (USBM 0074) show that 85 percent of the sulfur absorbed was accountable as SO_2 in the regenerator exit gas. The formation of sulfur in the case of the sorbent represented by Curve 5 needs further evaluation to determine whether direct sulfur formation is possible during regeneration.

Studies on Sorbent Attrition

In an actual commercial processing scheme, sorbent attrition is an important property contributing to the rate of sorbent makeup required. If attrition occurs during H_2S removal, the coal gas will carry additional particulate load which may interfere with the utilization of the gas. Ideally, an attrition loss of zero is desirable. However, catalyst attrition-loss rates of 0.3 wt %/hr (0.09 lb/bbl feed) in fluidized-bed cracking are known to be tolerable. In high-temperature coal gas desulfurization, an attrition loss of, say, 1.0 lb/million scf of gas treated* may be perhaps tolerable. It appears preferable that such loss occur during regeneration.

In the experiments reported here, the sorbents (fresh and after one cycle of acceptance-regeneration) were subjected to sieve analysis. The results are summarized in Table 4. Pure Fe_2O_3 and pure Component X disintegrate as well as agglomerate, as the data show. However, when the two are mixed, there is neither disintegration nor agglomeration. The USBM sorbent showed considerable particle disintegration and flake formation on the extrudates. In the case of sorbent BCL 29 E, the fines formed in Experiment 36 were very high, while in Experiment 37, a replicate, no fines were formed at all. This could probably be due to the overnight cooling of the absorbed sorbent before regeneration in Experiment 37, whereas in Experiment 36, there was no time lag between the acceptance and regeneration runs. Once again these data indicate the need for further studies of the regeneration mode. The strength of sorbent BCL 20 appears better in comparison with that of most other sorbents.

H_2S -Acceptance Thermodynamics

The performance of the mixture of Fe_2O_3 -Component X is enhanced over the performance of individual components, particularly in regard to physical strength. While this is an accidental discovery, the actual reasons are speculative and Component X may be a stabilizing agent. The partial pressure of H_2S in the exit gas stream is lower for the mixture than for both pure Fe_2O_3 and fly ash- Fe_2O_3 sorbent formulations.

The reaction mechanism of H_2S with Component X is not understood. Also free-energy data for component X are not available to compute equilibrium conversions. Experimental data at 1500 F show that the equilibrium conversion of H_2S with Component X is higher than with Fe_2O_3 ; however, the effect of steam on H_2S conversion with Component X cannot be predicted, and actual experiments are needed to obtain the data.

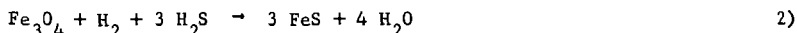
For Fe_2O_3 , considerable thermodynamic data are available. According to ICI, fresh iron oxide (Fe_2O_3) is converted to Fe_3O_4 in the presence of hydrogen above 350 F. (6) Thus, in the range of 650 to 1500 F, Fe_3O_4 is the sorbent.

* At 10 wt % desulfuricity, for an inlet gas containing 280 grains/100 scf H_2S (0.45 vol %) this is equivalent to an attrition loss of 0.025 wt % per cycle.

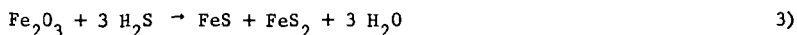
TABLE 4. SIZE ANALYSIS OF SELECTED SORBENTS TESTED

Average Particle Size	Grams of Sorbent in Size Mentioned													
	18, 23		20, 24		27, 28		29, 30		31		36		37	
	USBM	BCL	USBM	BCL	USBM	BCL	USBM	BCL	USBM	BCL	USBM	BCL	USBM	BCL
	0074	0074E	20	20E	21	21	26E	26E	29E(1)	29E(1)	36	36	37	37
<u>Fresh Sorbent</u>														
Pellet, 2680 μ	100	100	100	--	100	--	100	--	100	--	--	--	--	--
Extrudate, 1/8" x 1/4" long	--	--	--	100 ⁽⁵⁾	--	--	100	--	100	--	100	100	100	100
<u>Sorbent After Test Run</u>														
Total weight, all fractions	98.0	98.0	100.6	108.7	107.2	108.9	101.9	101.9	107.4	107.4	107.4	107.4	109.0	109.0
>2680 μ (agglomeration)	48.5	6.7	0	2.5	0	26.1	0	0	0	0	0	0	0	0
2680 μ	38.1	78.3	98.6	102.8	106.9	44.5	100.4	100.4	31.0	31.0	31.0	31.0	107.9	107.9
1420 μ	6.8	3.0	0.3	2.8	0.3	6.8	0.2	0.2	18.8	18.8	18.8	18.8	0.9	0.9
570 μ	2.3	8.8	0.7	0.5	0	11.7	0.2	0.2	25.2	25.2	25.2	25.2	0.1	0.1
200 μ	1.8	0.8	0.7	0.1	0	19.4	1.0	1.0	22.6	22.6	22.6	22.6	0.1	0.1
75 μ	0.5	0.3	0.3	0	0	0.4	0.1	0.1	7.7	7.7	7.7	7.7	0	0
40 μ	0	1.0	0.0	0	0	0	0	0	2.1	2.1	2.1	2.1	0	0
Fines formed (≤ 570)	4.6	10.9	1.7	0.6	0	31.5	1.3	1.3	57.6	57.6	57.6	57.6	0.2	0.2
Fused particles (>2680)	48.5	6.7	0	2.5	0	26.1	0	0	0	0	0	0	0	0
Finger crushing strength ⁽³⁾	P	S	E	G	G	P	G	G	G	G	G	G	G	G
Free flowing tendency	S	S	G	G	E	P	E	E	E	E	E	E	E	E
Flaking tendency ⁽⁴⁾	None	None	High	None	None	None	None	None	None	None	None	None	None	None

(1) Run 36 and 37 are same except for the difference in regeneration quality described before.
 (2) A test run includes one cycle of one acceptance run and one regeneration run.
 (3) P = poor, S = satisfactory, G = good, E = excellent.
 (4) Flaking is observable only on extrudates. The extrudates were covered with thin flakes.
 (5) 3/16-inch diameter and 1/4-inch long extrudates.



According to this reaction, each mole of Fe_2O_3 reacts with 2 moles of H_2S ; the theoretical desulfacity is 40 percent by weight. However, USBM reports that the following reaction takes place:



on this basis the desulfacity of Fe_2O_3 would be 60 percent by weight. The amount of water evolved by either reaction is the same. Actual experimental data on the fly ash + Fe_2O_3 sorbent (64 grams H_2S removed per 100 grams Fe_2O_3) support the USBM reaction mechanism (2) which can be utilized for computing the equilibrium conversions.

For Reaction 3), the standard free-energy change (ΔF° at 25 C and 1 atmosphere) is -26,270 cal/g-mole. Thus, the equilibrium constant

$$K = \exp\left(\frac{-\Delta F^\circ}{RT}\right) = 1.85 \times 10^{19} \text{ at } 25 \text{ C.}$$

K at 1000 F (537 C) can be computed using the equation

$$\frac{d \ln K}{dT} = \frac{\Delta H^\circ}{RT^2},$$

where ΔH , the heat of reaction can be shown to be substantially constant over the temperature range under study. Thus,

$$K_{1000 \text{ F}} = 8.6 \times 10^9.$$

The high K value indicates that conversions are very high and approach 100 percent. These reactions are heterogeneous and the change in number of moles of gas is zero. Therefore, there should be no effect of pressure on conversion.

The above calculations for Fe_2O_3 also hold for other dry oxides. Thus, BaO , CaO , CoO , Cu_2O , Na_2O , NiO , and ZnO all show high equilibrium conversions. Two oxides (MgO and ZrO_2) show positive standard free-energy changes, indicating thermodynamic infeasibility. Regeneration (reaction with oxygen) of the sulfides of all these sorbents is thermodynamically feasible.

Effect of Steam on Conversion

Coal gases usually contain steam, at least 10 percent by volume. Since steam is a product of the reaction of oxides with H_2S , the presence of steam in feed gas can reduce H_2S conversion. For the iron oxide sorbent, calculations show that at 1000 F ($K = 8.6 \times 10^9$), for a gas containing 5000 ppm H_2S and 10 percent steam, the equilibrium H_2S content in exit gas is 4.6 ppm based on the USBM reaction mechanism. If the ICI reaction is used, the equilibrium H_2S in exit gas is >300 ppm. These calculations cannot be made for Component X since thermodynamic data are not available. Further, the behavior of a mixture of materials reactive with H_2S as a sorbent in presence of steam is more complex than thermodynamics can predict.

A CONCEPTUAL PROCESSING SCHEME

It is important not only to have a good sorbent but also a processing scheme in which it can be used. Many processing schemes can be visualized to desulfurize hot coal gases. One such scheme is presented in Figure 4. The sorbent (pellets or extrudates) moves at a slow rate in a moving bed and discharges into a fluidized-bed regenerator. Air acts as the fluidizing medium and supplies the oxygen for the sulfide oxidation. The scheme has the advantages of a continuous process but reduces attrition problems during H₂S removal. Thus, no dust particles are introduced into the hot gas stream. This scheme is intended mainly for atmospheric pressure gases like K-T gas. The design of the H₂S-acceptance zone can be critical to the successful performance of the process.

CONCLUSIONS

A good desulfurizing sorbent should regenerate well, have a long life (activity) and high desulfacity. The SO₂ concentration in regenerator exit gas should be high with a sharp breakthrough. Also, the equilibrium H₂S concentration in exit gas during acceptance should be low, even in the presence of steam in feed gas. The attrition resistance should be high.

The fly ash--Fe₂O₃ sorbent did not show as good a resistance to attrition as BCL 20 sorbent. The BCL 20 sorbent showed lower exit equilibrium H₂S concentration and performed better at 1000 F than at 1500 F. The superior performance at lower temperature is in accordance with the thermodynamic rule that for exothermic reactions, the attained equilibrium conversion is higher at lower temperature. The addition of Component X improved the sorbent composition.

In conclusion, in this study, an effort has been made to define properties of a good sorbent, develop such a sorbent and conceptualize a processing scheme for its use. The commercial feasibility of the process can be demonstrated by using the sorbent in such a scheme over a number of acceptance-regeneration cycles. The following recommendations are made toward achieving that end.

RECOMMENDATIONS

The use of high-temperature H₂S removal technology should be investigated for the following cases.

- Low-Btu gasification and gas utilization in electric power plants
- Packaged coal-gasification plants (medium- and low-Btu gases)
- Synthetic natural-gas production.

High-temperature H₂S removal is a novel technology with good potential to compete with other desulfurizing processes. An overall process engineering and economic study of the novel technology vis-a-vis other processes (like Rectisol) is needed. Also needed is an experimental program to develop solid sorbents that can remove H₂S to less than 1-ppm levels. Both the Process engineering/economics study and the experimental program to screen sorbents should proceed concurrently. Intense efforts are needed to explore the full potential of this emerging technology and measure its impact on the national energy needs.

ACKNOWLEDGEMENTS

This work was supported by the Battelle Energy Program (BEP). The encouragement and cooperation of Dr. Frank G. Dawson and Mr. Jack G. Conner of BEP and Mr. Herman Feldmann, Dr. James E. Flinn, and Dr. Edward W. Ungar of BCL are sincerely appreciated.

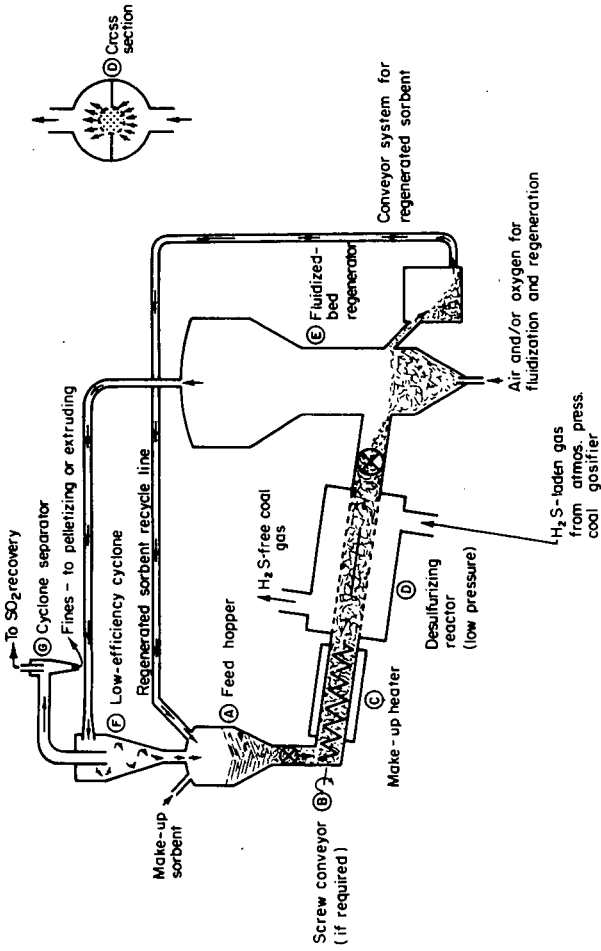


FIGURE 4. CONCEPTUAL PROCESS SCHEME FOR HIGH-TEMPERATURE, SOLID-GAS REACTION IN A MOVING BED WITH REGENERATION IN A FLUIDIZED BED

REFERENCES

- (1) "Report of the Cornell Workshops on The Major Issues of a National Energy Research and Development Program", Published by Cornell University, Ithaca, New York (December, 1973), p 76.
- (2) Abel, W. T., et al., "Removal of Hydrogen Sulfide from Hot Producer gas by solid Sorbents", RI 1947, Morgantown Energy Research Center, ERDA (1974).
- (3) Seil, Gilbert., E., DRY BOX PURIFICATION OF GAS, American Gas Association, New York, New York (1943), p 54.
- (4) Oldaker, E. C., et al., "Removal of Hydrogen Sulfide from Hot Low-Btu gas with Iron Oxide-Fly Ash Sorbents", Report No. MERC/TPR-75/1, ERDA, MERC, Morgantown, West Virginia (February, 1975).
- (5) Levenspiel, O., CHEMICAL REACTION ENGINEERING, 2nd Edition, John Wiley & Sons, Inc., New York (1972), p 215.
- (6) CATALYST HANDBOOK, Imperial Chemical Industries, Ltd., Distributed by Springer-Verlag, Inc., New York (1970), p 53.

SEPARATION OF COAL HYDROGASIFICATION GASES BY PERMSELECTIVE MEMBRANES

W. J. Schell

Chemico Process Plants Co.
El Monte, California 91734

INTRODUCTION

It has been recognized for many years that non-porous polymer films exhibit a higher permeability toward some gases than towards others. As early as 1831 (1), investigations were reported on the phenomenon of enrichment of air with rubber membranes; however, not until 1950 (2) had the practical possibility of this and other gas separations with permselective membranes been seriously studied. Weller and Steiner (2, 3) in their classic papers, demonstrated the feasibility of separating oxygen from air and described practical processes for separation of hydrogen and helium from methane. Although their results were highly valuable in the development of the science of membrane separation, the calculated membrane area requirements for industrial processes were enormous.

The technical breakthrough in the application of membranes to gas separation came with the development of a process for preparing cellulose acetate membranes in a state which retains the permselective characteristics of ordinary cellulose acetate but which yields vastly increased gas permeability. These cellulose acetate membranes are prepared from a solution of the polymer which is cast on a smooth surface, partially dried then set or gelled in an ice-water bath. At this stage the membranes are heated in water to improve their selectivity characteristics and are then dried by a solvent exchange technique. The reason for the highly permeability values, together with the permselective characteristics of ordinary cellulose acetate, is the formation of an "active" layer on the air-dried surface of the membrane. This active layer has characteristics similar to those of ordinary cellulose acetate and has a thickness of the order of 0.1 micrometer (μm) or less, whereas the total membrane thickness may range from approximately 75 to 125 μm . Thus, the membranes are said to be asymmetric. The major portion of the membrane is an open-pore sponge-like support structure through which gases may flow freely. The permeability and selectivity characteristics of these membranes are functions of casting solution composition, film casting conditions, and post-treatment and are relatively independent of total membrane thickness.

GAS SEPARATION THEORY

The steady state mass flux (J_i) of component i through a homogeneous film of uniform thickness separating two gaseous phases is given by Fick's "First Law" of diffusion:

$$J_i = -D_i \frac{dC_i}{dx} = \text{constant} \quad 1)$$

where D_i = local diffusivity (cm^2/sec)
 C_i = local concentration of component i
 x = the distance through the film

This relationship can be simplified when the gases do not chemically associate with each other and when the gases are sparingly soluble in the membrane material. In such cases, the diffusivity of the permeating gas is constant through the film and the solubility of the gas at the membrane surface is essentially directly proportional to its partial pressure in the gas phase adjacent to that surface, i. e., Henry's Law applies:

$$C_i = k_i P_i \quad 2)$$

where k_i is the solubility parameter and P_i is the partial pressure.

If we let superscript I refer to the high pressure or upstream side of the membrane and superscript II refer to the low pressure or downstream side of the membrane, Equation 1, after integration between C_i^I at $x = 0$ and C_i^{II} at $x = l$, becomes:

$$J_i = \frac{k_i D_i (P_i^I - P_i^{II})}{l} \quad 3)$$

The product $k_i D_i$ is termed the permeability coefficient (\bar{P}_i) of the membrane for component i. This coefficient is independent of membrane thickness and pressure differential and the frequently used units are, cc(STP)-cm/cm²-sec-cm Hg. Another parameter of interest is the permeability rate, defined as \bar{P}_i/l , which is a measured characteristic of a given membrane with units, cc(STP)/cm²-sec-cm Hg. The total pressures, P^I and P^{II} , are given by the sums, $P_i^I + P_j^I$ and $P_i^{II} + P_j^{II}$, respectively.

The ratio of fluxes of two gases through a membrane is given by:

$$J_i = \frac{\bar{P}_i (P_i^I - P_i^{II})}{\bar{P}_j (P_j^I - P_j^{II})} \quad 4)$$

The ratio \bar{P}_i/\bar{P}_j is defined as the ideal separation factor for component i with respect to component j in the membrane and is written $\alpha_{i/j}$.

From the previous discussion it can be seen that, if component i is the more permeable, increasing P_i^I , either by increasing the total pressure or the concentration of component i, will result in a higher membrane permeability rate. In addition, higher values for $\alpha_{i/j}$ result in greater efficiency in gas separation.

If we define a permselectivity of the membrane to component i with respect to component j by σ_{ij} ,

$$\sigma_{ij} \equiv \frac{P_j^I P_i^{II}}{P_i^I P_j^{II}} \quad 5)$$

it can be shown from Equations 4 and 5 that:

$$\sigma_{ij} = \alpha_{i/j} \frac{P_j^I}{P_i^I} \frac{(P_i^I - P_i^{II})}{(P_i^I - P_j^{II})} \quad 6)$$

It can be seen from Equation 6 that as $P^{II} \rightarrow 0$ or $P^I/P^{II} \rightarrow \infty$, the permselectivity of the membrane approaches the ideal separation factor, i. e.:

$$\lim_{P^{II} \rightarrow 0} \sigma_{ij} = \alpha_{i/j} \quad 7)$$

It is evident then that by increasing the feed pressure to product pressure ratio, P^I/P^{II} , an increase in the efficiency of the separation of the gas mixture is obtained.

Other system variables that will have an effect on the separation process are temperature and relative humidity of the gas. Usually an increase in temperature increases the permeability and decreases the separation factor. The effect of relative humidity is variable and has not been reported in the literature to any great extent.

MEMBRANES AND MEMBRANE SYSTEMS

The casting solutions for preparation of the membranes discussed herein contain cellulose diacetate, cellulose triacetate, acetone, dioxane, methanol and acetic acid or maleic acid. The solution is cast at a thickness of 0.010 in. and is gelled in ice water. The resulting membranes are heat-treated in water at 85 to 98°C for several minutes and are then dried by solvent exchanging the water with organic solvents followed by evaporation of the remaining solvent. Drying is necessary for application to gas separation and this procedure serves to prevent the membrane from shrinking and losing its asymmetric character upon removal of water.

The gas permeability measurements for the flat membranes were made in circular (2.93 cm² membrane area or 0.0316 ft²) test cells. Single gases at 23 to 25°C were brought into contact with the dense active layer side of the membrane at a regulated pressure of 15 to 750 psig, causing a portion of the gas to permeate through the membrane. The permeate gas was removed from the opposite side of the membrane at atmospheric pressure. The permeation rates were measured either by the displacement of a soap bubble in a 5 ml gas buret or with a wet-test meter. The measured permeation rates and separation factors for the single gases with flat-sheet membranes are shown in Table 1, measured at 100 psi pressure differential, along with literature values for 0.001-in. cellulose acetate films. It can be seen that the permeation rates of the asymmetric membranes range from 600 to over 1000 times those of the films while essentially retaining the selectivity for gases. The membranes exhibit an exceptionally high permeation rate for hydrogen and helium and are particularly permselective for hydrogen relative to carbon monoxide and methane. This evidence confirms the continuity of the thin active layer and demonstrates the improvement in membrane separation technology.

Cellulose acetate membrane modules have been manufactured in our facilities for several years now for use in water desalination. These modules have a spiral-wound configuration (6) that has the advantage of compactness and low cost. For example, the dimensions of such a module are 4-in. in diameter by 3-ft in length containing approximately 70 ft² of membrane. Development of similar modules with dry membrane for gas separation will provide gas permeability rates of the order of 3200 - 9500 SCFH at 750 psig for hydrogen.

TABLE I

PERMEABILITY PROPERTIES OF FLAT CELLULOSE ACETATE MEMBRANES AND FILMS

	Permeability*, $\frac{\text{cc(STP)} \times 10^8}{\text{cm}^2 \text{-sec-cm Hg}}$				Separation Factor, α							
	H ₂	CO ₂	O ₂	CO	CH ₄	N ₂	He/CH ₄	H ₂ /N ₂	H ₂ /CH ₄	H ₂ /CO	CO ₂ /CH ₄	O ₂ /N ₂
Film, 0.001-in. thick (4)	53.5	-	-	-	0.55	0.55	97	-	-	-	-	-
Film, 0.001-in. thick (5)	19.7	20-24	2.8-3.5	-	-	0.7-0.95	-	~25	-	-	-	~4.0
Membrane, Sample 1	32,400	28,000	15,800	2110	606	583	486	55	58	48	46	27
Membrane, Sample 2	32,800	29,310	16,100	2110	612	601	467	55	63	49	48	27
Membrane, Sample 3	33,900	28,600	16,400	2230	639	627	506	54	57	46	45	26

*A permeability of 30,000 cc(STP) $\times 10^{-8}$ /cm²-sec-cm Hg corresponds to 0.184 SCFH/ft² membrane/psi pressure differential.

APPLICATION OF MEMBRANE SYSTEM TO COAL UTILIZATION PROCESSES

The feasibility of adapting permselective membranes to coal utilization processes is described in the following paragraphs. Two processes were chosen from contract reports to the U. S. Department of Interior (7, 8).

In the two processes, the membrane separation units described are assumed to have the permeability and separation properties of the asymmetric cellulose acetates described previously in Table 1. It is also assumed throughout that all gas streams will have been pretreated for removal of acid gases. The resulting feed gases may then be considered to be a two-component system of hydrogen and methane-carbon monoxide (carbon monoxide and methane have similar permeabilities) and a computer program can be used to predict the permeate stream compositions.

Hydrogasification of Lignite

Figure 1 is a schematic diagram showing how membrane gas separators could be used to advantage in processing the gas from the hydrogasification of lignite. In this case the desired product is high Btu pipeline gas and the membrane separations are incorporated into the Institute of Gas Technology overall Process Block Flow Diagram (7) in order to reduce the size of several pieces of equipment and to produce 4% more methane with a higher Btu value.

The Prepurification Unit I effluent gas is cooled to 100°F to remove water and is then fed (Figure 1) into a spiral wound membrane separation unit which separates almost all of the hydrogen from the carbon monoxide and methane. The carbon monoxide and methane stream then has about 65% of the volume of the original stream and can be fed to a carbon monoxide shift reactor where the low concentration of hydrogen enables the reaction to be shifted further to the right ($\text{CO} + \text{H}_2\text{O} \rightleftharpoons \text{CO}_2 + \text{H}_2$), therefore consuming considerably less steam than otherwise required. The overall result is that the carbon monoxide shift reactor size is reduced and the heat load of the waste heat recovery unit is reduced. The hydrogen-bearing permeate stream comes from the membrane unit at low pressure and must be compressed and cooled before it is sent to the Prepurification Unit II. After removal of carbon dioxide and the trace of hydrogen sulfide, the hydrogen stream is fed to the methanation unit where carbon monoxide is converted into methane.

The second membrane separation unit processes the effluent gas after waste heat recovery by removing most of the 4.4% hydrogen and recycling it back to the methanation unit. The recovered hydrogen allows about a 4% increase in the volume of methane produced and an increase in the Btu value of the pipeline gas.

The cost of the membrane units is believed to be small in comparison with the savings to be gained by reducing the size of the carbon monoxide shift reactor and waste heat recovery unit and reducing the amount of steam consumed so that the overall plant should be less costly. In addition, the incorporation of the membrane separators should allow greater variation in operating conditions and compositions of intermediate gas streams.

Coal Oil Hydrogenation

Membrane gas separation may also be applied to coal oil hydrogenation such as the Coal Oil Energy Development (C. O. E. D.) process (8). The hydrogenation unit is fed C. O. E. D. oil from the pyrolysis unit along with a mixture of fresh and recycle hydrogen. The membrane separator removes most of the methane

and heavier hydrocarbons from the recycle hydrogen stream at high pressure. The one-pass membrane unit operating at 1050 psig increases the recycle hydrogen concentration from 43% to over 90%, with the accompanying improvement in the hydrogenation efficiency and reduction in size of the hydrogenation unit. The methane and hydrocarbon gas stream contains less than 2% hydrogen and after extraction of the higher hydrocarbons would be ideal for pipeline gas.

REFERENCES

1. J. V. Mitchell, J. Roy. Inst., 2, 101, 307 (1831).
2. Sol Weller and W. A. Steiner, J. Appl. Phys., 21, 279 (1950).
3. Sol Weller and W. A. Steiner, Chem. Eng. Prog., 46, 585 (1950).
4. P. K. Gantzel and U. Merten, Ind. Eng. Chem. Process Des. Develop., 9, 331 (1970).
5. Modern Plastics Encyclopedia, Oct. (1969).
6. U.S. Patent #3,417,870 by D. T. Bray, Assignment to Secretary of the Interior.
7. Institute of Gas Technology, Chicago, Ill., "Cost Estimate of a 500 Billion Btu/Day Pipeline Gas Plant via Hydrogasification and Electrothermal Gasification of Lignite," Office of Coal Research, R&D Report No. 22, Interim No. 4, pgs. 6-7, Contract No. 14-01-0001-381.
8. FMC Corporation, Princeton, New Jersey, "Char Oil Energy Development," Appendice I, Table XV, RSIS2, Office of Coal Research, Washington, D.C., Contract No. 14-01-001-235.

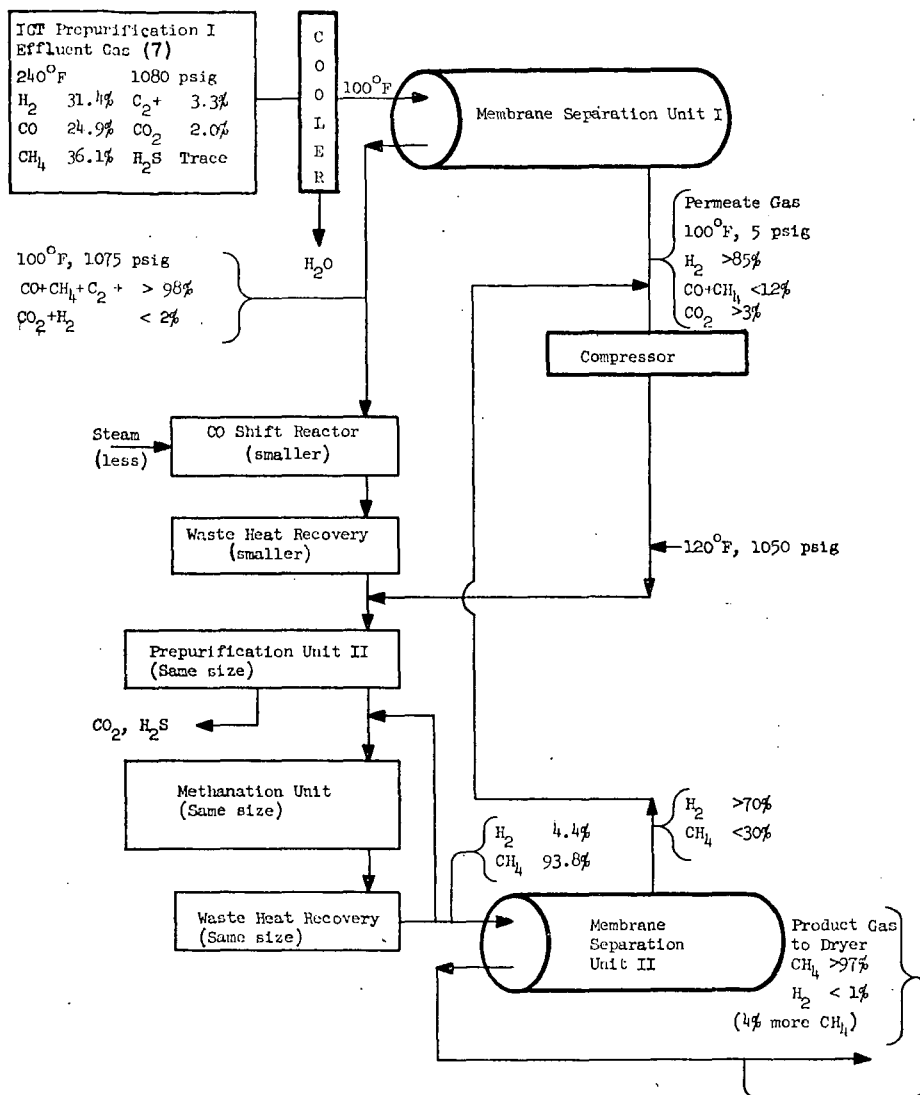


Figure 1. SCHEMATIC - APPLICATION OF MEMBRANE GAS SEPARATIONS IN A LIGHT GAS HYDROGASIFICATION PROCESS

COMBINED POWER CYCLE USING LOW

BTU GAS PRODUCED FROM THE KELLOGG MOLTEN SALT

COAL GASIFICATION PROCESS

C. A. KUMAR, L. D. FRALEY, S. E. HANDMAN

RESEARCH & ENGINEERING DEVELOPMENT

THE M. W. KELLOGG COMPANY

HOUSTON, TEXAS

INTRODUCTION

In recent years, it has become increasingly important to look for alternate sources of energy on a commercially feasible basis. In the midst of the present energy crisis, coal remains the most abundant source of energy in this country. However, the time honored techniques used to convert coal into electrical power no longer satisfy the needs of the power industry. Also, the public and the industry alike have grown to be ecology conscious; there is an ever increasing emphasis on burning "clean" fuel. A direction now established for increasing the economics of power generation is to exploit the use of a combined gas turbine-steam turbine power cycle. The relatively inexpensive gas turbine extends operation into the higher temperature range (presently 1950°F) and the temperature limit on gas turbine development has yet to be established. However, the gas turbine requires a clean fuel, natural gas or clean liquids. Low Btu fuel obtained from The M.W. Kellogg Molten Salt Coal Gasification Process, currently under development, when used in conjunction with a gas turbine-steam turbine combined power cycle system provides for an efficient method of generating electrical power from high sulfur, high ash coal while minimizing environmental pollution.

DISCUSSION

Gasification of coal using Kellogg's Molten Salt Process has been described in detail elsewhere (1, 2, 3). The overall process converts the heating value of high sulfur coal to fuel gas with a lower heating value of 100 to 150 Btu/SCF at a conversion efficiency of around 90% with most of the sulfur retained by the melt. The gasifier is set to operate at 260 psia and 1700°F and compressed air is used to partially burn coal to produce the fuel gas at these conditions.

The work to develop the Kellogg Molten Salt Coal Gasification Process for SNG (Substitute Natural Gas) has been modified to develop a process that is compatible with the combined cycle concept. (See Figure 1.)

There are four systems in the process:

1. Gasifier --a single pressure vessel where molten sodium carbonate catalyzes the partial oxidation of coal by air to produce a raw fuel gas. A typical composition is shown in Table 1.
2. Coal and Carbonate Feed --supply coal and make-up sodium carbonate at pressure to the gasifier.
3. Gas Conditioning --a series of heat exchanges and gas washes make the raw gas compatible with a gas turbine.
4. Carbonate Recycle --the stream which purges ash from the gasifier is approxi-

mately 70% sodium carbonate and 8% sodium sulfide. The system recovers the sodium for recycling to the gasifier.

COMBINED POWER CYCLE

The overall efficiency of a combined cycle power plant burning low Btu gas produced from the Kellogg process is dependent on the coal gasification efficiency--including the salt cleanup and regeneration--and the temperature-pressure conditions in the steam generation system. Salt recovery technique thus is one of the key features in the performance of this cycle. The sensible heat from the melt purge (@ 1700°F) is used to preheat the air supply to the gasifier (to 990°F). (See Figure 2.) Most of the salt is recovered by evaporation as carbonate for recycle and the heat for evaporation is provided from the gas turbine exhaust. Sulfur retained by the melt is converted to hydrogen sulfide by carbonation and then recovered as elemental sulfur in a nearby Claus plant.

The fuel gas leaving the gasifier is cooled in a series of heat exchangers to a temperature of around 175°F before being sent to a scrubber. The major part of this heat is utilized for the production of steam and BFW heat for the steam system (2400 psia/1000°F/1000°F) as well as for reheating the scrubbed fuel gas back to 500°F before being sent into the gas turbine. The scrubbing operation provides the CO₂ needed for carbonation of the salt, while scrubbing with water eliminates sodium. The only fixed nitrogen in the fuel is a trace of NH₃ and thus the fuel gas produced is quite clean. Also, sodium carbonate being a catalyst gasifies coal completely without the production of associated coal distillates. For example, using Ohio Clarion High Sulfur (4.65%) Coal in the Kellogg process, it has been determined that more than 90% of sulfur is retained by melt for recovery later. This results in 0.78 lb SO₂/MMBtu in the flue gas without any scrubbing to remove SO₂.

The gasification system distributes the heating value of the coal into four parts. (See Table 2.)

The sensible heat in the fuel gas is available at various temperature levels. This requires a close integration with the steam system of the combined cycle so that it is used in the most efficient manner.

The number and type of interfaces just described mean that the gasifier and combined cycle must be tightly integrated if the overall system is to be very efficient.

Figure 2 shows the result of just such an integration. A commercially available gas turbine with 1950°F inlet temperature and a 2400 psia/1000°F/1000°F steam cycle were used. The match up between the steam cycle and sensible heat, both in the fuel gas and flue gas, is shown in Figure 3.

These curves show that the heat interchanges are arranged in such a fashion that minimum temperature differentials of around 40°F are observed at the pinch points. This, along with the fact that heat available at the gasifier level is limited to steam generation, has required that BFW heating and steam generation be done in more than one step. The distribution of power among various components for a 120 eMW net plant is shown in Table 3.

It is estimated that integration of a gas turbine combined power cycle (with fully loading the gas turbine in conjunction with a 2400 psia/1000°F/1000°F steam system) with the Kellogg Molten Salt Coal Gasification process generates power at a net heat rate of around 9500 Btu/kw-hr or lower using available equipment (HHV).

UTILIZATION OF LOW ASH COAL

(e.g., Pittsburgh Seam Coal with 5.2% ash-1.3%S) Incorporating minor changes in the purge recycle and the power cycle discussed above, the molten salt process can be very effectively used with low ash coal. It is estimated that such a process would have a gasifier efficiency of over 95% with a 0.45 lb/MMBtu of SO₂ in the flue gas without any scrubbing. The overall efficiency of such a combined cycle power plant utilizing the low ash coal is estimated around 40% (8500 Btu/kwh based on HHV).

ECONOMICS

Any attempt at economic analysis in these days must be based more on underlying fundamentals of a system rather than on numbers.

However, in Table 4 is an attempt at a current analysis. This compares the cost of power generated by a conventional power plant equipped with a stack gas scrubber to the gasifier - combined cycle system. Both systems were considered to have an efficiency of 36%. Coal was assumed to be 20\$/ton, the conventional plant to cost 400\$/kw plus 55\$/kw for a scrubber. The gasifier - combined cycle system was estimated to be 375\$/kw. These parameters reflect the conditions at the end of 1974. Table 4 shows an 11% advantage for the gasifier - combined cycle system. This can be considered marginal since it is a system currently under development.

STATUS OF THE PROCESS

Extensive work has been done in testing the containment of the molten sodium carbonate bath for the production of high Btu pipeline quality gas (SNG). Basic data on the gasification process have been reported. Low Btu coal gasification is essentially an outcome of the Kellogg Molten Salt process for the production of SNG and as such most of the work done for the SNG process can easily be extended to the production of low Btu gas.

Thus, incorporating a combined cycle in conjunction with the Kellogg Molten Salt process, currently under development, for the production of low BTu gas, provides for a relatively easy way of obtaining power with the following advantages:

1. The Molten Salt gasifier will handle any type of coal including caking coals without pretreatment.
2. The catalytic action of the molten sodium carbonate promotes complete gasification of coal without the production of associated coal distillates, thus eliminating downstream fouling and some of the pollution control facilities that would otherwise be required.
3. The catalytic effect of sodium carbonate allows gasification at lower temperatures permitting higher gasification efficiency.
4. The system provides clean fuel gas for use in a gas turbine.
5. In the next five to ten years gas turbines possibly will be available with inlet temperatures of 2500°F and 3000°F. The power cycle efficiency in these cases are estimated to be 46% and 49%, respectively, based on HHV and low ash coal. And finally,
6. It is estimated that power plants using 3000°F inlet to gas turbine result in about 47% reduction in power costs compared to a conventional cycle (Table 4)

263
REFERENCES

1. Cover, A.E., W.C. Schreiner, and G.T. Skaperdas, "The Kellogg Coal Gasification Process", paper presented at American Chemical Society Meeting, Washington, D.C., Sept. 1971.
2. Cover, A.E., W.C. Schreiner, and G.T. Skaperdas, "Kellogg's Coal Gasification Process", Chemical Engineering Progress, March 1973.
3. Cover, A.E., and W.C. Schreiner, "The Kellogg Molten Salt Process", paper presented at the 4th Conference on Synthetic Fuels from Coal, Oklahoma State University, Stillwater, Oklahoma, May 1974.

TABLE 1
COAL AND FUEL GAS COMPOSITION

COAL PROXIMATE ANALYSIS

% ASH	16.87
% VOLATILE	39.44
% FIXED CARBON	<u>43.69</u>
	100.00
% SULFUR	4.65
% MOISTURE	3.43
HIGHER HEATING VALUE - 11273 BTU/LB	

FUEL GAS ANALYSIS

	WGT. FRACTION
N ₂	0.614
H ₂ O	.02
CO ₂	.04
CO	.31
CH ₄	.006
H ₂	.01
H ₂ S	<u>.0002</u>
	1.00
HIGHER HEATING VALUE - 137 $\frac{\text{BTU}}{\text{SCF}}$	

TABLE 2
 DISTRIBUTION OF HIGHER HEATING VALUE
 IN COAL AFTER GASIFICATION

1. FUEL GAS TO GAS TURBINE		
	HHV	72.5%
	NET SENSIBLE HEAT GAIN	1.8
2. STEAM GENERATED BY FUEL GAS		16.6
3. ASH PURGE LOSS		
	NET SENSIBLE HEAT LOSS	1.9
	COMBUSTIBLE (C, S)	6.7
4. SCRUBBER LOSS		<u>0.5</u>
		100%

GASIFIER EFFICIENCY (1) + (2) = 90.9%

TABLE 3
DISTRIBUTION OF POWER FOR 120 e MW PLANT
(REFER TO FIG. 1.) e

GAS TURBINE	69.3
STEAM TURBINE	<u>61.2</u>
GROSS	130.5 e MW
AUXILIARIES	6.5
BOOSTER COMPRESSOR	<u>4.0</u>
	10.5 e MW

POWER OUT (NET) = 120 e MW

OVERALL EFFICIENCY = 36%

TABLE 4
COMPARISON OF POWER COST FOR 480 MW CONVENTIONAL PLANT
WITH SCRUBBER VS. GASIFIER COMBINED CYCLE PLANT

	CONVENTIONAL WITH SCRUBBER		GASIFIER COMBINED CYCLE	
CAPITAL	15.8	<u>MILLS</u> <u>KWHR</u>	13.0	<u>MILLS</u> <u>KWHR</u>
LABOR	0.3		0.3	
OPERATING	<u>10.6</u>		<u>10.7</u>	
TOTAL	26.7		24.0	

FUTURE PLANTS
w/3000°F Inlet to
Gas Turbine

9.2	<u>MILLS</u> <u>KWHR</u>
0.2	
8.8	
<u>18.2</u>	

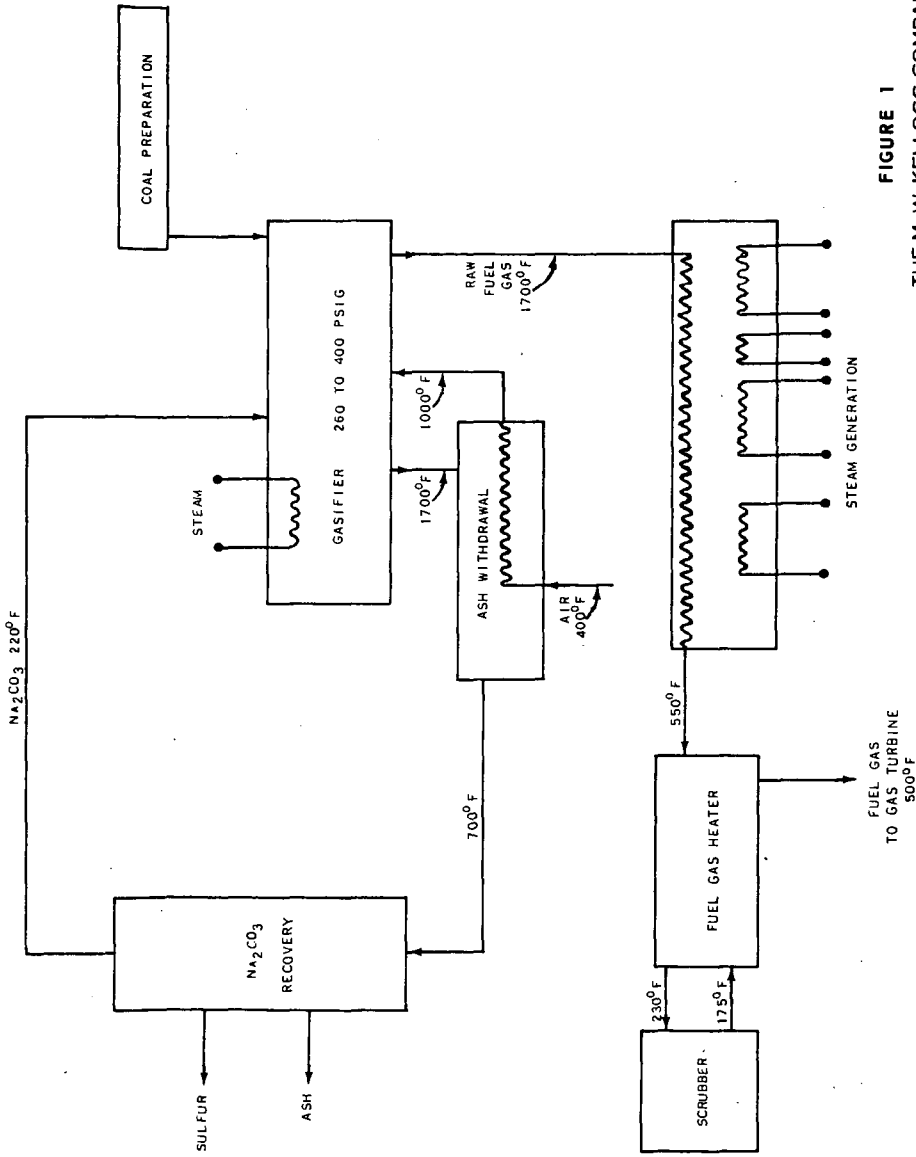
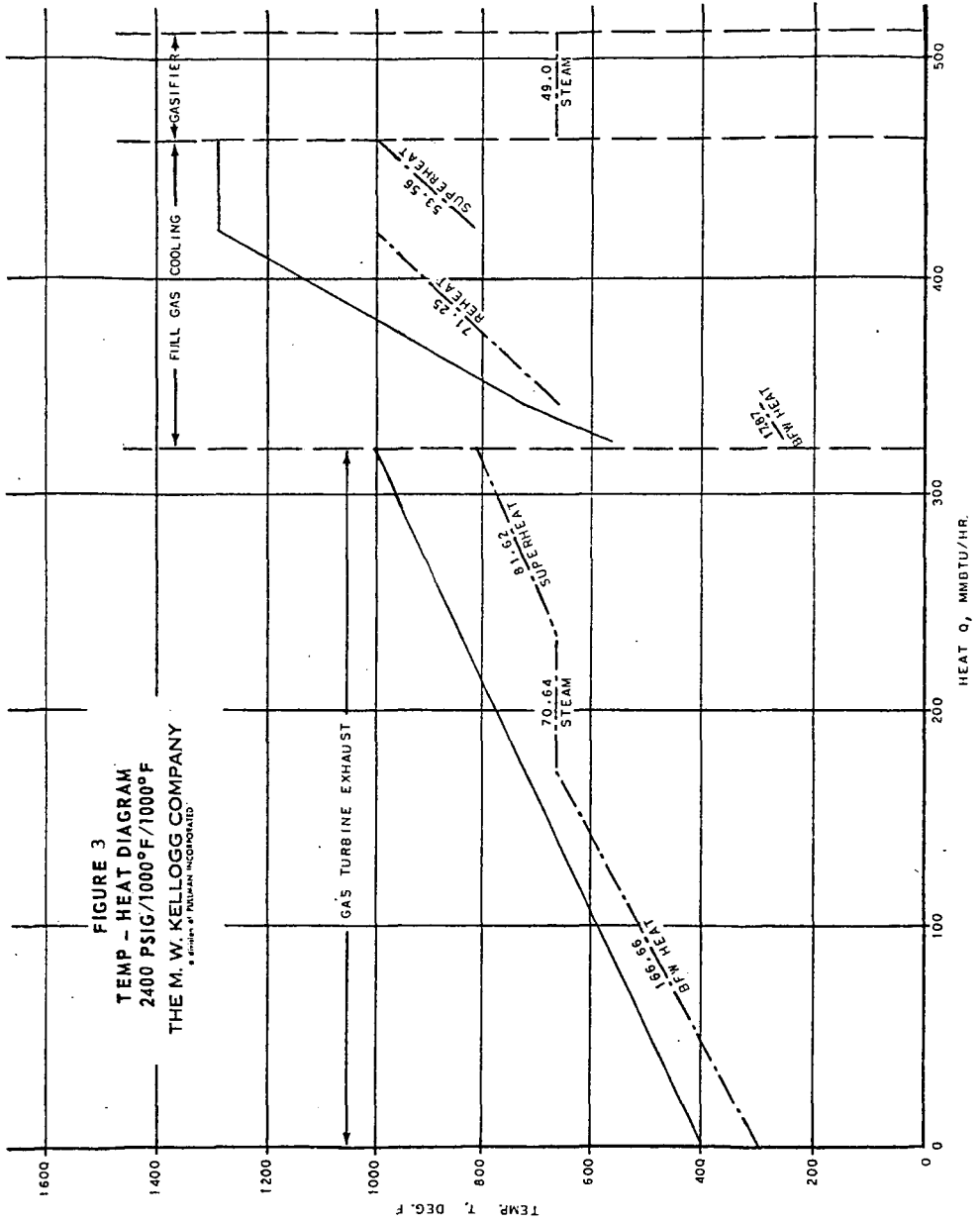


FIGURE 1
THE M. W. KELLOGG COMPANY
A DIVISION OF PHILAMAN INCORPORATED
MOLTON SALT COAL GASIFICATION



INTERACTION OF MOLTEN SODIUM CARBONATE WITH COAL ASH
COMPONENTS - ALUMINUM OXIDE. A. J. Darnell, Atomics
International Division of Rockwell International Corporation, 8900 DeSoto
Avenue, Canoga Park, CA 91304

A fundamental study is being made of the coal ash-melt interactions in relation to gasification of coal in molten sodium carbonate. In the present paper, the interaction of alumina with molten sodium carbonate is discussed. Alumina reacts with molten sodium carbonate to form sodium aluminate (NaAlO_2) and carbon dioxide, i. e., $\text{Al}_2\text{O}_3(\text{s}) + \text{Na}_2\text{CO}_3(\text{l}) \rightarrow 2\text{NaAlO}_2(\text{s}) + \text{CO}_2(\text{g})$. The sodium aluminate formed is very refractory (mp $>1700^\circ\text{C}$) and is only sparingly soluble (10-20 ppm) in molten sodium carbonate. The sodium aluminate forms a protective coating around the unreacted alumina which slows down further reaction with the molten sodium carbonate. The rate of the reaction between Al_2O_3 and Na_2CO_3 has been examined over the temperature range 900° to 1100°C under an atmosphere of CO_2 and with alumina particles ranging in size from $1\ \mu$ to $300\ \mu$. Temperature cycling did not affect the protective nature of the coating of NaAlO_2 on Al_2O_3 even though sodium aluminate is known to undergo a solid phase transition at 470°C . This was demonstrated in tests in which the temperature was cycled from ambient to 900°C and in tests in which the temperature was held at 900°C . Identical rate loss curves were obtained in the two sets of tests.

Supported by U.S. Energy Research and Development Administration.